Electrophysiological Investigation of Brain Stimulation Strategies to Improve Hearing Restoration via Auditory Neural Prostheses

A DISSERTATION
SUBMITTED TO THE FACULTY OF THE GRADUATE SCHOOL
OF THE UNIVERSITY OF MINNESOTA
BY

Malgorzata Maria Straka

IN PARTIAL FULFILLMENT OF THE REQUIREMENTS
FOR THE DEGREE OF
DOCTOR OF PHILOSOPHY

Dr. Hubert H. Lim, Advisor

December 2013

ACKNOWLEDGEMENTS

When I look back to who I was when I have started, I can see not only progress with my graduate work but also an incredible amount of growth within myself. None of these achievements would be possible without the support of the people around me and their encouragement to strive for more.

First, I would like to thank my mentor Hugh. You believed in me and equipped me with the tools I needed to be a scientist. Moreover, you continuously challenged me to perform better research, to present clearer, and to become increasingly independent. My committee members, including Matt Johnson, Tay Netoff, Theresa Nick, Andrew Oxenham, have guided my research and encouraged me throughout the process. I truly appreciate your helpful advice and positivity during this process.

I would like to acknowledge all of the undergraduate students who performed the histological reconstructions and normalizations presented in this work: Robby Hughes, Patrick Lee, Melissa McMahon, Rekha Narayanan, Jill Nelson, Dillon Schendel, Sam Schmitz, and Lindsey Sajevic. Thank you not only for contributing to this research but also helping me to better understand my work by teaching it. I enjoyed working with all of you and I am excited to see where your future takes you. I would also like to thank my fellow graduate students and lab siblings: Craig Markovitz, Cory Gloeckner, and especially Sarah Offutt. Your apt criticisms have guided me and have taught me skills that I will carry with me the rest of my life.

I would like to thank my parents and brothers, who have instilled the love of science in me. I am so grateful for my husband, Derek Straka, for his professional,

financial, and moral support. I could not have accomplished any of this and maintained my sanity without you. Your love has allowed me to take risks and grow in ways that I could not have otherwise done. And last, but most importantly, I would like to thank my Lord and Savior, Jesus Christ. Thank You for Your guiding hand and for giving me the opportunity to explore Your creation.

This research was funded by University of Minnesota start-up funds and NIH NIDCD R03DC011589.

DEDICATION

To my better half, my best friend, my partner, my heart. I could not have achieved this without you, Derek, and I would be a shadow of the person I am today without you. I am thankful for every day I share with you, and I love you more than I can express.

ABSTRACT

The auditory lemniscal system, the core pathway thought to be responsible for conducting high-fidelity auditory information, is yet to be well-understood, particularly at the level of the midbrain. The lack of understanding of the auditory lemniscal system resulted in limited performance of a central auditory neuroprosthesis called the auditory midbrain implant (**AMI**). The AMI is a linear array of 20 sites designed to stimulate the auditory lemniscal nucleus in the midbrain, the central nucleus of the inferior colliculus (**ICC**). In the first clinical trial, five patients were implanted with the AMI, which gave users improved lip reading abilities and environmental awareness. However, the AMI was unable to deliver sufficient temporal information, which is likely associated with suboptimal placement and stimulation strategies within the ICC.

This doctoral thesis project investigated the central lemniscal system in order to improve results for future AMI patients. First, the organization of responses to auditory stimuli was investigated within the auditory lemniscal midbrain. This study found different response properties within a rostral-lateral verses caudal medial ICC region, corresponding to subregions with differential input and output projection patterns. Next, we investigated various stimulation strategies that would allow the AMI to deliver sufficient temporal information. Repeated stimulation of a single site in the ICC, which was the initial strategy of the AMI, resulted in refractory effects in the auditory cortex that could only be overcome by co-activating neurons along a lamina of the ICC. This co-activation resulted in cortical activity that was enhanced beyond the sum of individual neural activation, with the greatest enhancement occurring in supragranular cortical

layers. Moreover, this enhancement was largest when stimulating the rostral-lateral rather than the caudal-medial ICC region. These ICC locations with different electrical stimulation properties matched the two subregions with different acoustic-driven response properties. Together, these studies found consistent differences in physiological properties within two subregions of the ICC, confirming the presence of dual lemniscal pathways from the midbrain to the cortex. In addition, these studies identified a potential stimulation strategy and implantation location for improving AMI performance: co-activating rostral-lateral neurons along the isofrequency laminae of the ICC.

TABLE OF CONTENTS

LIST OF TABLES

LIST OF FIGURES

ABBREVIATIONS LIST

ABI- Auditory Brainstem Implant

AC- auditory cortex

ACC- core auditory cortex regions

AMI- Auditory Midbrain Implant

A1- primary auditory cortex

BF- best frequency

CI- cochlear implant

CSD- current source density

ΔBF- Difference in BF between two sites

Di-I- 1, 1-dioctadecyl-3,3,3',3'-tetramethylindocarbocyanine perchlorate

DSR- Driven spike rate

DSS- Dual Site Stimulation: pulse stimulation of two or more sites along an isofrequency layer with varying inter-site delays

FRM- frequency response map

FSL- first spike latency

IC- inferior colliculus

ICC- central nucleus of the inferior colliculus

IPI- inter-pulse interval

IPI curves- lines showing how normalized responses vary with IPI when stimulating at one level for a single stimulation case

IPI-a curves- IPI curves which are averaged across levels

LFP- local field potential

Mean IPI-a curves- IPI-a curves averaged across stimulation-recording site pairs

MG- medial geniculate body

MGD- dorsal division of the medial geniculate body

MGM- medial division of the medial geniculate body

MGV- ventral division of the medial geniculate body

NF2-Neurofibromitosis Type II

Off-BF DSS- DSS applied on two ICC sites which are in different isofrequency laminae

PAF- posterior auditory field

pps- pulses per second

PSTH- Post-Stimulus Time Histogram

SSS- Single-Site Stimulation: pulse stimulation of a single site with two or more pulses with specific inter-pulse intervals

VRB- ventrorostral belt of the auditory cortex

CHAPTER 1: INTRODUCTION

ASCENDING AUDITORY PATHWAYS: THE LEMNISCAL VS. NONLEMNISCAL SYSTEM

The gross anatomy and physiology of the ascending auditory pathway has been well-defined and characterized throughout literature (Rees and Palmer 2010; Webster et al. 1992; Yost 2007). Sound travels through the air in pressure waves and is converted to mechanical motion and vibrations at the eardrum and through the middle ear via small bones called ossicles, focusing this mechanical energy into the inner ear structure, the cochlea. The cochlea, and in particular the stereocilia within its organ of Corti, convert this mechanical energy into electrical impulses to the auditory nerve, which sends information to the central auditory system. The first nucleus that receives the auditory nerve fibers is the cochlear nucleus, which is found ipsilateral to the incoming sound source. In addition to sending some projections within the ipsilateral side of the ascending auditory system, the cochlear nucleus sends projections that decussate through the trapezoid body towards the contralateral superior olivary complex, which is the first nucleus to receive bilateral information. The cochlear nucleus then sends axons through the lateral lemniscus en route to the inferior colliculus (**IC**), a nearly mandatory relay to the auditory thalamus. The auditory thalamus, the medial geniculate body (**MG**), projects the auditory cortex (**AC**), where perception is thought to occur. This simplistic and brief introduction of the ascending pathway is by no means comprehensive, for there are many

complex projection patterns to contralateral nuclei throughout the pathway. In addition, there is a vast descending projection system which provides feedback to the central ascending system (Winer 2006; 2005).

The ascending auditory pathway has traditionally been separated into two pathways, the lemniscal "core" pathway and the nonleminscal pathway. The lemniscal pathway projects from the brainstem up through the ICC, the ventral division of the medial geniculate body (**MGV**), and core auditory cortex regions (**ACC**), which includes the primary auditory cortex (**A1**) (Rouiller 1997). Neurons within the lemniscal pathway are tonotopically organized and primarily code for auditory information (Ehret and Romand 1997; Lee and Sherman 2010a; b). In contrast, neurons within the nonlemniscal pathway project to regions outside of ICC, MGV, and ACC, have poor or no tonotopic organization and code for multimodal information. In general, it is thought that the lemniscal system acts as a driver or information-bearing pathway, while the nonlemniscal system acts as a modulator that alters the principle driver streams (Lee and Sherman 2010a). Similar parallel pathways are observed throughout the somatosensory systems, and can be distinguished by both anatomical and physiological features within thalamocortical circuits. In contrast to the modulator pathways, the driver pathway inputs have thicker axons, denser arbors, and more proximal dendrites (Lee and Sherman 2009; Lee and Sherman 2011). In addition, driver pathways typically observe large EPSPs and paired-pulse depression, only responding to ionotropic glutamate receptors (Sherman and Guillery 2001). In contrast, modulator pathways have smaller, graded EPSPs and paired-pulse facilitation, activating both ionotropic and metabotropic glutamate receptors.

Differences between subnuclei of the inferior colliculus highlight the anatomical and physiological features that distinguish between the auditory lemniscal and nonlemniscal pathway. As shown in Figure 1A, the ICC is composed of flat and less-flat neurons, which are also known as disc-shaped and stellate neurons (Faye-Lund and Osen 1985; Malmierca et al. 1993; Malmierca and Hackett 2010; Morest and Oliver 1984). The fibrodendritic arbors of the flat cells are arranged parallel to ascending fibers and form laminae along the dorsoventral axis, with less flat cells found in small inter-laminar compartments (Malmierca et al. 1993). These laminae constitute the tonotopic axis as shown in Figure 1B, where dorsal laminae respond best to low frequencies and ventral laminae respond best to high frequencies (Malmierca et al. 2008; Schreiner and Langner 1997). Each frequency lamina, approximately 175 μm in cat (Schreiner and Langner 1997) and 150 μm in rat (Malmierca et al. 2008), typically constitutes a bandwidth of approximately 0.3 octaves (Malmierca et al. 2008; Schreiner and Langner 1997). The ICC is surrounded dorsal-caudally, laterally, and rostrally by the dorsal, rostral, and external nuclei of the inferior colliculus (ICD, ICR and ICX, respectively) that are part of the nonlemniscal system. The cells in these nuclei are morphologically distinct from those in the ICC and include flattened neurons as well as small, medium, and large multipolar neurons, as shown in Figure 1C. The cortices lack isofrequency laminae and do not have a clear or consistent tonotopic frequency organization (Oliver 2005). Both Golgi and Nissl staining can be used to differentiate between the subnuclei, though determining the precise border between regions remains difficult and regions that have

been determined anatomically and physiologically have been controversial (Oliver 2005; Portfors et al. 2011) .

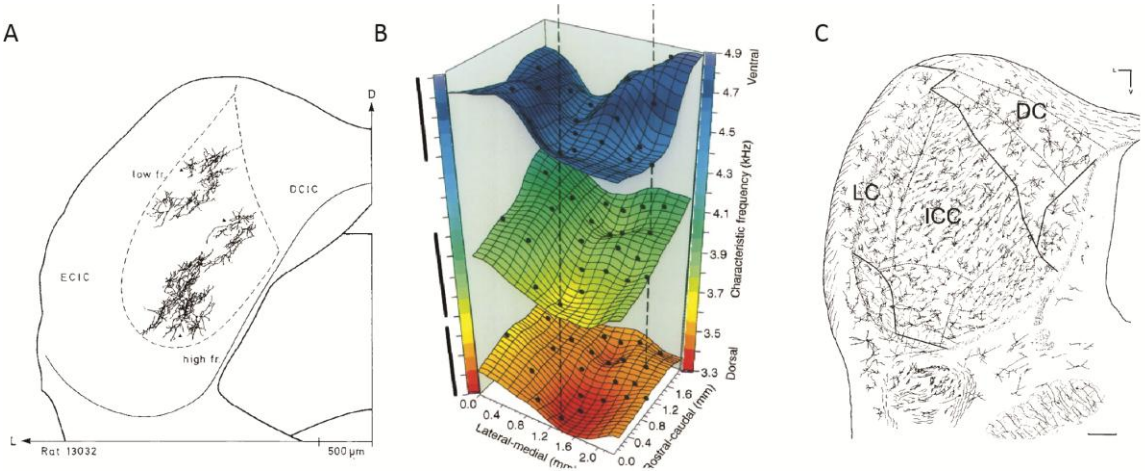

Figure 1: The ICC primarily consists of flat neurons **(A)**, whose dendritic organization forms the basis of the isofrequency laminae (**B**). The ICC is surrounded by the external (ECIC, or the lateral nucleus LC) and dorsal (DC or DCIC) nuclei of the IC. The three subnuclei have cells that are morphologically distinct, as seen with this Golgi-impregnated section (**C**). Figures reproduced with permission from (Malmierca et al. 1993), (Schreiner and Langner 1997), and (Morest and Oliver 1984). L, lateral; V, ventral; D, dorsal.

The IC's central nucleus and cortices also differ in input and output projection patterns. The ICC receives projections from the contralateral anteroventral, posteroventral, and dorsal cochlear nuclei, the ipsilateral ventral nucleus of the lateral lemniscus and medial superior olive, and bilateral dorsal nuclei of the lateral lemniscus and lateral superior olive (Brunso-Bechtold et al. 1981; Cant and Benson 2006; Loftus et al. 2004; Malmierca 2003). While the ICC receives projections mainly from auditory nuclei, the IC cortices also receive projections from the somatosensory (Aitkin et al. 1978; Aitkin et al. 1981; Zhou and Shore 2006) and visual systems (Hyde and Knudsen 2000; Knudsen 2002), and thus are important for multi-sensory integration features such

as sound localization. In addition, descending corticofugal and thalamotectal projections primarily terminate in the cortices (Malmierca and Ryugo 2011). The output of the ICC is to the MGV with projections that are tonotopically arranged, while the cortices project to nonlemniscal thalamic nuclei (Calford and Aitkin 1983; Winer and Schreiner 2005).

In addition to these anatomical and projection differences, the ICC also has different physiological responses than the cortices of the IC. In general, the ICC has lower thresholds, stronger responses, and shorter response latencies to acoustic stimuli than the surrounding cortices (Syka et al. 2000). In addition, the tuning to specific frequencies is sharper and spontaneous activity is stronger in the ICC (Aitkin et al. 1994; Syka et al. 2000). In response to tones and noise stimuli, sustained firing patterns were most often found in the ICC while onset patterns were more commonly found in the cortices (Aitkin et al. 1994; Syka et al. 2000). Finally, most of ICC neurons respond to binaural inputs though some of the cortices (e.g., ICX) primarily respond only to inputs from the contralateral ear (Aitkin et al. 1975).

The lemniscal auditory thalamus is the MGV, which is the largest division of the MG, as shown in Figure 2. MGV contains bushy tufted cells which, similar to the ICC, have a characteristic organization of their fibrodentritic arbors that construct tonotopic frequency laminae (Banks and Smith 2011; Cetas et al. 2001; Imig and Morel 1985). The non-lemniscal divisions of the MG include the dorsal (**MGD**) and medial (**MGM**) divisions, which are composed of more diverse neurons, including tufted and stellate cells, that result in greater physiological diversity (Bartlett and Smith 2002). The MGV has sharp tuning, precise tonotopy, short response latencies, and primarily single spikes and onset

responses (Calford and Aitkin 1983; Edeline 2011; Hu 1995; Winer and Schreiner 2005). In contrast, the MGD and MGM have broad tuning, weak tonotopic arrangements, and longer latencies. In addition to the vast descending corticothalamic projections, the MGV primarily receives ascending input from the ICC while the MGD and MGM's inputs include the cortices of the IC as well as non-auditory information (Calford and Aitkin 1983; Winer and Schreiner 2005). MGV neurons then project in a tonotopic organization to the ACC regions, which are also tonotopically organized, while MGM and MGD project to a greater number of non-tonotopic auditory and non-auditory cortical fields (Banks and Smith 2011; Hu 2003; Morel and Imig 1987; Winer and Schreiner 2005).

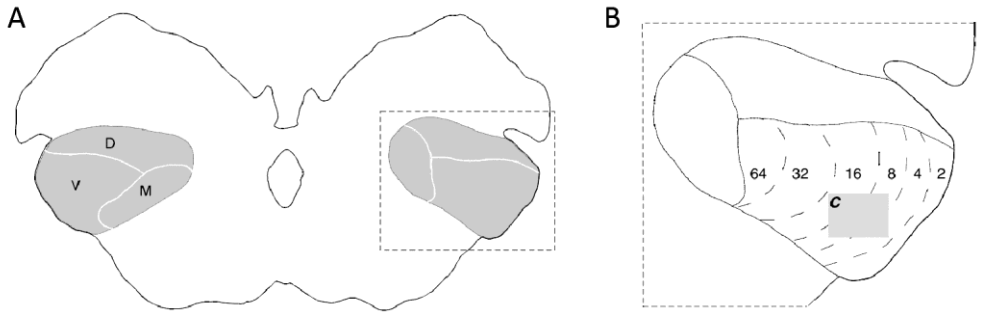

Figure 2: A, The MG consists of three major subnuclei, including the ventral (V), dorsal (D), and medial (M) divisions. **B**, The right MGV is composed of fibrodendritic laminae which correlate to tonotopic organization (C and gray box in C not relevant in this figure). Figure reproduced from (Winer and Schreiner 2005).

The auditory cortex is much more complex and diverse than the IC or MG, with the number of subdivisions greatly varying between species, from approximately five traditionally accepted regions in rats, to twelve in monkey, with different naming conventions between different animals (for example, see Figure 3A and B to compare cat and guinea pig). A common theme across species is that a core region, which includes A1

and up to two other tonotopically organized fields, is surrounded by a belt region. By definition, the core regions are lemniscal and belt regions are non-lemniscal. While A1 responds with short latencies to pure tones and noise, has narrow spectral tuning, and consists of a strong tonotopic organization, belt regions have weaker or no tonotopic organization and broad spectral tuning, typically responds with longer latencies, and sometimes responds only to noise bursts or complex stimuli (Malmierca and Hackett 2010). The tonotopic organization of ACC regions consists of an arrangement of columns with neurons that respond to similar BFs and are organized into layers with different neurons and function (Malmierca and Hackett 2010; Mitani et al. 1985; Winer and Schreiner 2010). Supragranular layers, or layer I-II, have fewer neurons and many horizontal projections that primarily project to other cortical areas. Granular layers, or layer III and IV, are the primary input layers receiving thalamocortical projections (where layer III/IV is the primary input layer in guinea pig (Huang and Winer 2000; Smith and Populin 2001), and layer IV is the primary input layer in higher species (Jones and Burton 1976; Mitani et al. 1985)). Primarily composed of pyramidal neurons, the granular layers predominantly project to supragranular layers and to the contralateral AC. Infragranular layers, or Layer V and VI, are output layers that form vast descending projections, where corticothalamic projections are present in both layers and corticotectal projections are predominantly found in layer V (Doucet et al. 2003; Mitani et al. 1985).

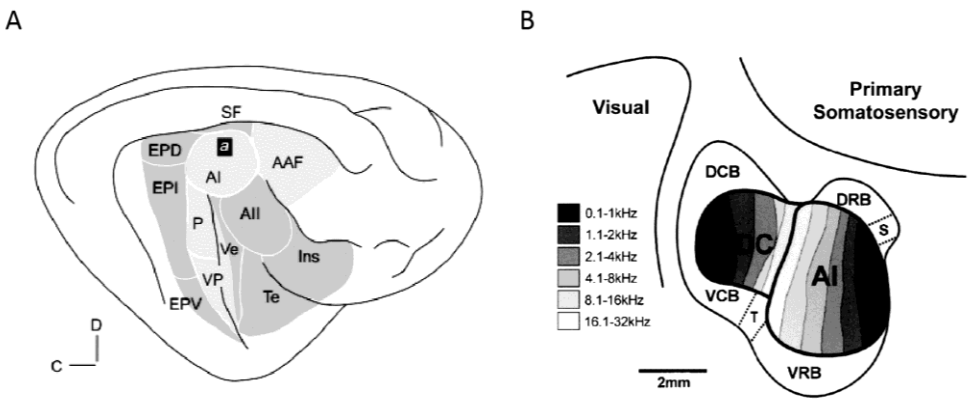

Figure 3: The auditory cortex of cat (**A**) and guinea pig (**B**) vary in the number of defined areas, but both consist of tonotopically organized lemniscal (light gray in A and shaded regions in B) and less organized belt regions (dark gray in A and white in B). Though the ventrorostral belt (VRB) here is denoted as a non-lemniscal region, it has a weak tonotopic organization and therefore can also be classified as a lemniscal region. Figures reproduced from (Read et al. 2002) and (Wallace et al. 2000).

This classical view of the central auditory system, with lemniscal and non-lemniscal parallel pathways, has served as an organizing principle for studying, modeling, and understanding sound coding within the brain. These two centers work together to interpret auditory information and integrate it with other senses for important multi-sensory tasks. As the primary channel for transmitting high fidelity auditory information, the functional properties of the lemniscal system appears to be more suitable for stimulation with auditory neuroprostheses. Therefore, different lemniscal nuclei from the brainstem up to the cortex have been considered for targets of auditory neuroprostheses.

CENTRAL AUDITORY PROSTHESES: THE AMI

Auditory prostheses have been treating hearing loss for decades with the best-performing cochlear implant (**CI**) users able to converse on the telephone (Adams et al.

2004). By stimulating along the tonotopic gradient of the auditory nerve within the cochlea, the CI is able to provide sufficient temporal and spectral cues required for speech understanding (Kral and O'Donoghue 2010; Shannon et al. 1995; Zeng 2004). However, many people are ineligible for CIs due to un-implantable cochleas or damaged auditory nerves, which often occurs in patients with neurofibromatosis type II (**NF2**). By the late 1970s, central auditory implants called auditory brainstem implants (**ABIs**) were developed to provide an alternative by implanting electrode arrays in the cochlear nucleus, which is accessible during the tumor removal surgery (Schwartz et al. 2008). However, ABI performance has been varied, with only a small fraction of patients achieving open-set speech perception. One study found that ABI patients with NF2 performed significantly poorer than patients without NF2, most likely because of damage to the cochlear nucleus by the tumor and tumor-removal surgery (Colletti and Shannon 2005). This made it necessary to consider other implantation areas with surgical accessibility, a clear neuronal organization, and no tumor-related damage (Lim et al. 2009).

To address these concerns, and as an alternative approach to the ABI, a new AMI was developed to stimulate along the tonotopic gradient of the ICC. After safety was confirmed with animal studies (Lenarz et al. 2007), an AMI clinical trial was performed with five patients (Lim et al. 2008b; Lim et al. 2007). As shown in Figure 4, the AMI consisted of a single shank electrode array with 20 contacts.

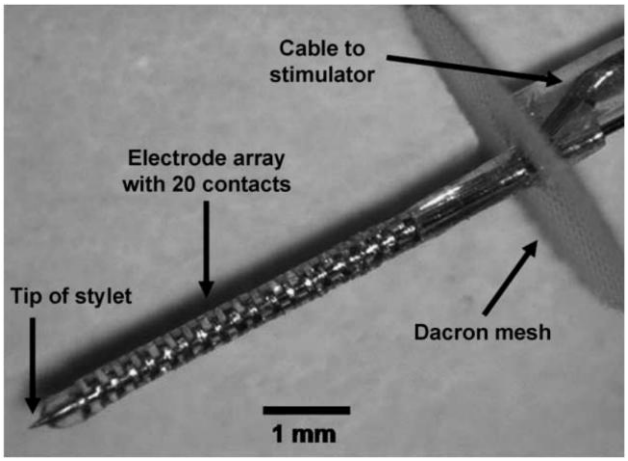

Figure 4: The AMI array consists of 20 platinum ring electrodes with a 0.4 mm diameter, 0.1 mm width, and ~0.00126 mm^2 surface area, each separated by 0.2 mm (center-to-center). The array was developed by Cochlear Ltd. Figure was reproduced from (Lenarz et al. 2006b).

For the published data on the first three patients, common results included increased environmental awareness and enhanced lip-reading abilities. Performance was strongly correlated with implantation location, as the only ICC-implanted patient achieved the highest test scores. However, even this patient did not achieve open set speech perception, which may in part be due to implanting in a sub-optimal location within the ICC. One indication of suboptimal placement is the unexpectedly high current thresholds required for perception, which were similar to those required for CI stimulation (Lim et al. 2007; Pfingst et al. 1997; Shannon 1985). Considering that AMIs directly stimulate neurons while CIs stimulate through a bony modiolar wall to activate the distant auditory neurons, AMIs should require significantly lower current levels. Animal studies suggest the high thresholds, which are likely linked to the poor perception, may be due to implanting caudally rather than rostrally in the ICC and may result in poor A1 activation (Calixto et al. 2010; Lim et al. 2007).

Rostral and caudal regions within the ICC and MGV appear to exhibit different neural coding properties even though both regions are part of the lemniscal system. In the cat, single units responding to acoustic stimuli in the rostral MGV are homogenous, sensitive to broad band stimuli and pure tones, and respond with excitatory discharge patterns, precise time-locking, and short latencies with low jitter (Rodrigues-Dagaeff et al. 1989). In contrast, caudal units are more heterogeneous and complex, with broader ranges of different response patterns. These properties may correlate with behavioral features such as thresholds, loudness discrimination, and temporal coding properties. Moreover, tonotopicity, a measure of the degree of frequency organization, linearly decreases from the rostral to caudal regions, meaning the rostral region has a stricter organization for frequency, which would be important for frequency-specific coding with an auditory implant. In addition to these functional differences, the rostral and caudal locations appear to project differentially from the brainstem to the ICC (Cant and Benson 2006) and from the ICC to MGV (Cant and Benson 2007) in anatomical gerbil studies. While there have also been segregated projections reported from these regions of the MGV to the auditory cortex (Morel and Imig 1987; Redies et al. 1989a; Rodrigues-Dagaeff et al. 1989), the specific cortical areas between these studies have been inconsistent and should be further investigated to determine if they are a result of differences in species.

Overall, the functional and anatomical differences between the rostral and caudal regions suggest that there may be at least two sub-region pathways within the lemniscal system. This is further supported by experiments showing that stimulation of the rostral

and caudal regions of the ICC elicits different responses in A1. In addition to properties such as longer latencies, larger discriminable level steps and lower magnitudes of evoked potentials (**EPs**) in A1, stimulation of the caudal ICC is known for higher activation thresholds than the rostral region in the guinea pig (Lim and Anderson 2007b; Neuheiser et al. 2010). This suggests that perhaps the high current thresholds required for the AMI user implanted in the ICC may be a direct result of being implanted in a caudal rather than a rostral region. Thus, caudal-rostral differences are directly relevant for AMI implantation since differences in temporal, level, and frequency coding properties will likely affect overall hearing performance.

In addition to the caudal-rostral functional effects, the poor performance in the AMI patient implanted in the ICC may also be due to a lack of sufficient temporal cues that require effective activation across the isofrequency layers. Although the distribution of some temporal properties such as latencies, intensity-related responsiveness, and azimuth angles within the isofrequency layers are known, response interactions among neurons within a layer to complex stimuli are not clearly understood (Ehret and Romand 1997). At least some evidence shows that temporal response properties, such as best modulation frequency and latency, can vary topographically along a direction orthogonal to the frequency axis (Langner et al. 2002; Schreiner and Langner 1988), which would predict inadequate temporal transmission with only a single-shank AMI. Supporting this prediction, AMI patients scored poorly on consonant and sentence recognition tests (Lim et al. 2007), which rely on sufficient temporal cues (Shannon et al. 1995). The temporal information may be partly limited due to the lack of temporal integration for AMI

stimulation that is generally achieved for CI or acoustic stimulation. More specifically, increasing stimulation rates above 500 pulses per second (pps) ceased to decrease perceptual thresholds, in contrast to CI and normal hearing subjects whose thresholds continue to decrease (or loudness increase) with increasing rates, seen in Figure 5 (Kreft et al. 2004; Lim et al. 2008b). Moreover, McKay et al. (2013) modeled the perceptual effects of temporal parameters and found that AMI stimulation had a significantly wider integration window than CI stimulation. In other words, this model indicated that AMI users had decreased temporal resolution compared to CI users.

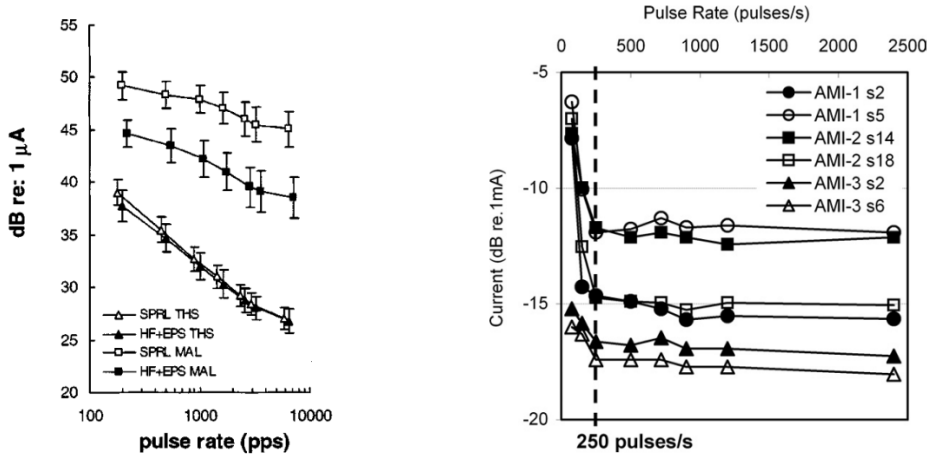

Figure 5: The effect of pulse rate on perceptual thresholds in CI (**A**) and AMI (**B**) users. Increasing the pulse rate continuously decreases perceptual thresholds (THS) and maximum allowable loudness (MAL) in CI users, but AMI users do not exhibit a decrease in thresholds above about 250-500 pulses/s. In (**A**), THS and MAL refer to different detection techniques and SPRL and HF+EPS to different electrode arrays, while in (**B**) numbers refer to different subjects. Figure (**A**) reproduced from (Kreft et al. 2004) and (**B**) from (Lim et al. 2008b).

The unexpected perceptual threshold effect with pulse rate in Figure 2 was further investigated in guinea pigs in which A1 local field potentials (**LFPs**) were measured in

response to ICC stimulation. When one site was stimulated with two pulses with varying inter-pulse delays (i.e., different pulse rates), referred to here as single-site stimulation (SSS), the total area of the LFP began to decrease for inter-pulse intervals shorter than 2 ms (i.e., >500 pps; Figure 3) (Calixto et al. 2012). This decrease could be attributed to some refractory effects since the ratio of LFP area to two pulses approached the area to a single pulse (equal to 0.5) for shorter delays, indicating that the second pulse did not contribute to the LFP already elicited by the first pulse. In addition, these refracorty-like effects could also be due to inhibitory tectothalamic projections, which may result in suppression of responses (Calixto et al. 2012)

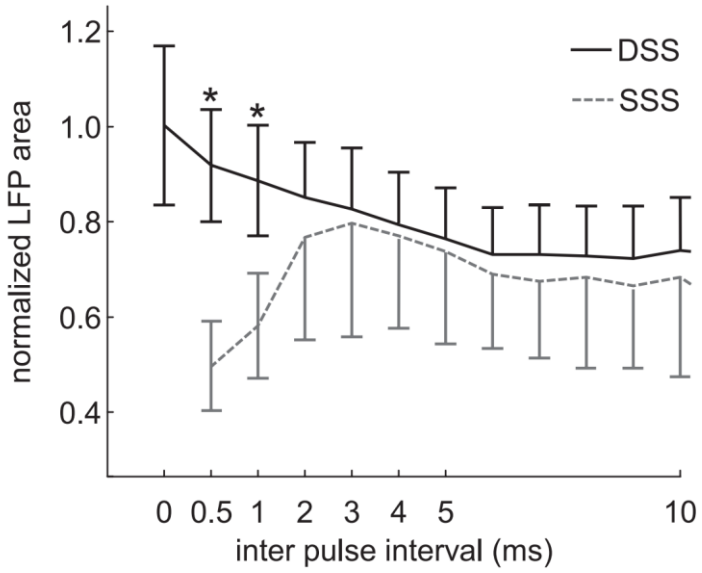

Figure 6: Normalized areas for all animals, with SSS (dashed grey) normalized by two times the first LFP and DSS (black) normalized to the sum of LFPs for the individual sites. Values above one reflect enhancement. A refractory effect is seen with SSS responses before 2ms, but not with MSS. Figure reproduced from (Calixto et al. 2012).

However, stimulating with two sites across the isofrequency layer via dual-site stimulation (**DSS**) overcomes this refractory effect. The normalized activity shows an

increasing LFP with shorter inter-pulse delays (or higher rates). The LFPs could be considered enhanced because they exceeded the sum of the individual response for each site (>1). Thus, it appears stimulating several sites within a layer may be necessary for the cortex to receive adequate temporal information because DSS not only overcomes refractory effects but also results in enhanced cortical activity within an approximately 5 ms window. While this result was unexpected, it is not necessarily unintuitive. Since the ICC consists of two-dimensional layers, which are known to have different temporal coding features (Langner et al. 2002; Schreiner and Langner 1988), it is reasonable to assume that stimulation across these layers would be necessary to provide a full temporal code. In addition, in Figure 6 both DSS and SSS appear to have similar overall shapes above 2 ms, which suggests that the enhancement seen in DSS is not a result of artificial normalization procedures but rather would also be expected with SSS if the neurons did not enter a refractory state. Moreover, the DSS enhancement may be the physiological correlate to the well-known psychophysical phenomenon termed temporal integration (i.e., related to a window of roughly 5 ms), which results in a decrease in perceptual thresholds in normal hearing and CI subjects when presented with a pair of stimuli with decreasing inter-stimulus intervals (McKay and McDermott 1998; Viemeister and Wakefield 1991).

These results suggest that the benefits of the AMI in the first clinical trial are likely limited due to issues with sub-optimal implantation location and stimulation strategy. Therefore, before future clinical trials can proceed, there must be an increased understanding of temporal information coding within the ICC to improve stimulation

strategies. Since DSS appears to be an important factor in improving temporal coding, the mechanism of how it affects cortical activity must also be further investigated. Moreover, the location effects within the ICC must be assessed for both of these studies in order to determine an optimal implantation location. As detailed below, the work presented in this manuscript attempts to address these questions.

GOAL OF THIS THESIS

The lack of thorough understanding of the lemniscal system has been a limiting factor in developing and improving central auditory neuroprostheses, particularly in the midbrain. Since the coding patterns of sound stimuli along the isofrequency laminae of the ICC are poorly understood, it is difficult to develop improved stimulation strategies for activating neurons across the ICC with the AMI. Moreover, different responses across the lemniscal system would be expected, since previous anatomical studies have found differential and segregated projection patterns existing from the midbrain, through the thalamus, and to the cortex. However, physiological studies only found different response properties matching the organization of these segregated anatomical projection patterns in the thalamus and cortex. The study in Chapter 2 investigates this missing link, and probes whether physiological responses along the isofrequency laminae of the ICC differ in functional properties in regions consistent with those segregated ascending patterns. In order to address this, we presented pure tones and investigated different response properties for neurons along a given ICC lamina. We analyzed both LFPs and spiking parameters to analyze synaptic inputs as well as neural outputs. With this study we found clusters of activity, where the caudal-medial and rostral-lateral regions of the ICC

showed different responses to sound. The rostral-lateral recording locations respond with greater spatial and temporal synchrony than caudal-medial locations. Thus, there are separate regions along the ICC lamina with different physiological properties, which are consistent with the segregated ICC regions that have shown to receive as well as send differential projection patterns. In addition to confirming that dual lemniscal projections exist at the level of the midbrain, the results presented in Chapter 2 provide insight as to optimal target locations for neuroprostheses within the lemniscal system.

The next goal of this manuscript was to better identify stimulation strategies and locations in order to improve the implementation of the AMI. The Calixto et al. (2012) study demonstrated that that three-dimensional stimulation may be required to sufficiently code for temporal information through DSS to improve hearing performance. The results in Chapter 3A extended this study by using smaller electrode sites (413 μm^2 versus 126,000 μm^2), which allowed for more local stimulation of the ICC to minimize the current spread and antidromic activation effects that limited their analysis of spiking activity. With these smaller stimulation sites, both LFP and spiking activity could be recorded throughout cortical layers to determine whether further processing occurs in the cortex after the main thalamocortical input (i.e., LFPs into layer III/IV). First, this study confirmed that the refractory effect was observed when stimulating with SSS, despite the fact that current spread in the ICC was much smaller. Secondly, DSS resulted in enhanced cortical activity at short IPIs for both LFPs and spiking for all cortical layers, and the greatest amount of enhancement was found in supragranular layers. This enhancement was only observed when co-activating neurons along an ICC isofrequency

lamina and not across different isofrequency laminae. Thus, this study determined that there is a mechanism which integrates activity across several locations from the ICC isofrequency lamina that is further enhanced in supragranular cortical layers.

From the acoustic response characterizations in Chapter 2, it was known that locations along the ICC isofrequency lamina have different neural properties. Therefore, in Chapter 3B we investigated location trends of DSS, both in the ICC and in A1. Cortical enhancement, which was not dependent on recording A1 locations, was greatest when stimulating rostral-lateral rather than caudal-medial ICC regions. These locations were compared to other studies, including the locations in Chapter 2, and we determined that they correspond to those that differ in acoustic response properties. The differences in cortical responses to DSS further confirm the presence of dual sub-projection pathways throughout the lemniscal system. Moreover, the results from Chapter 3A and B suggest that the next AMI clinical trials need to likely co-activate neurons across an ICC lamina and target neurons within the rostral-lateral region. Thus, the results presented in this manuscript will prove vital in understanding the lemniscal auditory pathway and improving clinical outcomes for central auditory neuroprostheses. Chapter 4 provides future research and clinical directions for the presented thesis project.

In addition to the studies in Chapters 2 and 3, we also performed experiments investigating the descending projection patterns from different primary auditory cortical regions to the ICC. The initial motivation of this study was to assess if there were any differences in projection patterns to the rostral-lateral versus caudal-medial ICC, which would demonstrate the existence of segregated lemniscal projection patterns not only

within the ascending system but also the descending system. Interestingly, we observed differences in cortical descending projection patterns to the ICC with some patterns consistent with the dual lemniscal pathways. Since this study is outside of the scope of the main goals of the thesis project, it is included as an Appendix chapter at the end of the manuscript.

CHAPTER 2: ACOUSTIC-DRIVEN RESPONSES VARY ACROSS THE ICC LAMINA

The central auditory system has traditionally been divided into the lemniscal and the nonlemniscal pathway through the midbrain, thalamus, and cortex. This view of the auditory system has served as an organizing principle for studying, modeling, and understanding sound coding within the brain. However, there has been increasing evidence that the lemniscal pathway should be further divided into two sub-pathways that code for sound in different ways. Using multi-site array recordings in response to pure tone stimuli and three-dimensional brain reconstruction techniques, we investigated this dual lemniscal organization within the ICC of ketamine-anesthetized guinea pigs. In contrast to caudal-medial ICC regions, neurons within rostral-lateral ICC regions responded with shorter first-spike latencies with less spiking jitter, shorter durations of spiking responses, more proportion of spikes occurring near the onset of the stimulus, and larger local field potential peaks with shorter latencies. Further analysis of these response properties revealed two distinct clusters of values corresponding to the caudal-medial region and the rostral-lateral region along the isofrequency laminae of the ICC. We also found that acoustic thresholds were generally lower in rostral compared to caudal locations. Thus, we discovered substantial differences in coding properties between two regions of the midbrain that were consistent with the dual anatomical pathways of the lemniscal system identified in previous studies. Together, these findings indicate that the

classical view of the lemniscal pathway needs to be redefined, which will motivate new and potentially more refined studies and models of the auditory system.

INTRODUCTION

The ascending auditory pathway has traditionally been separated into two pathways, the lemniscal "core" pathway and the nonleminscal pathway (Lee and Sherman 2010a; b; Rauschecker and Romanski 2011; Rouiller 1997). The lemniscal pathway projects from the brainstem up through the ICC, the MGV, and ACC. Neurons within the lemniscal pathway are tonotopically organized and primarily code for auditory information. In contrast, neurons within the nonlemniscal pathway project to regions outside of ICC, MGV, and ACC, have poor or no tonotopic organization, code for multimodal information, and are thought to modulate lemniscal responses (Ehret and Romand 1997; Lee and Sherman 2010a; Malmierca and Hackett 2010; Oliver 2005; Winer and Schreiner 2010). This classical view of the central auditory system has served as an organizing principle for studying, modeling, and understanding sound coding within the brain.

While the lemniscal pathway has traditionally been treated as a single pathway, differences in its projection patterns through the central auditory system suggest that at least two sub-projection pathways exist. In the gerbil, two subregions have been identified within the ICC: a rostral-lateral region and a caudal-medial region that receive different brainstem projections and also project to the rostral region and the caudal region, respectively, of the MGV along its isofrequency dimension (Cant and Benson 2007; 2006). In addition, studies in the cat and rat have demonstrated that the rostral MGV projects throughout the auditory cortex, including A1, whereas the caudal MGV

projects to regions predominantly outside of A1 (Morel and Imig 1987; Polley et al. 2007; Rodrigues-Dagaeff et al. 1989; Storace et al. 2012; Storace et al. 2010).

The dual lemniscal projections from the ICC up to ACC are further supported by electrophysiological studies suggesting that the "rostral" pathway exhibits stronger and more temporally and spectrally precise activation than the "caudal" pathway. One study in guinea pig showed that electrical stimulation of the rostral-lateral ICC compared to the caudal-medial ICC along its isofrequency laminae required lower levels for activating A1 and elicited stronger spiking and LFP magnitudes, shorter latencies, less spiking jitter, and smaller discriminable level steps (Lim and Anderson 2007b). In the cat, neurons responding to acoustic stimuli in rostral MGV compared to caudal MGV exhibited stronger excitatory activation, more precise time-locking to click trains, shorter latencies, less spiking jitter, and stricter tonotopic organization with narrower tuning curves (Rodrigues-Dagaeff et al. 1989). Consistent with these results, the caudal MGV projects mainly to regions outside of A1 that can exhibit responses with longer latencies, greater spiking jitter, less excitatory activity, and less precise tonotopic organization compared to A1, which receives its inputs primarily from the rostral MGV (Morel and Imig 1987; Polley et al. 2007; Rodrigues-Dagaeff et al. 1989; Schreiner et al. 2011; Storace et al. 2012; Storace et al. 2010).

Remarkably, this dual lemniscal organization from the midbrain to the cortex has been observed across multiple species. However, the missing link in confirming this hypothesis is that a study has not yet shown a clear functional division of acoustic responses within the ICC to match the segregation identified from the ICC up to the

ACC. In terms of similar features investigated in those previous studies above, shorter latencies tend to be observed in more lateral versus medial regions along an ICC lamina in chinchilla and cat (Langner et al. 2002; Schreiner and Langner 1988) and ventral-lateral versus dorsal-medial in the medial division of the ICC in bat (Hattori and Suga 1997; Portfors and Wenstrup 2001). In addition, faster following responses (i.e., best modulation frequencies) tend to be observed in more lateral versus medial regions along an ICC lamina in chinchilla, cat, and guinea fowl (Langner 1992; Langner et al. 2002; Schreiner and Langner 1988), though the topographic pattern for best modulation frequencies can be complex (e.g., concentric and varying across frequency regions) and even level dependent (Krishna and Semple 2000; Schreiner and Langner 1988). Lower thresholds and/or narrower tuning have also been observed in more central versus outer regions along an ICC lamina in mouse and cat (Hage and Ehret 2003; Schreiner and Langner 1988; Stiebler 1986). Thus, key discrepancies arise between the spatial coding patterns of acoustic responses and the expected caudal-medial versus rostral-lateral organization of the dual lemniscal pathways. Species differences alone cannot explain these discrepancies, as this dual organization has been demonstrated across multiple species. It is possible that some acoustic properties may not exhibit the dual organization until the MGV. However, since anatomical segregation has shown to exist at the level of the ICC, there should be differences in at least some acoustic coding properties between the rostral-lateral versus caudal-medial ICC.

In this study, we performed a detailed mapping of acoustic-driven responses across the ICC. We presented short tone pips, in addition to the longer pure tone stimuli used in

previous studies, to assess whether spatial differences in coding properties were masked by analyzing longer stimulus responses. Unlike the previous studies described above, which did not delineate the lamina borders in three dimensions, we used multi-site arrays as well as histological and computational reconstruction techniques to ensure that we fully sampled locations throughout and up to the borders of a given isofrequency lamina. We then analyzed a wide range of response features based on LFPs and spikes that revealed obvious and substantial differences in multiple response properties between the caudal-medial versus rostral-lateral ICC. These results demonstrate that there are at least two sub-projection pathways through the ICC, providing further evidence for redefining the auditory lemniscal pathway.

METHODS

Neural responses were recorded in the ICC of ketamine-anesthetized guinea pigs using a four shank, 32-site array and in response to 10 or 20 kHz pure tone stimuli. Basic surgical procedures and methods for neural recording and acoustic stimulation were similar to those presented in previous work (Lim and Anderson 2007a; 2006; Straka et al. 2013). The array was inserted into multiple locations within each experiment and across a total of 12 male and female guinea pigs (391 ± 57 g). We compared the responses to short (0.5 or 1 ms) and long (50 ms) pure tone stimuli to assess whether spatial differences in coding properties along an ICC lamina were masked by analyzing long stimulus responses in the previous studies described in the Introduction. We used histological and computational reconstruction techniques to ensure that we fully sampled locations throughout and up to the borders of a given isofrequency lamina. We then analyzed a

wide range of response features based on LFPs and spikes, and mapped how these responses changed with location along an ICC lamina.

SURGERY

Basic surgical procedures and methods for neural recording and acoustic stimulation were similar to those presented in previous (Lim and Anderson 2007a; 2006; Straka et al. 2013). Ketamine-anesthetized guinea pigs were used in accordance with policies of the University of Minnesota's Institutional Animal Care and Use Committee. Experiments were performed on 12 male and female Hartley guinea pigs (391 ± 57 g, Elm Hill Breeding Labs, Chelmsford, MA). Animals were initially anesthetized with an intramuscular injection of ketamine (40 mg/kg) and xylazine (10 mg/kg) and were given periodic supplements to maintain an areflexive state. Atropine sulfate (0.05 mg/kg) was periodically administered via an intramuscular injection to reduce bronchial secretion. A warm water heating blanket monitored by a rectal temperature probe was used to maintain the body temperature at 38 ± 0.5 °C. The heart rate and blood oxygen level were also monitored.

After fixing the animal into a stereotaxic frame (David Kopf Instruments, Tujunga, CA), we exposed the right side of the cortex from the caudal end of the occipital lobe to the caudal end of the temporal lobe. The dura was removed and micromanipulators were used to insert a silicon-substrate, 32-site electrode array (NeuroNexus Technologies, Ann Arbor, MI) into the ICC. The array consisted of four 8-mm-long shanks separated by 500 μm. Sites were linearly spaced at 100 μm along the shank (8 sites per shank) and each had an area of about 700 μm^2. The array was placed at a 45° angle to the sagittal plane

through the visual cortex into the inferior colliculus in order to be aligned along the tonotopic axis of the ICC (Malmierca et al. 1995; Snyder et al. 2004). Array placements were confirmed with acoustic-driven responses (Lim and Anderson 2007b; Snyder et al. 2004), and the exposed brain was covered with agarose gel.

RECORDING SETUP

All experiments were performed in an acoustically and electrically-shielded chamber and controlled by a computer interfaced with TDT System 3 hardware (Tucker-Davis Technology, Alachua, FL) using custom software written in MATLAB (MathWorks, Natick, MA). Sound was presented via a speaker coupled to the left ear through a hollow ear bar. The speaker-ear bar system was calibrated using a 0.25-in. condenser microphone (ACO Pacific, Belmont, CA) connected to the ear bar via a short plastic tube representing the ear canal.

All neural signals were passed through analog DC-blocking and anti-aliasing filters from 1.6 Hz to 7.5 kHz. The sampling frequency used for acoustic stimulation was 195 kHz and for neural recording was 24 kHz. The recording ground needle was positioned directly in the brain in the parietal lobe.

PLACEMENT OF ARRAY

To guide the array placement, various levels of pure tones and broadband noise (50 ms in duration with 5 ms and 0.5 ms rise-fall ramp times, respectively) were presented in the left ear to elicit acoustic-driven activity in the contralateral ICC. Post-stimulus time histograms (**PSTHs**) and frequency response maps (**FRMs**) were plotted online to confirm the array's position along the tonotopic axis of the ICC. All FRMs and responses

to pure tones were analyzed offline for greater accuracy. Details on these analysis methods and example plots for similar types of arrays are presented in previous publications (Lenarz et al. 2006; Lim and Anderson 2006). Briefly, we bandpass filtered the neural signals (300-3000 Hz) on each site and detected spikes that exceeded a threshold of three standard deviations above the background activity. To create FRMs, four trials were presented for each pure tone (1-40 kHz, 8 steps/octave) and level (0-70 dB, 10 dB steps) stimulus in a randomized sequence. The best frequency (**BF**) was taken as the centroid of frequencies at 10 dB above the visually-determined threshold. As shown in Fig. 1A, FRMs for each site were found to determine the frequency tuning properties for each neural population, and array placement in ICC was confirmed when shallow to deep sites along the shank systematically responded with low to high BFs, respectively. Across an ICC lamina, no clear spatial organization of tuning widths was found (see *Discussion: Comparison to previous studies* for further details).

ACOUSTIC STIMULI

Two durations of pure tones at 10 or 20 kHz were each presented 20 times at varying levels in 2 dB increments. In 12 animals, we presented short tones, which were 5 periods of a stimulus (i.e., 0.5 or 1 ms for 10 and 20 kHz, respectively) with a 2.5 period $\cos^2$ up- and down-ramps. In four of these animals, we also presented 50 ms long tones, with 5 ms $\cos^2$ up- and down-ramps, which was chosen to compare the results of our short tones to those of long tones presented in literature. Both the 10 and 20 kHz stimuli were randomly presented across varying levels and stimuli durations, at a rate of 2/s. These stimuli were presented at levels of up to 80 dB SPL, though this upper limit could be lower for

different placements in which we already observed strong or saturating activity at lower levels. For each shank in the ICC, we analyzed the site that responded with the closest BF to the stimuli presented. For the 10 kHz stimuli, the average BF was 10 ± 1 kHz (mean ± STDV) for short tones (n = 119 sites) and long tones (n = 54). For the 20 kHz, the average BF was 19 ± 1 kHz for short tones (n = 99) and long tones (n = 52). An ICC isofrequency lamina has a bandwidth of approximately 0.28 octaves in cat (Schreiner and Langner 1997) and 0.29 octaves in rat (Malmierca et al. 2008). Although the average BF across ICC sites for the 20 kHz stimuli was slightly lower at 19 kHz, this was still within one critical bandwidth, and thus was still considered as the 20 kHz lamina. For all of the stimuli, our bandwidth of 0.15 octaves STDV for 10 kHz and 0.11 octaves STDV for 20 kHz were much smaller than the expected bandwidths of each isofrequency lamina (i.e., 0.28 or 0.29 octaves), and supports that the BF-matched sites were within the same 10 or 20 kHz lamina.

HISTOLOGY AND MIDBRAIN RECONSTRUCTIONS

Prior to placement, the array was dipped in a red stain (Di-I: 1, 1-dioctadecyl-3,3,3',3'-tetramethylindocarbocyanine perchlorate, Sigma-Aldrich, St. Louis, MO) to later identify the array locations across the ICC during histological analysis. Detailed description of the histological procedure, midbrain reconstruction, normalization, and approximation of frequency lamina is provided in a previous publication (Markovitz et al. 2012). Briefly, the midbrain was fixed with 3.7% paraformaldehyde and cryosectioned into sagittal sections at 60 µm using a sliding microtome (Leica, Buffalo Grove, IL). Images of each slice were taken using a Leica MZ FLIII fluorescence stereomicroscope

(Leica, Buffalo Grove, IL), Leica DFC412 C peltier cooled CCD camera, and Image-Pro software (MediaCybernetics, Bethesda, MD). A single reflection white light image using a variable intensity fiber optic light source (Fiber-Lit-PL800, Dolan-Jenner Industries, Boxborough, MA) was taken to determine the outline of each slice. Fluorescence images were later superimposed on the white light images for visualization of the reference and array shank points stained with Di-I. The brain was then reconstructed in three dimensions using Rhinoceros (Seattle, WA), and the positions of the arrays were estimated by creating best fit lines through the points on individual slices.

The reconstructions for each brain were then normalized to one standard brain using a reference needle point at the intersection of the superior colliculus, thalamus, and lateral extension from the IC, as well as the curvature of the IC. These anatomical features have shown to be reliable and consistent for normalizing brains across animals in previous studies from our lab (Markovitz et al. 2012; Markovitz et al. 2013). The laminae were approximated by creating a plane orthogonal to the average insertion angle of all best fit lines of the array placements. To determine the depth of each lamina, we calculated the distance from the surface of the IC, where neurons do not respond to broad-band noise, to locations where neurons respond with specific BFs from previously published data (Markovitz et al. 2012). This distance was multiplied by a scaling factor to account for tissue changes due to the histological process.

Though the true frequency laminae are curved throughout the ICC (Malmierca et al. 2008; Malmierca et al. 1995), the approximation of the lamina as a flat plane was necessary for the analysis of how responses vary across each lamina. Thus, the locations

along a lamina are a projection of points onto this plane. However, since the electrode shanks are approximately parallel to each other, the positions of the points maintain their relative location to each other along an ICC lamina, which is sufficient to determine differences in coding properties between the caudal-medial versus rostral-lateral regions.

In order to record from both the 10 and 20 kHz BF-matched neurons for each placement, the depth of the array was adjusted for each stimulus. For each depth, FRMs were acquired and placements were classified as inside, on the border, or outside the ICC, as shown in Figure 7A. Placement in the ICC was defined by observing FRMs that exhibited an orderly shift from low to high BFs for superficial to deeper sites, respectively, along a shank (Lim and Anderson 2006; Snyder et al. 2004). Shanks were labeled 'border' if the FRMs showed broad tuning with orderly shifts or if a neighboring shank (which was simultaneously recorded) was outside the ICC. In addition, shanks were designated as a border position if the sites along the shank showed tonotopic shifts for only four to six consecutive sites, one of which being the BF-matched site to the stimulus. Shanks were determined to be outside the ICC if the tonotopic shift of increasing BFs with deeper sites was not present. The reconstructions of each array placement within the normalized brain, as well as the 10 and 20 kHz laminae, can be seen in Figure 7B. For the shanks which were inside or on the border of the ICC (Figure 7C), sites with similar BFs to the stimulus were analyzed for the different LFP and spiking properties. Though large vasculature on the surface of the visual cortex impeded our ability to insert the arrays more medially in Figure 7C, the FRMs indicated that our most medial sites were located at the border of the ICC.

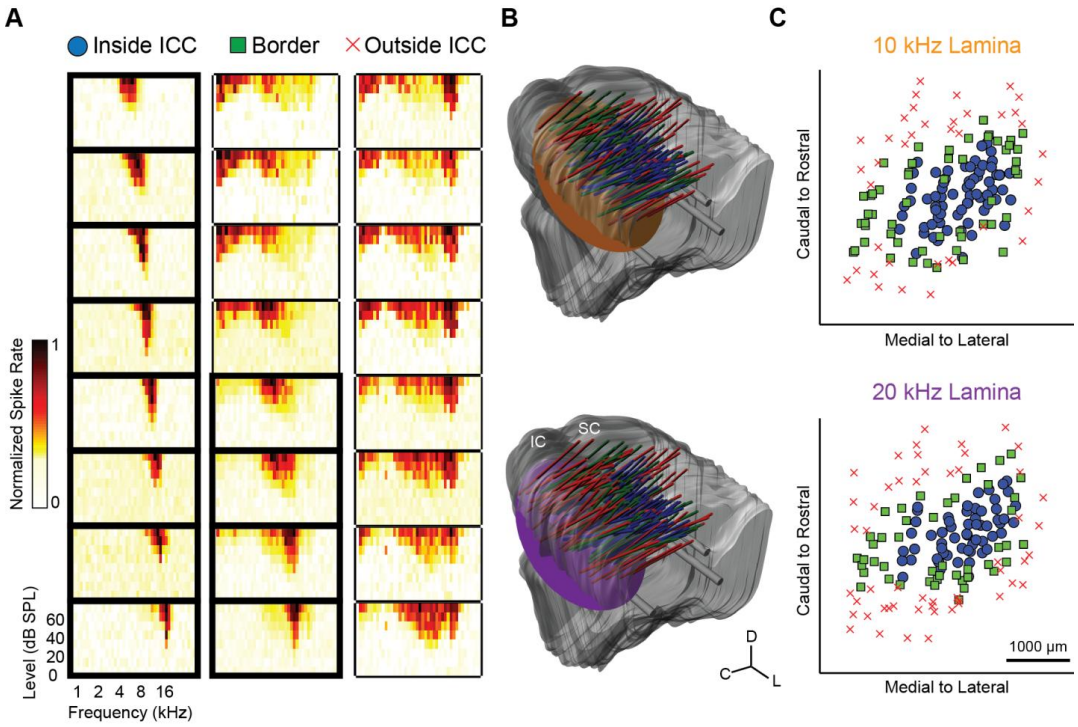

Figure 7: Histological Reconstructions and Physiological Responses were used to Determine ICC Recording Locations and Delineate Borders. **A**, Each placement was determined to be inside the ICC, on the border, or outside of the ICC based on FRMs of a single array shank, which had eight sites spanning different frequency layers. Placements were considered inside the ICC when shallow to deep sites along the shank systematically showed low to high BFs, respectively. Placements were considered to be on the border of the ICC if there was only a partial BF shift across the shank, as shown in the figure, or if a neighboring shank within the same array placement was outside the ICC. Placements which did not show any systematic BF shift were considered outside of the ICC. Bolded FRMs were sites considered inside the ICC and, of these sites, only those with a BF of 10 or 20 kHz were further analyzed. **B**, The midbrains and array placements were reconstructed in three dimensions and normalized onto a single brain (see *Materials and Methods: Histology and midbrain reconstructions* for details). The 10 and 20 kHz isofrequency laminae (orange and purple planes, respectively) were approximated by planes at depths which correspond to neurons with those respective BFs. C, caudal; D, dorsal; L, lateral; IC, inferior colliculus; SC, superior colliculus. **C**, The location of each recording site was determined across the isofrequency laminae. For symbol definition, see A.

DATA ANALYSIS

Local Field Potential Activity

LFPs were obtained by averaging (across 20 trials) the neural signals recorded on one site. LFP threshold was determined by finding a response that was three standard deviations above the background activity, which was taken from the 40 ms window preceding the acoustic stimulus of pre-averaged data. The time of the averaged LFP peak (i.e., for the minimum point of the negative peak) was calculated at the lowest level which elicited a LFP peak at threshold. The magnitude of the negative averaged LFP peak, which was subtracted from the baseline, was determined at a level 4 dB above the threshold for each site. We found these criteria to be the minimum stimulation levels which were not strongly influenced by noise. The most caudal-medial locations of the ICC usually did not exhibit activity that surpassed these criteria even up to our maximum level of 80 dB SPL. Despite this limitation, similar trends in response properties were still observed across ICC locations.

Spiking Activity

Spikes were detected offline using the same online method described above. Then the window length of the PSTH was visually assessed by estimating the start and end times. A signal detection theory (**SDT**) paradigm was used to calculate d', which describes the separation between the driven and spontaneous activity distributions in the units of the standard deviation of the spontaneous activity distribution obtained for the 40 ms window preceding the acoustic stimulus (Britten et al. 1992; Green and Swets 1966). All spiking parameters, including PSTH duration, were calculated at the lowest level

which elicited a spiking response of d'=1 and d'=3, which we refer to as threshold and suprathreshold, respectively, throughout this paper.

During our analysis, it was evident that PSTHs had different shapes along with different durations, especially for long tone stimuli. In order to quantify these shapes, we created a parameter called halftime. The halftime is the time required for half of the total spikes within the PSTH to occur. Therefore, a short halftime is indicative of the majority of the spikes occurring at the beginning of the PSTH (i.e., with a predominant onset shape), while a long halftime is indicative of the majority of spikes occurring later in the PSTH (i.e., with a predominant sustained shape).

The first spike latency (**FSL**) and FSL jitter were calculated by computing the mean and STDV, respectively, of the first spike latencies across all 20 trials. The minimum latency for a given trial was at least 4 ms after the onset of the acoustic tone, which was the shortest latency previously reported for the ICC (Schreiner and Langner 1988; Syka et al. 2000). If the first spike for a given trial did not occur by the 'lock-out' time, which was the end of the PSTH window, it was counted as a 'miss' and that trial was not included in the analysis.

Steepest Gradient Axis

Response properties were fit to the ICC locations using two-dimensional, linear multiple regression analysis, in which a site's location across the lamina was a predictor of the response property. The model determined the slope parameter, which we call the steepest gradient axis (i.e., the vector of greatest increase) for each response parameter.

Thresholds

Within a single placement of the four shank array, the thresholds of BF-matched sites on the most rostral shank to the most caudal shank in the ICC were compared. Comparisons were only made for placements with at least two shanks inside the ICC. At least one of the sites had to reach threshold activity; if the other site did not reach threshold, threshold was estimated by adding 2 dB to the highest level presented for that site. The highest stimulus level used for each placement was varied within experiments in order to accommodate the rising thresholds that occurred with each placement, and allowed us to ensure that activation of most ICC neurons was sufficient for analysis. This estimated threshold did not affect our findings because it was a more conservative estimate of threshold for our analysis (i.e., the threshold for such a site would be equal to or even higher than what we estimated). Spiking thresholds were determined at threshold and suprathreshold levels, which were the lowest levels which elicited a spiking response of d'=1 and d'=3, respectively. LFP thresholds were determined at the level that elicited a response three standard deviations above the background activity. The difference between the caudal shank threshold to rostral shank threshold was determined for each placement, and this difference was determined to be positive or negative. Significance across all placements was determined using the sign test, which uses the binomial test to assess the null hypothesis that there are equal numbers of positive and negative differences.

RESULTS

CASE EXAMPLE OF RESPONSES

As evidenced by both LFPs and PSTHs, evoked responses to pure tones varied

systematically across an isofrequency lamina of the ICC. Figure 8 shows a case example, where an electrode array was placed several times within a single animal and neural activity in response to short and long 10 kHz tones at 70 dB SPL were recorded on sites within the 10 kHz lamina.

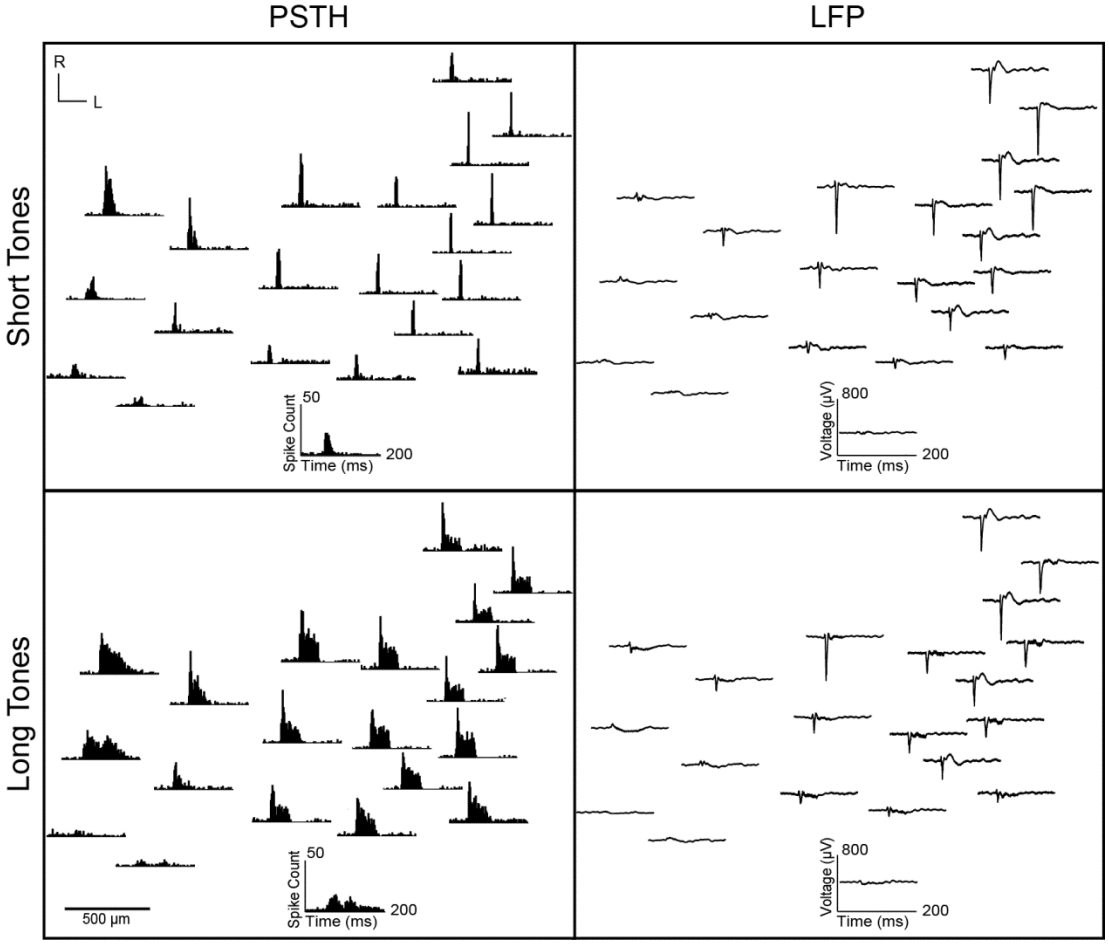

Figure 8: After the placement of each site was determined by histological reconstructions, the PSTH and LFP responses to 10 kHz short and long tone stimuli at 70 dB SPL were plotted across an ICC lamina (each box). All sites were recorded in a single animal. The PSTHs of sites in the rostral-lateral locations had pronounced onset spiking which grew wider in caudal-medial regions in response to short tones. In response to long tones, most sites responded with sustained spiking, but the onset was more pronounced in rostral-lateral regions while the sustained activity was more pronounced in the caudal-medial regions. In

addition, sites in rostral-lateral regions responded with larger LFPs to both stimuli, while caudal-medial regions had weak LFPs. R, rostral; L, lateral.

In response to the short tone stimuli, PSTHs in the rostral-lateral region had a sharp onset response that grew wider caudal-medially. In response to the long tone stimuli, PSTHs throughout a lamina showed sustained activity. However, in the rostral-lateral region, the amount of spiking in the onset portion is much larger than the sustained portion. In contrast, more caudal-medial locations exhibit more complex and/or longer lasting responses. For both short and long tone stimuli, LFP peaks were large in the rostral-lateral locations and grew weaker in more caudal-medial locations. In the most caudal-medial region, LFPs were small and never exceeded threshold above background activity regardless of the stimulus level. Despite the weak LFPs, these caudal-medial locations still exhibited strong spiking responses, and thus the inputs must not have sufficient temporal and spatial synchrony to elicit larger LFPs.

Response Parameter Maps across the ICC Lamina

The consistent trends observed in response types encouraged us to further investigate how specific properties of the responses varied across the ICC lamina. In this analysis, neural responses at a similar activation level were analyzed for each location trend. For spiking, this was accomplished using SDT to determine levels which elicited threshold and suprathreshold responses at d' levels of 1 and 3, respectively (see *Materials and Methods: Data analysis* for details). Several spiking parameters were analyzed, including PSTH duration, halftime, FSL, and the FSL jitter. Since we observed different PSTH shapes, we also analyzed halftime, which is the amount of time for half of the total spikes

to occur. Halftime is indicative of the PSTH shape since longer halftimes occur with stronger sustained spiking while shorter halftimes occur with stronger onset spiking. The maps of how spiking parameters varied across the ICC lamina in response to 10 and 20 kHz short tones can be seen in Figure 9. The values decreased from large PSTH durations, halftimes, FSLs, and FSL jitters caudal-medially to smaller values rostral-laterally for both threshold and suprathreshold levels. This trend was also similar for 10 and 20 kHz long tone responses, as seen in Figure 10.

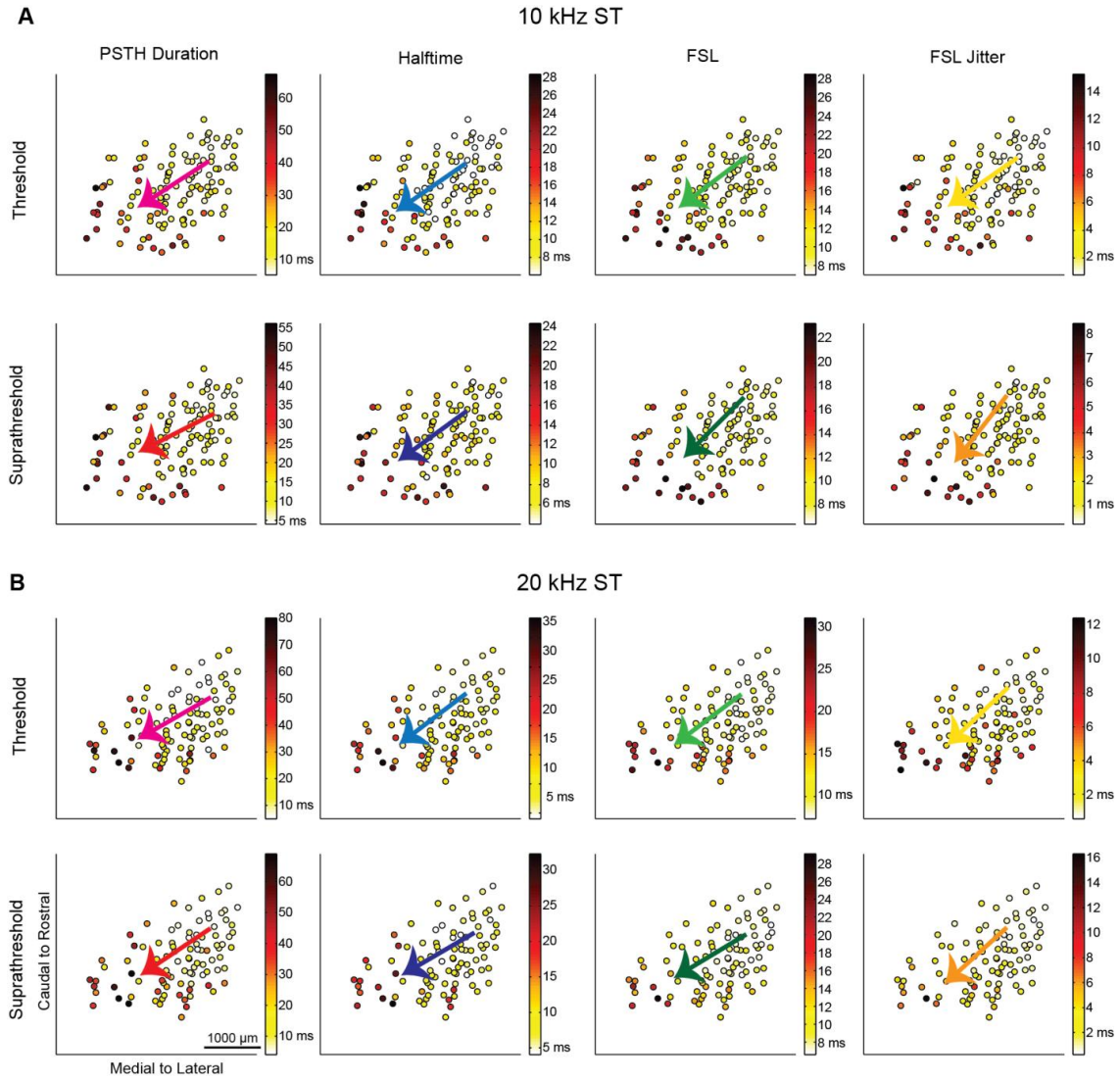

Figure 9: Spiking Responses to Short Tones (ST) Vary from Caudal-Medial to Rostral-Lateral across the Lamina. The maps of spiking in response to 10 kHz (**A**) and 20 kHz short tones (**B**) show response parameters recorded at each location. Multiple regression was performed to determine the steepest gradient axis (arrows, colors are indicative of response parameter and threshold variables). The spiking properties of PSTH duration, halftime, FSL, and FSL jitter were determined for each site at threshold and suprathreshold levels. See Table 1 for details on the regression statistics and Figure 10 for spiking response maps for the long tone stimuli.

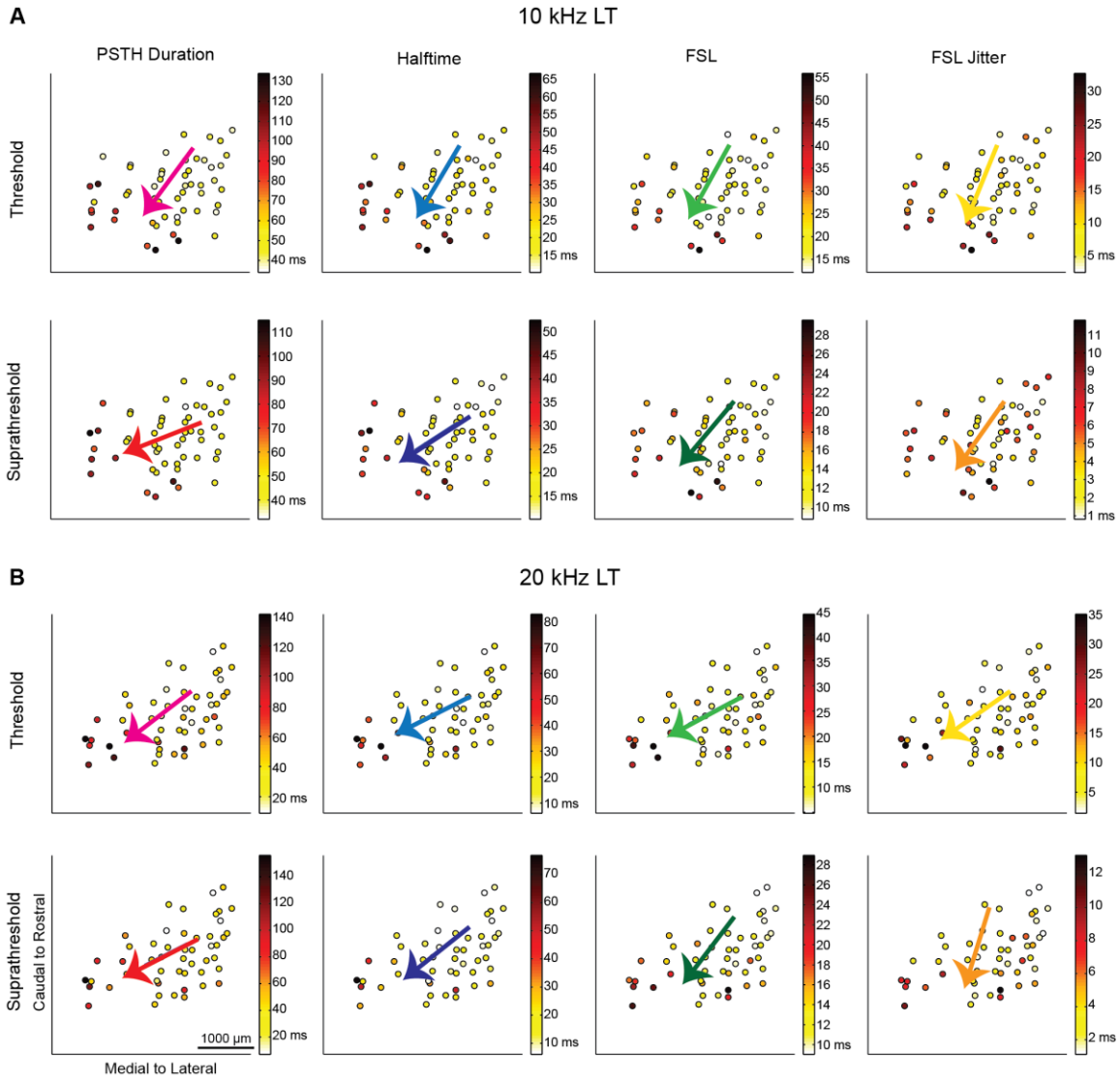

Figure 10: Spiking Responses to Long Tones (LT) Vary from Caudal-Medial to Rostral-Lateral across the Lamina. The maps of spiking in response to 10 kHz (**A**) and 20 kHz long tones (**B**) show response parameters recorded at each location. Similar to short tone responses in Figure 9, the responses varied from rostral-lateral to caudal-medial across the lamina.

In addition to spiking parameters, we also analyzed how LFP parameters varied across the ICC lamina. The LFP threshold was defined as three times the standard deviation of the spontaneous activity. LFP peak time was determined at the lowest

stimulus level which surpassed this threshold, and the magnitude of the LFP peak was found at 4 dB above this threshold. In choosing these criteria, we attempted to find the lowest elicited threshold which would provide consistent results while minimizing noise effects. However, the responses in the most caudal locations still did not exceed spontaneous activity. These caudal locations were set to 0 μV for the analysis of LFP peak magnitudes but were not included for the analysis of LFP peak time. The maps of LFP parameters in response to 10 and 20 kHz short and long tones are shown in Figure 11, where caudal-medial regions have smaller or subthreshold LFP peaks that occur later and rostral-lateral regions have larger LFP peaks that occur earlier.

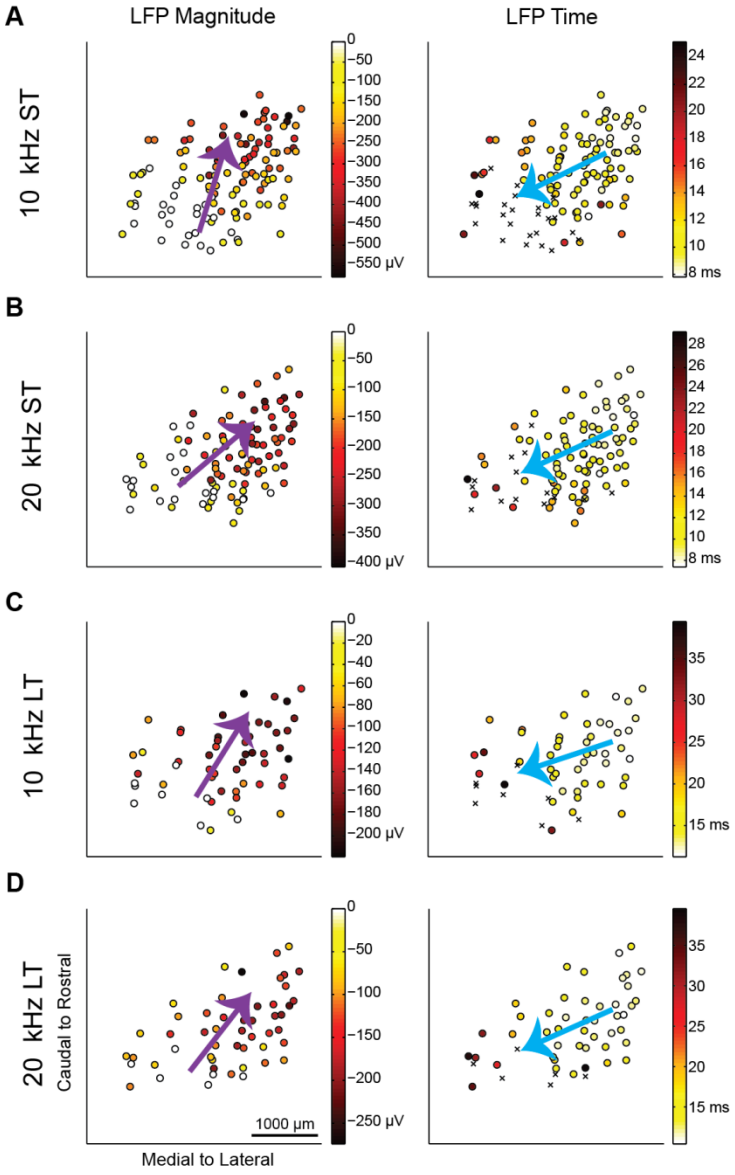

Figure 11: LFP Response Properties Vary from Caudal-Medial to Rostral-Lateral across the Lamina. The maps of LFP properties in response to 10 kHz short tones (**A**), 20 kHz short tones (**B**), 10 kHz long tones (**C**), and 20 kHz long tones (**D**) show response parameters recorded at each location. Multiple regression was performed to determine the steepest gradient axis (arrows). The LFP peak time was determined at threshold and the LFP magnitude was determined at 4 dB above threshold. If the site did not exceed threshold, the LFP magnitude was labeled as 0 µV and included in the data analysis. Those locations were

not included in the LFP peak time analysis, and are marked as X's in the LFP Time plots. See Table 1 for details on the regression statistics.

In order to quantify the gradient directionality of these different response maps, a line was fit to the data using linear, two-dimensional multiple regression analysis to find the steepest gradient axis, or the direction at which the response increased the most. The steepest gradient axes (the directional arrows) for each parameter are overlaid on the location data in Figure 9 for the short tone spiking parameters, Figure 10 for the long tone spiking parameters, and Figure 11 for short and long tone LFP responses. Directions for all parameters, summarized by the steepest gradient axes lines in Figure 12, show that all of the different response properties varied in a caudal-medial to rostral-lateral direction. The regression fit for each parameter was found to be significant, and details on the angle value and statistics can be found in Table 1.

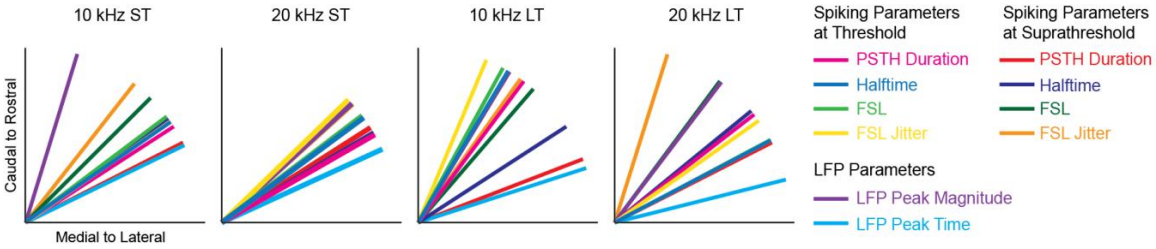

Figure 12: Multiple regression was performed to determine the steepest gradient axis (colored lines), which highlights the directionality for each parameter across the ICC lamina. Responses to all spiking and LFP parameters varied caudal-medially to rostral-laterally for the 10 and 20 kHz short and long tone responses.

Table 1: Multiple Regression Statistics Summary. Multiple regression was performed to determine the directionality of how each response parameter varied across the isofrequency lamina. The angle θ across the isofrequency lamina is the inverse tangent of the slope of the regression, where caudal to rostral would

be 90° and medial to lateral would be 0°. Each regression was performed on the number of sites N, with the descriptive statistics of a coefficient of determination R^2 and probability P.

		Spiking Parameters								LFP Parameters	
		At Threshold				At Suprathreshold					
		PSTH Duration	Half-time	FSL	FSL Jitter	Width	Half-time	FSL	FSL Jitter	Peak Mag.	Peak Time
10 kHz Short Tones	θ	33.3	34.6	37.4	35.0	27.1	36.1	45.4	51.5	73.5	25.8
	N	119	119	119	119	113	113	113	113	119	95
	R^2	0.47	0.48	0.57	0.48	0.48	0.45	0.57	0.57	0.64	0.50
	P	7E-17	3E-17	4E-22	4E-17	2E-16	5E-15	4E-21	1E-20	3E-26	2E-14
10 kHz Long Tones	θ	53.3	59.4	61.3	67.3	21.1	33.0	49.3	54.6	58.8	18.0
	N	55	55	55	55	53	53	53	53	55	47
	R^2	0.43	0.43	0.32	0.27	0.44	0.49	0.39	0.12	0.62	0.54
	P	5E-07	5E-07	4E-05	3E-04	5E-07	4E-08	4E-06	4E-02	1E-11	3E-08
20 kHz Short Tones	θ	30.0	36.5	37.3	44.2	32.6	30.6	30.4	42.2	42.5	24.6
	N	99	99	99	99	93	93	93	93	99	85
	R^2	0.40	0.46	0.56	0.50	0.46	0.47	0.56	0.41	0.49	0.58
	P	3E-11	1E-13	9E-18	4E-15	1E-12	3E-13	1E-16	5E-11	1E-14	3E-16
20 kHz Long Tones	θ	37.8	27.8	28.0	35.3	27.0	39.3	53.4	72.6	52.8	14.1
	N	52	52	52	52	50	50	50	50	52	46
	R^2	0.39	0.38	0.38	0.29	0.36	0.39	0.48	0.28	0.31	0.64
	P	7E-06	8E-06	9E-06	2E-04	3E-05	9E-06	3E-07	4E-04	1E-04	4E-10

Across the 10 kHz and 20 kHz laminae, the spiking and LFP response gradients varied from 24-74° rostral-laterally in response to short tones and 14-73° rostral-laterally in response to long tones, where 90° would be aligned along the caudal to rostral axis and 0° would be aligned along the medial to lateral axis.

Next we investigated whether the variation in angles across the ICC lamina depended on different properties, laminae, or stimulus duration. We compared the mean

angles between these specific variables by averaging across all other properties and stimulus conditions, as summarized in Figure 13.

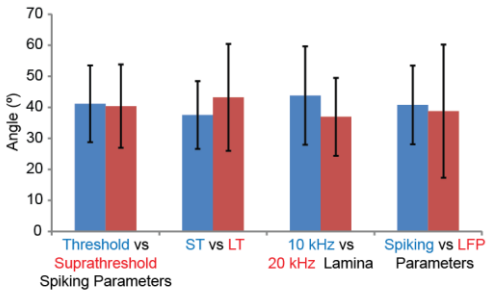

Figure 13: The angles of the responses, averaged across relevant response parameters (i.e., all other parameters and stimuli conditions except those directly being compared), were similar when comparing between different conditions. Average angles across all spiking parameters, BF laminae, and stimuli length were comparable between threshold and suprathreshold conditions. Average angles across all LFP and spiking parameters were similar when comparing between tone lengths or BF laminae. Finally, the average angles were similar between spiking and LFP parameters. Data is represented as mean ± STDV.

The mean angle was 41 ± 12° (mean ± STDV, n = 16 parameters) for threshold and 40 ± 13° (n = 16) for suprathreshold spiking parameters, when averaging across the four parameters each for the 10 and 20 kHz short and long tone stimuli. The similarity between the two suggests that this directionality is maintained across stimulation levels for spiking responses. The mean angle across all properties was 37.5 ± 11° (n = 20) for the short tones and 43 ± 17 ° (n = 20) for long tones, when averaging across the four spiking parameters at each of the two threshold levels and LFP parameters for both frequency laminae. Therefore, response properties were similar between short and long tone stimuli, though long tones resulted in greater scatter of angles potentially due to the fewer number of sites sampled. In addition, the average angle for all properties and

stimuli was 44 ± 16° (n = 20) for the 10 kHz lamina and 39 ± 22° (n = 20) for the 20 kHz lamina, which indicates that the two lamina also showed similar trends across properties. Across all stimuli, the average angle was 41 ± 13° (n = 32) for spiking parameters and 39 ± 22° (n = 8) for LFP parameters. The similarity of trends for both LFP and PSTH response characteristics further supports the main trends in response differences between rostral-lateral and caudal-medial regions of the ICC. There were no significant differences between all four of these group comparisons ($P > 0.05$, using the Mann-Whitney test). Therefore, we conclude that the directionality of property differences from caudal-medial to rostral-lateral is consistent across the parameters used in this study, including short and long tone stimuli, the 10 kHz and 20 kHz lamina, threshold and suprathreshold spiking activity, as well as spiking and LFP activity.

Two Spatially Distinct Regions along an ICC Lamina

While the steepest gradient axis was an important tool in determining the directionality of response gradients, we needed to further investigate how the responses vary along these gradients. Based on previous anatomical and physiological studies, it has been proposed that at least two spatially segregated lemniscal pathways exist from the ICC (i.e., caudal-medial versus rostral-lateral regions) up to ACC. Thus, it would be expected that response parameters would exhibit at least two clusters of response values between the caudal-medial and rostral-lateral regions of the ICC rather than a smooth gradient of values across that dimension. In order to address this question, we projected each recording location onto the steepest gradient axis by determining the shortest distance between the two. We then plotted the response properties for each location as a

function of distance from the vertex (i.e., the most caudal-medial point on the steepest gradient axis), as shown in Figure 14 in response to short tones.

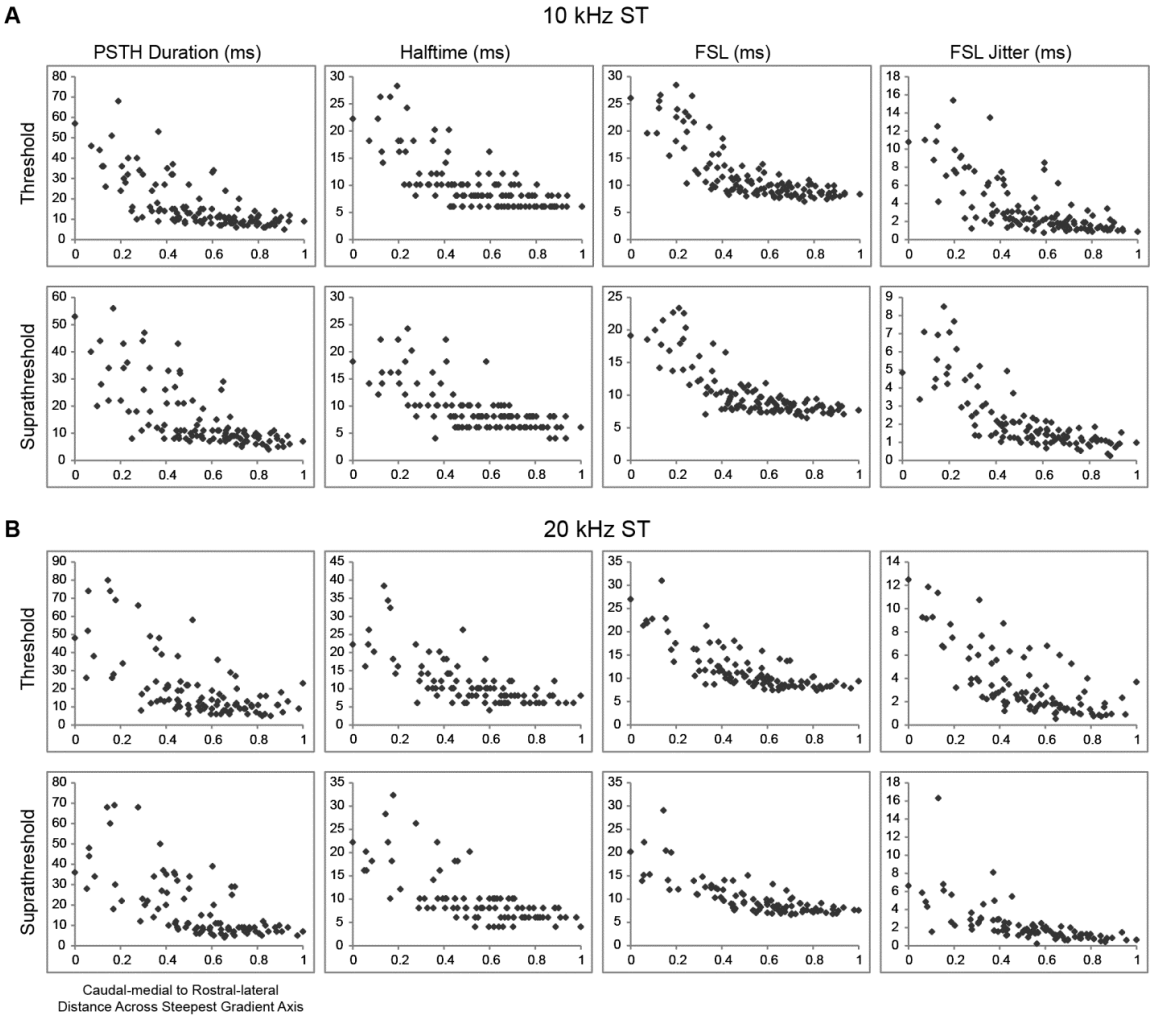

Figure 14: In Response to Short Tones, Differences of Spiking Properties between the Caudal-Medial and Rostral-Lateral Regions Suggests that the Two are Distinct Clusters. The values of spiking parameters were plotted along the steepest gradient axis from the caudal-medial (0) to the rostral-lateral (1) endpoints along an ICC lamina in response to a 10 kHz (**A**) or 20 (**B**) kHz ST. The spiking parameters are small and similar in rostral-lateral regions and increase rapidly in amount and scatter towards more caudal-medial regions. Trends in spiking responses were similar across different stimulus levels. See Figure 15 for spiking responses to the long tone stimuli.

For the spiking parameters in Figure 14, at least two clusters of values can be seen along the caudal-medial to rostral-lateral dimension. This is most clearly observed for the FSL parameter, where latencies are short in the rostral-lateral region and become longer in the caudal-medial region. At a distance of about 0.5 up to 1 (i.e., along the abscissa and in the rostral-lateral region), there is no or minimal change in values. However, for smaller distances below about 0.5 (i.e., in the caudal-medial region), the values increase rapidly with greater heteroscedasticity. This basic pattern can be observed for all the other spiking parameters and for long tone stimuli (see Figure 15).

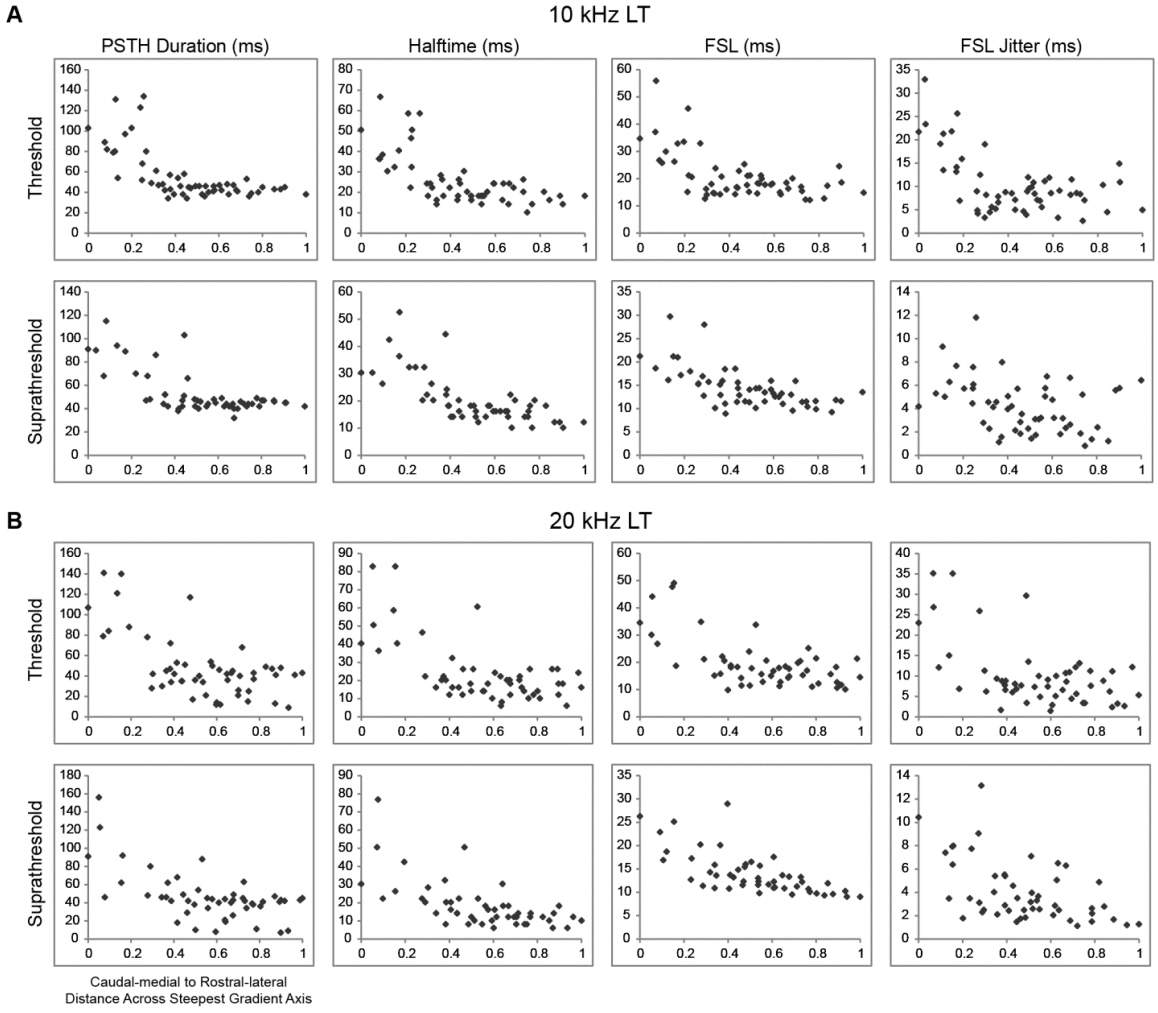

Figure 15: In Response to Long Tones, Differences of Spiking Properties between the Caudal-Medial and Rostral-Lateral Regions Suggests that the Two are Distinct Clusters. The values of spiking parameters were plotted along the steepest gradient axis from the caudal-medial (0) to the rostral-lateral (1) endpoints along an ICC lamina in response to a 10 kHz (**A**) and 20 (**B**) kHz LT. Similar to short tone stimuli in Figure 14, the spiking parameters are small and similar in rostral-lateral regions and increase rapidly in amount and scatter towards more caudal-medial regions.

In addition, this basic pattern can be partially observed for LFP peak time but not for LFP peak magnitude, as shown in Figure 16. It is important to note that the LFP corresponds to activity recorded across a large population of neurons surrounding the

recording site that can span a distance of hundreds of microns whereas our multi-unit spiking activity corresponds to a spatial span of tens of microns (Eggermont and Smith, 1995; Humphrey and Schmidt, 1991; Leung, 1990; Mitzdorf, 1985). Thus, the limited spatial resolution of the LFP response likely smeared any clustering effect along the caudal-medial to rostral-lateral distance.

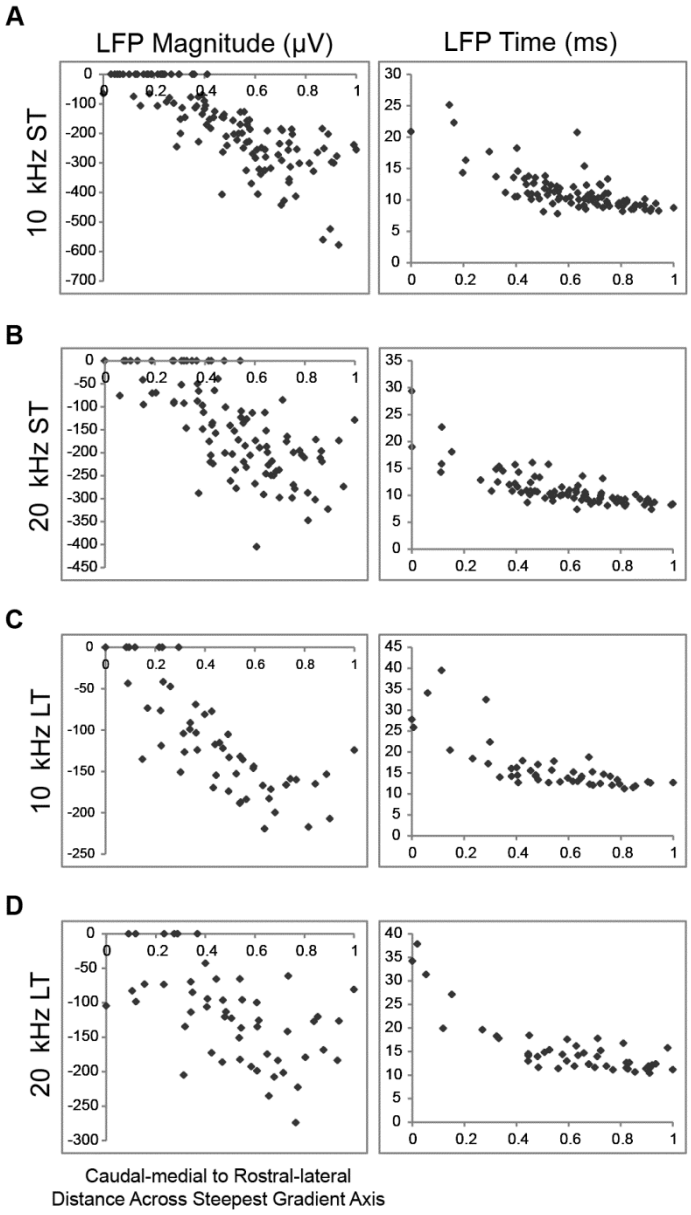

Figure 16: Differences of LFP Properties between the Caudal-Medial and Rostral-Lateral Regions Suggests that the Two are Distinct Clusters. The values of LFP parameters were plotted along the steepest gradient axis from the caudal-medial (0) to the rostral-lateral (1) endpoints along an ICC lamina in response to 10 kHz short tones (**A**), 20 kHz short tones (**B**), 10 kHz long tones (**C**), and 20 kHz long tones (**D**). The LFP times are small and similar in rostral-lateral regions and increase rapidly in amount and scatter towards more caudal-medial regions. LFP magnitudes are large in rostral-lateral regions while rarely exceeding threshold in caudal-medial regions.

THRESHOLD ANALYSIS

The previous results were all compared at levels which elicited a similar extent of activity for each site. We also wanted to analyze whether thresholds varied across locations. Unfortunately, each subsequent array insertion slightly increased the threshold of response regardless of location, possibly due to minor tissue damage, swelling over time, or adaptive effects. This limitation restricted us from analyzing location maps for threshold across all our array shank locations and animals. Since we used a four shank array in which the shanks were separated by 500 µm and aligned along the caudal to rostral direction of the ICC, we instead compared the thresholds of BF-matched sites on the most rostral shank versus the most caudal shank for each placement. These rostral and caudal sites were distributed throughout the rostral and caudal ICC locations over all of the animals, as shown in Figure 17.

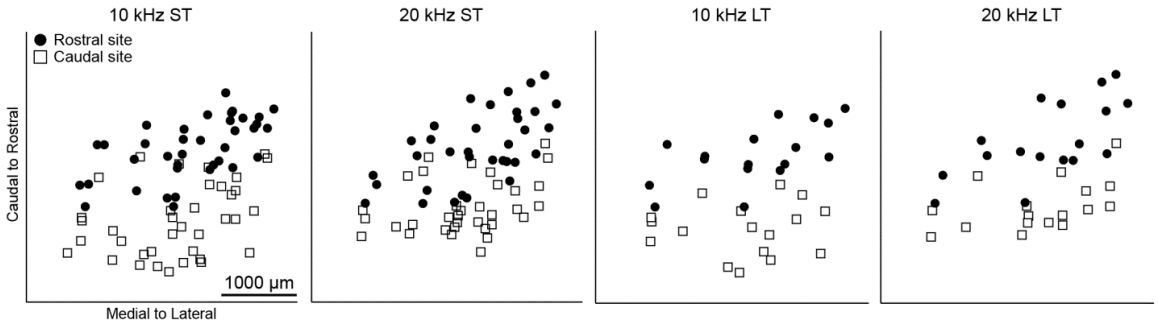

Figure 17: Distribution of the Most Rostral and Most Caudal Shank for Each ICC Array Placement. The most rostral shank (circle) and the most caudal shank (square) in the ICC for each array placement are shown for the different stimuli. Since placements of rostral and caudal points were distributed throughout the rostral and caudal half of the ICC, respectively, this suggests that comparing the thresholds of the rostral and caudal shank for each placement (i.e., BF-matched sites) is an appropriate way to compare threshold differences between the rostral versus caudal regions along an ICC lamina.

As described previously, the spiking threshold and suprathreshold values were determined using SDT at stimulation levels which elicited spiking activity at d' values of 1 and 3, respectively. For each placement, we determined the differences between the caudal shank and rostral shank threshold. We used the sign test to test the null hypothesis that, across all placements, the number of occurrences of positive differences was equal to that of the number of negative differences. We found that thresholds were significantly lower for rostral compared to caudal shanks for spiking in response to 10 kHz short tones at spiking threshold ($P < 5x10^{-4}$, N = 37 comparisons) and suprathreshold levels ($P < 4 x10^{-3}$, N = 37). Similar trends were observed for the other stimuli, though these trends did not reach significance. In addition, LFP thresholds were lower for rostral compared to caudal shanks for the 10 kHz short tones ($P < 9x10^{-10}$, N = 36), 10 kHz long tones ($P < 6x10^{-5}$, N = 17), and 20 kHz short tones ($P < 7x10^{-3}$, N = 31). A similar trend was observed for the 20 kHz long tones but it did not reach significance. Perhaps not all of these conditions reached significance because of the orientation of the shanks along the caudal to rostral dimension instead of the caudal-medial to rostral-lateral dimension. Nevertheless, all of the conditions still exhibited similar trends of lower thresholds in more rostral locations, which is consistent with what is expected for the dual lemniscal organization. In particular, the rostral (and lateral) ICC projects up to the rostral MGV and A1, which have both shown greater sensitivity and/or stronger neural activity compared to the caudal MGV and regions outside of A1 that receive projections from the caudal-medial ICC.

DISCUSSION

Summary of Results

In response to pure tones, we found a differential pattern of activity to BF-matched sites across the isofrequency laminae of the ICC. In contrast to caudal-medial regions, rostral-lateral regions responded with shorter PSTH durations, more proportion of spikes occurring earlier in the PSTH, shorter first-spike latencies with less FSL jitter, and larger LFP peaks with shorter latencies. The larger LFP peaks relate to greater spatial and/or temporal synchrony across neurons. Using multiple regression, we found this caudal-medial to rostral-lateral directionality of response properties (i.e., along the steepest gradient axis) to be significant when investigating responses to both short and long stimuli. Further analysis of the response properties revealed two distinct clusters of values along the steepest gradient axis, corresponding to a caudal-medial and a rostral-lateral region along the isofrequency laminae of the ICC. We also found that acoustic thresholds were generally lower in rostral versus caudal locations.

Methodological Considerations

In order to fully map numerous locations across and up to the border of a given ICC lamina, we targeted only two isofrequency laminae of the ICC: the 10 kHz and 20 kHz lamina. Since the typical hearing range of the guinea pig spans frequencies from tens of hertz up to 40-50 kHz (Prosen et al. 1978), we cannot claim that the two distinct clusters of response properties between the caudal-medial versus the rostral-lateral regions along an isofrequency lamina occurs throughout the ICC. However, we arbitrarily selected these two different laminae and observed similar trends in response properties. Previous studies have also demonstrated a dual lemniscal organization that spans across different

frequency regions from the brainstem up through the ICC, MGV, and ACC. In gerbil, this segregated organization from the ICC up to MGV was anatomically demonstrated throughout most of the ICC spanning low, middle, and high frequency regions (Cant and Benson 2007; 2006). In cat, this segregated organization from MGV up to ACC with their different coding properties was demonstrated across a wide frequency range of approximately 0.2 to 50 kHz (Rodrigues-Dagaeff et al. 1989). In rat, the anatomical segregation from MGV to ACC was only investigated for a frequency region around 8 kHz, but the differences in response properties between subregions within ACC (i.e., A1 versus ventral auditory field or caudal suprarhinal auditory field) that are the targets of the dual lemniscal pathways from MGV were demonstrated across a wide frequency range of about 1-30 kHz within the same studies (Polley et al. 2007; Storace et al. 2012). In guinea pig, the spatial segregation of activation properties from the caudal-medial versus the rostral-lateral ICC up to A1 was shown for different frequency laminae spanning 9-23 kHz (Lim and Anderson 2007b). Considering the consistency in results across frequency regions for these different studies and species, we expect that the distinct cluster of response properties identified between the caudal-medial and the rostral-lateral regions of the 10 and 20 kHz laminae would also occur in other isofrequency laminae throughout the ICC.

In our study, we used an anesthetized preparation that enabled us to position the electrode array into numerous locations throughout the ICC in each animal. We selected ketamine as the anesthetic because previous studies have shown that it has minimal or no alterations in ICC activity compared to the awake state, including minimal or no changes

for FSL, FSL jitter, trial-by-trial reliability, temporal synchronization capabilities, and acoustic-driven firing rate (Astl et al. 1996; Suta et al. 2003; Ter-Mikaelian et al. 2007). Similar to our study, several studies used a combination of ketamine and xylazine in guinea pigs and reported no or minimal changes compared to the awake state for spontaneous activity, firing patterns in response to pure tones, and tuning properties based on Q10 values (Astl et al. 1996; Suta et al. 2003; Torterolo et al. 2002). In one study that used barbiturate-ketamine anesthetic in gerbil (Ter-Mikaelian et al. 2007), some neurons exhibited greater firing rate adaptation over a longer period of time compared to the awake condition. However, this adaptation occurred on a time scale (> 500 ms) longer than our analysis period (< 160 ms), and thus is unlikely to have affected our results. It is important to note that different types of anesthetics (i.e., ketamine, pentobarbital, or nitrous oxide) were used in all the previous studies we have described above that have demonstrated distinct and consistent response properties between the dual lemniscal pathways through the MGV and ACC. Therefore, it is unlikely that the differences in response properties between the dual lemniscal pathways are caused by any specific type of anesthetic.

COMPARISON TO PREVIOUS STUDIES

We observed differences in thresholds and latencies between the caudal-medial and rostral-lateral regions along an ICC lamina, which aligns with the expected dual lemniscal organization. However, these results contrast those of previous studies that showed a concentric map for thresholds (Hage and Ehret 2003; Stiebler 1986) or a medial to lateral organization for latencies (Langner et al. 2002; Schreiner and Langner 1988)

along an ICC lamina. This discrepancy in results could be associated with our reconstructions of the recording sites that enabled more accurate identification of response locations throughout and up to the borders of each ICC lamina across animals. For example, it can be seen in the data in Fig. 9 presented by Langner et al. (2002) that more recordings from locations closer to the borders of the ICC could have revealed a caudal-to-rostral component in their latency map, which would have led to a caudal-medial versus rostral-lateral organization rather than a medial versus lateral organization. In that same figure, however, it does not appear that recording more ICC border locations would have resulted in a periodicity map consistent with our dual lemniscal organization. Considering the complexity and/or differences in periodicity maps shown across studies and species as well as their dependence on level (Krishna and Semple 2000; Langner 1992; Langner et al. 2002; Schreiner and Langner 1988), it is possible that this feature may be integrated across the dual lemniscal pathways. Similarly, other coding properties such as frequency modulation, binaural interactions, and sound source localization may also be integrated across the dual lemniscal pathways considering that topographic maps for these acoustic features have shown to be different than the dual lemniscal anatomical segregation (Cohen and Knudsen 1999; Heil et al. 1992; Langner et al. 2002; Middlebrooks and Zook 1983; Rodrigues-Dagaeff et al. 1989; Schreiner and Langner 1988; Wenstrup et al. 1994).

In this study, we did not find a consistent organization of tuning curve width (i.e., Q10 and Q30 values) or tonotopicity (detailed analysis will be presented in a future publication). With regard to frequency tuning properties, it was shown in anesthetized

mouse that neurons with narrower tuning were located in more central regions of an ICC lamina that then broadened in more outward locations (Hage and Ehret 2003; Stiebler 1986). However, a more recent study in awake mouse performed detailed histological reconstructions of all the recording site locations and found no spatial trend along an ICC lamina for tuning curve width (Portfors et al. 2011). As suggested by the authors of this study, the discrepancy in results could be associated with the use of histological reconstructions for more accurately combining response locations across animals that was not performed in the previous studies. It appears that differences in spectral coding properties between the dual lemniscal pathways may not occur until the MGV up to ACC (Polley et al. 2007; Rodrigues-Dagaeff et al. 1989; Storace et al. 2011).

A Dual Lemniscal Organization

The concept of a dual lemniscal organization was first revealed in the 1980s (Morel and Imig 1987; Rodrigues-Dagaeff et al. 1989), specifically for projections from MGV up to ACC in a cat model. The dual lemniscal hypothesis was further expanded in 2006 to 2007 to include pathways from the brainstem up through the ICC, MGV, and ACC across several species, including gerbil, rat, and guinea pig (Cant and Benson 2007; 2006; Lim and Anderson 2007b; Polley et al. 2007). Together, these studies revealed two segregated anatomical pathways through the ICC (caudal-medial versus rostral-lateral regions), MGV (caudal versus rostral regions), and ACC (A1 versus core regions outside of A1). They also demonstrated different coding properties between these pathways within the MGV and ACC, and for electrical activation of ICC up to ACC. More recently, a series of anatomical and functional studies in rat further support this dual

lemniscal organization from the MGV up to ACC and also reveal differences in gene expression for type 1 vesicular glutamate transporter that may contribute to the distinct coding properties between pathways (Storace et al. 2012; Storace et al. 2010; 2011).

Figure 18A provides a simplified schematic summarizing the dual lemniscal pathways through the ICC, MGV, and ACC. The differences in coding properties between the rostral versus caudal MGV demonstrated by Rodrigues-Dagaeff (1989) in cat and listed in Figure 18B suggest that the rostral pathway is designed for stronger excitatory activation and more temporally and spectrally precise transmission of information up to higher centers. Many of these differences in coding properties between the dual pathways have also been shown in ACC and listed in Figure 18B (Phillips et al. 1995; Polley et al. 2007; Schreiner et al. 2011; Storace et al. 2012; Wallace et al. 2000).

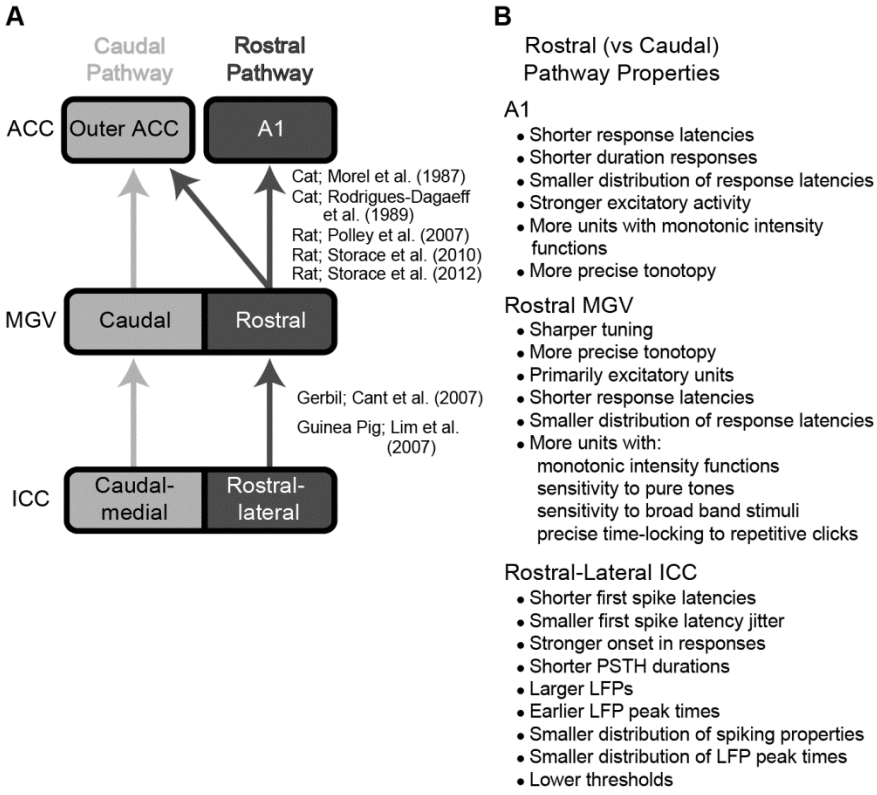

Figure 18: Schematic of Anatomical Projections and Summary of Physiological Differences that Indicate the Lemniscal Pathway is Segregated into Two Sub-projection Pathways. A, The rostral and caudal ascending pathways show spatially segregated anatomical projections from the ICC up to ACC. Overlapping projections between the two pathways are not shown. B, In contrast to the caudal pathway, the rostral pathway also shows different responses to acoustic stimuli in A1 (Phillips et al. 1995; Polley et al. 2007; Storace et al. 2012; Wallace et al. 2000), the rostral MGV (Rodrigues-Dagaeff et al. 1989) and the rostral-lateral ICC (as shown in this study). Figure adapted from Lim et al. (2008a).

The key finding of our study is the confirmation of distinct regions along the ICC laminae that code for sound in different ways and align with the dual lemniscal pathways identified in the previous studies listed in Figure 18. Except for the spectral coding properties, the differences in response properties in ICC are consistent with those identified for MGV, further supporting that the rostral pathway is designed for stronger

activation and more precise transmission of sound information to higher centers compared to the caudal pathway.

There is undoubtedly a complex and heterogeneous organization of different sound features across the ICC and up to ACC, some of which are organized into topographic maps that may or may not align with each other. However, a consistent organization of at least two spatially segregated pathways through the ICC, MGV, and ACC with different coding properties has been observed across several studies spanning multiple species. While these studies investigated mammals including rodents and cats, the presence or organization of dual lemniscal pathways in bats or birds is uncertain because of neuroanatomical and physiological differences in these species (Butler and Hodos 2005; Popper and Fay 1995). Moreover, the role of these dual pathways is not yet clear. A recent study demonstrated that electrical stimulation of A1 elicits descending excitatory activation in the caudal-medial ICC but with little or no activation within the rostral-lateral ICC (Markovitz et al. 2013). Combined with the robust and precise activation properties of the rostral pathway that projects up to A1, these findings suggest that the rostral pathway may serve as the main ascending auditory pathway while the caudal pathway, at least within the midbrain, may serve a more modulatory role for sound processing.

What is clear from multiple studies and our recent findings is that the lemniscal pathway can no longer be considered as a single pathway through the ascending auditory system. Just as studies have differentiated between different subregions associated with the lemniscal versus the nonlemniscal pathway (e.g., ICC versus the external inferior

colliculus) to better understand and model the central auditory system, it will also be important to differentiate between the dual lemniscal pathways through the ICC, MGV, and ACC. Further studies are also needed to identify how brainstem and higher cortical regions interact with this dual lemniscal system as well as the functional role of these segregated pathways for sound coding and perception. Clinically, these types of studies will reveal appropriate targets and stimulation patterns for improving central hearing prostheses, such as the auditory brainstem implant and the auditory midbrain implant (Colletti et al. 2012; Lim et al. 2009; Schwartz et al. 2008).

CHAPTER 3A: DSS EFFECTS ON THE CORTEX

While the cochlear implant has successfully restored hearing to many deaf patients, it cannot benefit those without a functional auditory nerve or an implantable cochlea. As an alternative, the AMI has been developed and implanted into deaf patients. Consisting of a single-shank array, the AMI is designed for stimulation along the tonotopic gradient of the ICC. Although the AMI can provide frequency cues, it appears to insufficiently transmit temporal cues for speech understanding because repeated stimulation of a single site causes strong suppressive and refractory effects. Applying the electrical stimulation to at least two sites within an isofrequency lamina can circumvent these refractory processes. Moreover, co-activation with short inter-site delays (<5 ms) can elicit cortical activation which is enhanced beyond the summation of activity induced by the individual sites. The goal of our study was to further investigate the role of the auditory cortex in this enhancement effect. In guinea pigs, we electrically stimulated two locations within an ICC lamina or along different laminae with varying inter-pulse intervals (0-10 ms) and recorded activity in different locations and layers of A1. Our findings reveal a neural mechanism that integrates activity only from neurons located within the same ICC lamina for short spiking intervals (<6 ms). This mechanism leads to enhanced activity into layers III-V of A1 that is further magnified in supragranular layers. This integration mechanism may contribute to perceptual coding of different sound features that are relevant for improving AMI performance.

INTRODUCTION

Auditory prostheses have been treating hearing loss for decades, with the CI being able to provide sufficient temporal and spectral cues required for speech understanding (Kral and O'Donoghue 2010; Shannon et al. 1995; Zeng 2004). For people without a functional auditory nerve or an implantable cochlea, central prostheses have been implanted in the brainstem since 1979. Unfortunately, the performance of the ABI has generally been less successful than the CI, particularly for patients with NF2, one of the key target populations for the implant (Colletti et al. 2009; Lim et al. 2009; Schwartz et al. 2008). While some ABI patients have shown performance levels approaching that of CI patients (Colletti et al. 2012; Sennaroglu et al. 2011), continued research into central auditory implants needs to be performed in order to improve hearing perception for the majority of patients who cannot benefit from a CI.

As an alternative approach to the ABI, particularly for the NF2 population, deaf patients have been implanted with a new AMI consisting of a single-shank array (20 sites) designed for stimulation along the tonotopic gradient of the ICC (Lim et al. 2009; Lim et al. 2007). While AMI stimulation can activate frequency-specific neurons and transmit spectral cues to higher auditory centers, it appears to exhibit limited temporal coding abilities (Lenarz et al. 2006a; Lim and Anderson 2006; Lim et al. 2013; Lim et al. 2008b; McKay et al. 2013).

Calixto et al. (2012) investigated this limited performance of the AMI by stimulating the ICC of guinea pigs with the AMI array and recording the evoked LFPs in the A1. Repeated stimulation of a single site caused refractory and suppressive neural

effects, which likely resulted in the inadequate temporal coding. These negative effects could be overcome by stimulating at multiple sites within an isofrequency lamina. In addition, co-activation of sites with short delays (<5 ms) resulted in cortical activity that was enhanced beyond a linear sum of activation elicited by the individual sites. However, their interpretation of A1's role in this enhancement effect was limited because they only analyzed LFPs in the main input layer III/IV (i.e., corresponding to thalamic input into A1). They also did not analyze spike activity in A1 because of the prevalence of antidromic field potentials from ICC stimulation that could partially mask the orthodromically activated spikes across cortical layers. As a result, they were unable to determine if this enhancement effect was solely produced within the tectothalamic pathway or if it also occurred within the thalamocortical and corticocortical pathways. Moreover, they were unable to determine whether this enhancement effect could be observed when stimulating across different ICC laminae or if it solely occurred when stimulating within a lamina.

The purpose of this study was to further investigate the role of A1 in the enhancement effect by expanding the study performed by Calixto et al. (2012). We presented two electrical pulses with varying inter-pulse intervals (0-10 ms) to one or two sites within an isofrequency lamina or in different laminae of the ICC. By stimulating the ICC with much smaller electrode sites than the AMI sites (413 μm^2 versus 126,000 μm^2), we could stimulate more locally within the ICC, which resulted in less antidromic activation of corticocollicular neurons and thus the antidromic field potential was isolated to layer V as reported in a previous study (Lim and Anderson 2007a). Using 32-site

electrode arrays, we recorded LFPs and multi-unit spike activity simultaneously within different cortical layers to determine if activity is further enhanced or altered by neuronal mechanisms within A1. We also investigated how the enhanced cortical activity varied across different locations in A1. Our results confirm that a neural mechanism exists within the ICC-to-A1 pathway for eliciting enhanced activity in A1. This neural mechanism integrates activity from different ICC neurons which reside only within the same lamina and are co-activated within a brief time window (<6 ms). Our results also indicate that this integration effect is further enhanced up to supragranular layers of A1. Moreover, this integration effect exhibits similar properties to that of perceptual data obtained for short-interval stimuli in humans. These findings reveal a neural mechanism that may contribute to perceptual processing of different sound features based on an inter-spike interval or synchrony code across ICC neurons, and needs to be considered for improving AMI stimulation strategies.

METHODS

OVERVIEW

Basic surgical procedures and methods for neural recording and stimulation were similar to those presented in previous work (Lim and Anderson 2007a; 2006; Straka et al. 2013). This study was approved by the University of Minnesota's Institutional Animal Care and Use Committee. Silicon-substrate, 32-site Michigan electrode arrays (NeuroNexus Technologies, Ann Arbor, MI) were used to electrically stimulate the ICC and record the corresponding neural responses within A1 of ketamine-anesthetized guinea pigs. Appropriate placements of the array sites within the ICC and A1 were

guided by acoustic-driven responses (Lim and Anderson 2007b; Snyder et al. 2004; Wallace et al. 2000). Neuronal action potentials (spikes) and LFPs recorded in response to application of two pulses at 1 ICC site were compared to neuronal activity induced by application of a single pulse at each of 2 sites, with varying delays between the two pulses. The two stimulated sites were either within the same isofrequency lamina or across different laminae. These experiments investigated how activation of similar versus different neurons within and across frequency laminae activated different regions and layers of A1.

SURGERY

Experiments were performed on 14 male and female Hartley guinea pigs (373 ± 46 g, Elm Hill Breeding Labs, Chelmsford, MA). Animals were initially anesthetized with an intramuscular injection of ketamine (40 mg/kg) and xylazine (10 mg/kg), and were given periodic supplements to maintain a non-reflexive state. After fixing the animal into a stereotaxic frame (David Kopf Instruments, Tujunga, CA), we exposed the right side of the cortex from the caudal end of the occipital lobe to the middle cerebral artery of the temporal lobe. The dura was removed, micromanipulators were used to insert the arrays into the ICC and A1, and the exposed brain was covered with agarose gel.

STIMULATION AND RECORDING SETUP

All experiments were performed in an acoustically- and electrically-shielded chamber and controlled by a computer interfaced with TDT System 3 hardware (Tucker-Davis Technology, Alachua, FL) using custom software written in Matlab (MathWorks, Natick, MA). For acoustic stimulation, sound was presented via a speaker coupled to the left ear through a hollow ear bar. The speaker-ear bar system was calibrated using a 0.25-

inch condenser microphone (ACO Pacific, Belmont, CA) connected to the ear bar via a short plastic tube representing the ear canal.

All neural signals (i.e., LFPs and spiking activity) were passed through analog DC-blocking and anti-aliasing filters from 1.6 Hz to 7.5 kHz. The sampling frequency used for acoustic stimulation was 195 kHz and for neural recording was 24 kHz. Electrical stimulation up to 100 μA was presented on different sites on the ICC array in a monopolar configuration with a ground return in the neck muscles. The pulses were biphasic, charge-balanced, cathodic-leading and 205 μs/phase. The recording ground needle was positioned either under the skin approximately 2 cm rostral to bregma or directly in the brain in the parietal lobe. No obvious differences in results were observed when using the different recording grounds.

PLACEMENT OF ARRAYS

PSTHs and FRMs were plotted online to confirm the array's position within the ICC or A1. Details on these analysis methods and example plots for similar types of arrays are presented in previous publications (Lenarz et al. 2006a; Lim and Anderson 2006; Neuheiser et al. 2010). Briefly, we bandpass filtered the neural signals (300-3000 Hz) on each site and labeled a spike as any negative peak that exceeded a threshold of three standard deviations above the background activity. Thus, all analysis was performed on multiunit spike data. For frequency response maps, four trials were presented for each pure tone (1-40 kHz, 8 steps/octave) and level (0-70 dB, 10 dB steps) stimulus. The BF was taken as the centroid of frequencies which elicited spiking responses at 10 dB above the visually-determined threshold.

The A1 array consisted of four 5-mm-long shanks separated by 400 μm. Sites were linearly spaced at 200 μm along the shank and each had an area of 177 μm^2. The array was inserted approximately perpendicular to the cortical surface in an attempt to align each shank along a column in A1 (Abeles and Goldstein 1970; Redies et al. 1989b; Wallace et al. 2000). The average difference of BFs (**ΔBF**) between sites in layers I/II, III/IV, and V along each shank was 0.09 ± 0.08 octaves (mean ± standard deviation). Placement into A1 was confirmed when tonotopic shifts of low to high BFs were observed for ventral-rostral to dorsal-caudal locations (Wallace et al. 2000). Only A1 sites with similar BFs to the stimulated ICC sites were analyzed.

The identification of A1 layers was accomplished by performing current source density (**CSD**) analysis (Kral et al. 2000; Mitzdorf 1985; Muller-Preuss and Mitzdorf 1984) in response to 70 dB SPL broadband noise (100 trials) using the finite difference formula:

$$CSD(z) = \sigma_z \frac{\phi(z+\Delta z) - 2\phi(z) + \phi(z-\Delta z)}{(\Delta z)^2}$$

where ϕ is the averaged LFP across trials, z is the depth location of each site along an A1 array shank, Δz is the differentiation step size, and σ_z is the component of conductivity in the z-direction. Δz was equal to the A1 site spacing of 200 μm and σ_z was set to one since absolute CSD values were not required for analysis. The one-dimensional CSD approximation provides a consistent representation for the current sinks and sources associated with columnar synaptic activity in the guinea pig auditory cortex (Lim and Anderson 2007a; Middlebrooks 2008). The main input layer of A1, which is layer III/IV

in guinea pig (Huang and Winer 2000; Smith and Populin 2001), corresponded to the site with the shortest latency current sink (i.e., positive CSD peak). Layer V was identified as the site with a current source (i.e., negative CSD peak), typically being two electrode sites (or 400 μm) deeper than the site corresponding to layer III/IV. Supragranular layers, here combined as layer I/II, corresponded to two electrode sites (or 400 μm) shallower than the site corresponding to layer III/IV.

The ICC array consisted of two 10-mm-long shanks separated by 500 μm. Sites were linearly spaced at 100 μm along the shank and each had an area of 413 μm^2. Prior to the experiment, the sites on the ICC array were activated using cyclic voltammetry to enable both recording and stimulation up to 100 μA (Anderson et al. 1989; Lim and Anderson 2006). The ICC array was placed at a 45° angle to the sagittal plane through the visual cortex in order to be aligned along the tonotopic axis of the ICC (Malmierca et al. 1995; Snyder et al. 2004). Proper array placement in the ICC was confirmed by observing frequency response maps that exhibited an orderly shift from low to high BFs for superficial to deeper locations, respectively, along a shank (Lim and Anderson 2006; Snyder et al. 2004).

ELECTRICAL STIMULATION PARAMETERS

As depicted in Figure 19, we used three protocols to electrically stimulate one or two sites within the ICC and characterize the corresponding LFP and spiking activity within A1 supragranular layers I/II, main input layers III/IV, and output layer V.

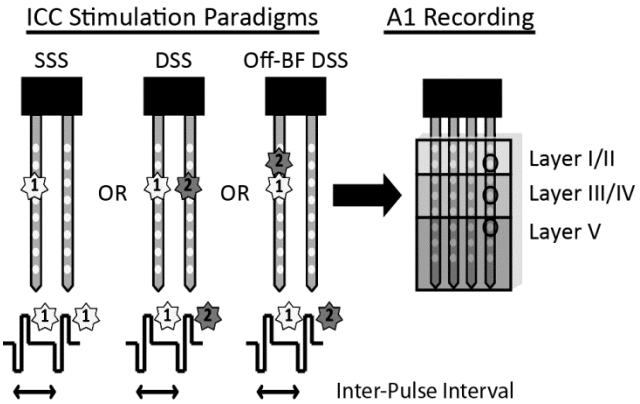

FIGURE 19: Summary of ICC electrical stimulation protocols and elicited responses recorded in A1. In the SSS protocol, two pulses were delivered to one site at specific IPIs. In the DSS protocol, one of two pulses were each delivered to two sites 500 μm apart along an ICC isofrequency lamina, with corresponding IPIs. For both SSS and DSS, all ICC stimulation sites have similar BFs to the recording sites in A1. In the Off-BF DSS protocol, the second pulse was sent to a site in a neighboring frequency lamina 100 μm from site 1 on the same array shank and responses were recorded on an A1 site with a similar BF to that of site 1. Neural responses in A1 were recorded at sites (circles) in layers I/II, III/IV, and V within the same cortical column. Figure is not drawn to scale and not all sites are shown on the ICC arrays. A1, primary auditory cortex; BF, best frequency; ICC, central nucleus of the inferior colliculus; IPI, inter-pulse interval.

In the first two protocols, we stimulated within an ICC isofrequency lamina either by delivering two pulses on the same site (single-site stimulation, **SSS**) or one pulse on each of two sites with similar BFs (dual-site stimulation, **DSS**). For the DSS protocol, the average ΔBF between the ICC sites was 0.05 ± 0.06 octaves, which is below the bandwidth of ~0.3 octaves seen in an isofrequency lamina of cat (Schreiner and Langner 1997) and rat (Malmierca et al. 2008). The analysis was performed on the A1 sites with similar BFs to the stimulated ICC laminae (ICC-to-A1 ΔBF: 0.2 ± 0.2 octaves). We also presented two pulses in the third protocol, with one on an ICC site BF-matched to the A1

site and the other on a neighboring ICC site 100 μm away along the same shank for the **Off-BF DSS** protocol. Stimulating sites further than 100 μm along the tonotopic gradient required current levels typically exceeding our 100 μA limit to effectively activate the A1 site, which is consistent with different ICC regions projecting to and activating different regions of the MGV and A1 in a tonotopic pattern (Lim and Anderson 2006; Malmierca et al. 1997; McMullen et al. 2005; Velenovsky et al. 2003). The average ΔBF between the two ICC sites was 0.2 ± 0.1 octaves. While 0.2 octaves is smaller than the bandwidth of an isofrequency lamina, which is approximately 150 μm at 0.3 octaves (Malmierca et al. 2008), this separation still allowed us to stimulate different populations of neurons residing in neighboring laminae to achieve the goal of this study. The Off-BF DSS protocol was used in three animals, in which two of the animals also received the SSS and DSS protocol. For the DSS protocol, a total of 25 ICC site pairs were stimulated and responses were recorded in 57 A1 locations from thirteen animals. Every DSS stimulation site was also used in the SSS protocol for a total of 50 stimulation sites. For the Off-BF DSS protocol, a total of 9 ICC site pairs were stimulated and responses were recorded in 36 A1 locations.

Electrical stimulation was presented with different levels and varying inter-pulse intervals (**IPIs**), with each stimulus being randomly presented for a total of 20 trials. For the SSS protocol, the IPIs included 0.5, 1, 2, 3, 4, 5, 6, 8, and 10ms, and both pulses were always presented at the same stimulus level. For the DSS and Off-BF DSS protocols, an IPI of 0 ms (simultaneous stimulation) was also used. The DSS stimulation levels varied between the two pulses on different sites because stimulation of different ICC locations

elicits A1 activity with different thresholds (Lim and Anderson 2007b; Neuheiser et al. 2010). Due to restrictions in time, we identified only two or three levels above threshold for one of the sites while stimulating the other site with up to ten levels above its threshold across a 12 dB range. Only levels eliciting A1 activity above threshold but below saturation levels were analyzed. An average of six levels for SSS, 12 levels for DSS, and 11 levels for Off-BF DSS were used for each stimulation case (i.e., ICC-A1 stimulation-recording site pair). For each level, we plotted IPI curves in which the A1 response was shown as a function of IPI. Note that for a given pair of ICC sites for the DSS protocol, we could obtain two different IPI curves by reversing the order of which ICC site was stimulated first. Due to inherent differences in neural activation patterns, we considered each of these two scenarios as different stimulation cases when later presenting the summary data and statistical analyses. This was further validated when fitting neural responses to a linear mixed model, where the predictors were IPI and stimulation order and the random variable was the location of the electrode array. Stimulation order and IPI proved to be significant predictors ($P < 2x10^{-16}$). Linear mixed models were performed using the nlme library in R (Team 2013).

DATA ANALYSIS

Evoked Potential Activity

For IPIs up to 10 ms, only one negative LFP peak was present (e.g., Figure 20A) and the area of the negative peak was calculated. The LFP response, which corresponds to a voltage recording over time, is proportional to current over time based on Ohm's Law (assuming neural tissue can be approximated as a linear medium). Therefore the LFP area

reflects the total charge (i.e., area under a current versus time curve), which is related to the amount of synaptic input into A1 surrounding the recording site (Eggermont and Smith 1995; Mitzdorf 1985). In this study, the LFPs shown were not filtered beyond the filters used in data collection in order to avoid altering the LFP shape, which can vary dramatically depending on the filter range and type. However, averaging the LFP traces across trials in effect is a low-pass filter that smoothed the curves, resulting in a response that is an order of magnitude longer than the time scale of spikes (Figure 20A; tens of milliseconds versus milliseconds).

Calculation of a given LFP area consisted of three steps: removal of the electrical artifact from each recorded LFP trace, averaging the LFP traces across trials, and calculation of the LFP area from the averaged curve by determining the onset, the negative peak, and the end of the LFP. The onset of the LFP was the last transition point before the peak, which was the negative inflection point at least 4 ms after the electrical stimulus. Following the peak, the end of the LFP was the zero-crossing (a return to the y-value of the onset point). Thus a horizontal line was created from the baseline just before the peak to the rising portion of the LFP, and the LFP response was quantified by calculating the area underneath this line with a trapezoidal function.

An issue with LFP area calculation was that the shape, particularly the start point, was sensitive to irregular trials. The auditory cortex is known to be highly sensitive to preceding activity, with periods of synchronized states exhibiting larger, lower frequency waves (Harris et al. 2011). Strong oscillatory responses have also been observed in ketamine anesthetized preparations (Eggermont 1992; Kisley and Gerstein 1999;

Rennaker et al. 2007) and are strongest in medium anesthesia depths (Kisley and Gerstein 1999). To reduce variability in the LFP area calculation, we removed trials that exhibited large sporadic activity preceding our stimulus-driven activity. A trial was removed if the absolute difference between its slope and that of the average slope for a given 25 ms sliding window was greater than three standard deviations. An average of about 17 trials, with a minimum of 14 trials, was included in the calculation of the LFP area for each stimulation case and level.

Spiking Activity

Spikes were detected offline using the same online method described above. The electrical artifact was already removed from the signal for each trial during LFP analysis and prior to filtering the signals from 300-3000 Hz for spike detection. Spikes were summed across a 45 ms window following the onset of the electrical stimulus for all of the same trials included for the LFP analysis. This window was sufficiently long to fully capture the A1 activity elicited by ICC stimulation. The driven spike rate (**DSR**) per trial was calculated by subtracting the spike rate obtained for this 45 ms window by the spontaneous rate obtained for the 20 ms window preceding the electrical stimulus. The FSL was calculated by computing the mean latency of the first spike across all 20 trials. The minimum latency for a given trial was at least 4 ms after the onset of the acoustic tone, which was the shortest latency previously reported (Schreiner and Langner 1988; Syka et al. 2000). If the first spike for a given trial did not occur within 45 ms (i.e., the window also used for DSR calculation), it was counted as a 'miss' and that trial was not included.

The FSL was calculated by computing the mean latency of the first spike across all 20 trials. The minimum latency for a given trial was 3 ms after the onset of the stimulus, which is the shortest latency observed in our data (unpublished observation). If the first spike for a given trial did not occur within 45 ms (i.e., the window also used for DSR calculation), it was counted as a 'miss' and that trial was not included.

Spiking activity in layer V often had putative antidromic activity, which was evident because the spikes exhibited short latencies, low temporal jitter, a sudden increase from no activity to robust spiking per trial with a slight increase in current level above threshold, and isolated activity predominantly in layer V as characterized in a previous publication (Lim and Anderson 2007a). Due to the difficulty of accurately isolating antidromic spikes from the multiunit orthodromic activity, LFP analysis for layer V is included while DSR and FSL analysis for layer V is not.

Normalization

Responses to individual pulses from each stimulation site were also recorded concurrently with each protocol. Because hardware limitations required two stimuli to be presented, a second pulse was applied after the completion of the response to the first pulse at a 60 ms delay (see Figure 20A, Figure 21A, and Figure 22A). Only the response to the first pulse was analyzed and taken as the response to the individual pulse. LFP and DSR responses to the stimulation protocols were normalized by the sum of activity to two individual pulses. Normalized values greater than one were classified as enhanced.

Statistical Analysis

After a Friedman test detected statistically significant differences of normalized

activity with varying IPIs, Wilcoxon Signed-Rank tests were used for comparisons between specific IPIs and the 10 ms IPI. The 10 ms IPI was used as a relative comparison between different IPIs because it was the longest IPI that resulted in a single continuous LFP and spiking response in the cortex. Significance corresponded to $P < 0.05$ after applying the Bonferroni correction for multiple comparisons.

RESULTS

TYPICAL RESPONSES IN DIFFERENT A1 LAYERS

Cortical responses to ICC stimulation greatly varied depending on whether pulses were delivered to one neural population (SSS protocol) or two neural populations (DSS protocol) within the same ICC isofrequency lamina for short delays between the pulses. Figure 20A shows a typical example of how cortical activity from one site in layer III/IV varied in response to the SSS or DSS protocols at one stimulation level.

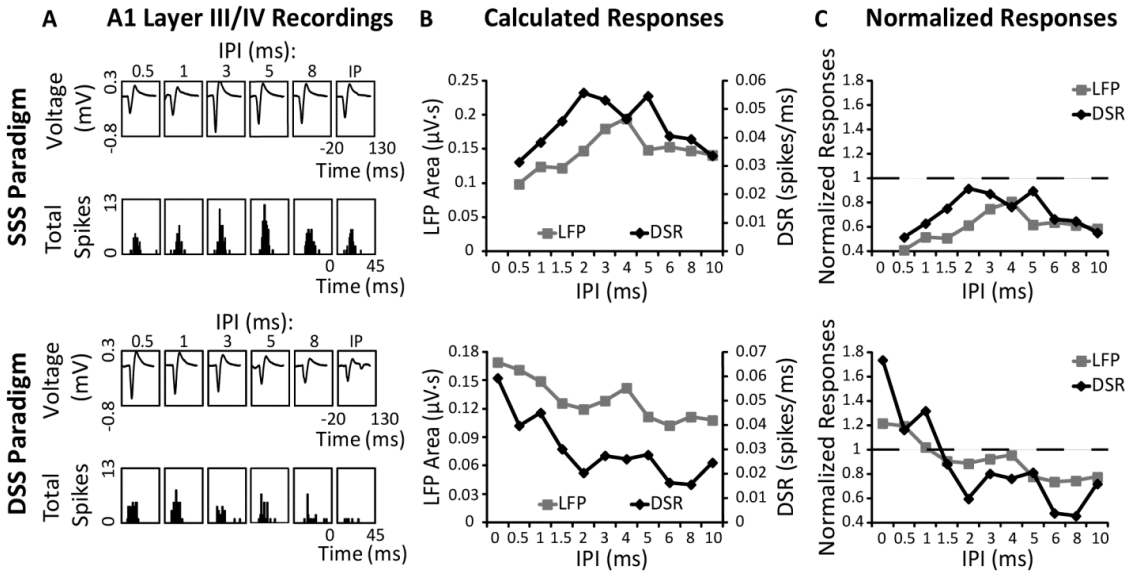

Figure 20: Repeated stimulation of a single site in the ICC (SSS protocol, top half) elicited different response trends in layer III/IV of A1 than stimulating along an isofrequency lamina (DSS protocol, bottom half). In these case examples, the LFP and spiking activity was each recorded in layer III/IV for one stimulation case within one animal in response to one stimulation level. (**A**) LFP and PSTH responses to stimuli with IPIs from 0.5 to 10 ms (left to right columns). Responses to an individual stimulus are also shown, where only the first response was analyzed (see Methods for further explanation). (**B**) Calculated LFP areas and DSRs were then normalized in (**C**) by the sum of responses to the individual pulses to create IPI curves. The normalization factor 1 is indicated by the dashed line. Cortical responses to the SSS protocol first increase as IPI decreases, and then sharply decrease at delays less than about 2-3 ms. In contrast, responses to DSS continue to increase with shorter IPIs and is even enhanced (>1) for very short IPIs. Electrical artifacts were removed in (**A**). Time is relative to initial stimulus onset. DSR, driven spike rate; IP, individual pulse; LFP, local field potential; PSTH, post-stimulus time histogram.

As delays decreased from about 10 to 3 ms, LFP areas and driven spike rates increased for both protocols. However, for IPIs less than about 2-3 ms, the activity decreased for the SSS protocol but continued to increase for the DSS protocol. Responses were

quantified (Figure 20B) and then normalized to the sum of individual responses (Figure 20C) to show IPI curves. **IPI curves** show how normalized responses vary with IPI when stimulating at one level for a single stimulation case (i.e., one A1-ICC location pair from one animal). Across levels and layers, we systematically found that responses to the SSS protocol decreased at very low IPIs. This is likely due to refractory effects, for at very short pulse delays the responses equal that of a single pulse, or a normalized value of 0.5. This indicated that the second pulse did not contribute to the evoked potential already elicited by the first pulse. In contrast, responses to DSS stimulation continued to increase for shorter IPIs, resulting in enhanced cortical activity above a linear sum of the individual responses, or a normalized value of 1.

Using our multi-site arrays, we simultaneously recorded from neural populations across layer I/II, layer III/IV, and layer V of A1. As the IPI decreased, the cortical activity increased in all three layers in response to the DSS protocol, and the extent of increase was much greater for layer I/II compared to the other layers (Figure 21A).

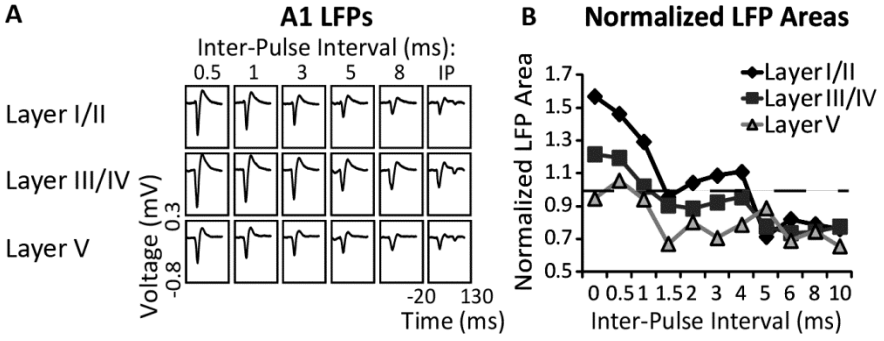

Figure 21: A comparison of LFP responses and IPI curves measured simultaneously in layer I/II, layer III/IV, and layer V of a single A1 shank for one stimulation case. While all cortical layers show larger LFP areas with shorter IPIs when stimulating along an ICC lamina (DSS protocol), layer I/II exhibits the greatest amount of enhancement. (**A**) LFPs recorded in layers I/II (top), III/IV (middle), and V (bottom) of

A1 in response to DSS at IPIs from 0.5 to 10 ms (left to right columns), as well as the response to an individual pulse. (**B**) LFP areas were normalized to the sum of the responses to the individual pulses for the different layers to create IPI curves.

This greater increase is evident in the raw data, for the LFP peak for layer I/II was about half the size of that for layer III/IV at 8 ms IPI but became closer in size as the IPI decreased down to 0.5 and 0 ms. The normalized curves in Figure 21B highlight this layer difference, showing stronger activity at shorter delays for the more superficial layers compared to the deeper layers. We also observed greater spiking activity at short delays for layer I/II as compared to layer III/IV (Figure 22).

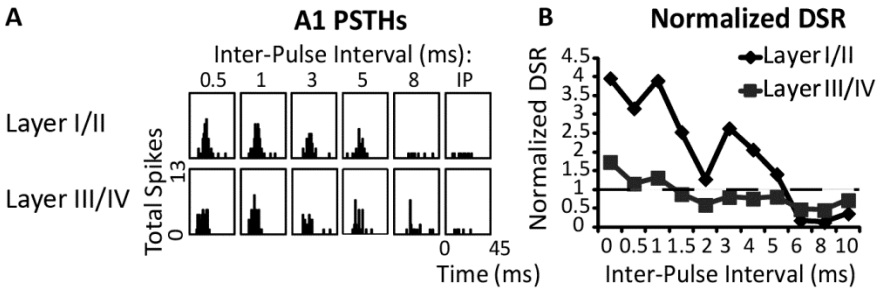

Figure 22: A comparison of DSR responses and IPI curves measured simultaneously in layer I/II and layer III/IV of a single A1 shank for one stimulation case. While both layers I/II and III/IV have greater spiking activity at shorter IPIs when stimulating along an ICC lamina (DSS protocol), layer I/II exhibits a greater amount of enhancement. (A) PSTHs were recorded in layers I/II (top) and III/IV (bottom) of A1 in response to DSS at IPIs from 0.5 to 10 ms (left to right columns) as well as the response to an individual pulse. (B) DSRs were normalized to the sum of the responses to the individual pulses for the different layers.

In the PSTH plots, spiking activity for both layer groups exhibits similarly low responses to an individual pulse. However, the spiking activity increased to a larger extent in layer I/II for shorter IPIs, even exceeding that of layer III/IV. While it was not typical to see

greater levels of neural activity in supragranular layer I/II compared to layer III/IV, it was common to see a greater increase in normalized activity for layer I/II as shown in Figure 22B.

While Figure 20, Figure 21, and Figure 22 highlight responses at specific amplitudes of electrical stimulation, we recorded cortical activity across many stimulation levels in order to investigate potential trends. Figure 23 shows normalized IPI curves recorded in layer III/IV of A1 in response to ICC stimulation across valid levels (see Methods for criteria).

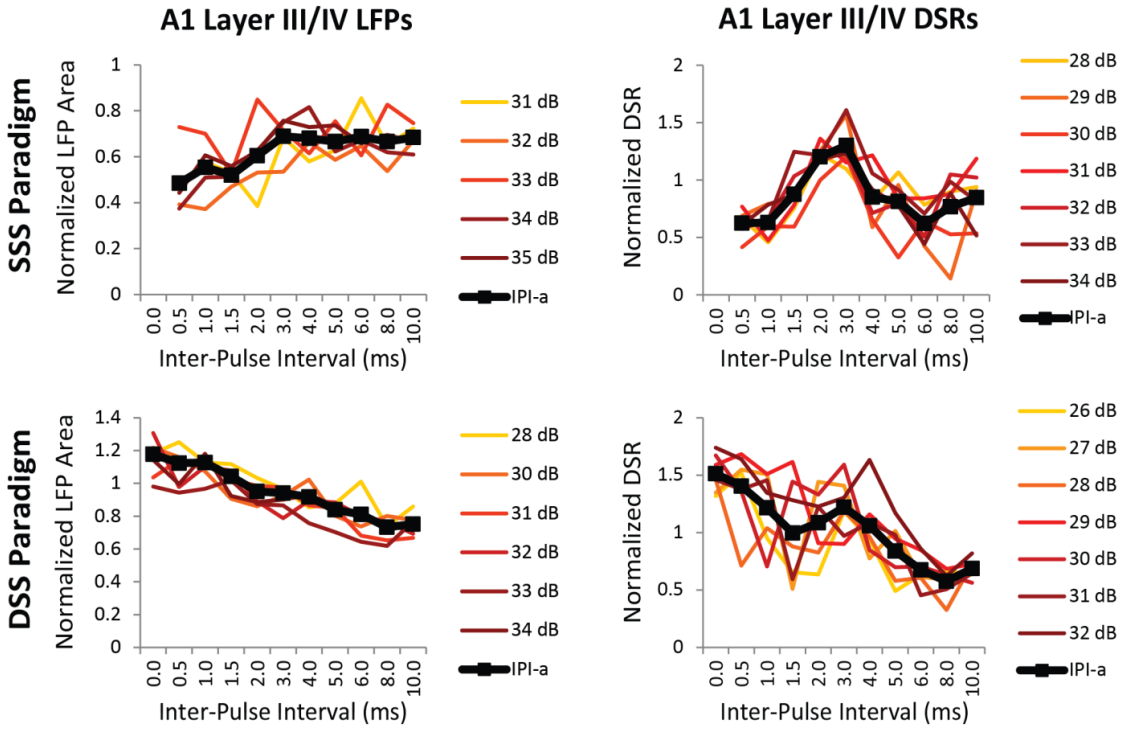

Figure 23: The effects of different stimulation levels on the normalized responses recorded in layer III/IV of A1 for one stimulation case. For the SSS protocol (top row), both pulses were stimulated at the same level. For the DSS protocol (bottom row), one site was stimulated at a constant level while the other site was stimulated at the labeled level on the right side of each plot. The IPI curves for the different levels in each plot were averaged to calculate the IPI-a curve in black. While there were some minor differences in

curves across levels, there were no obvious or consistent trends in level effects observed for both the SSS and DSS protocols for the normalized LFP or DSR data.

These levels were averaged to calculate the **IPI-a curves** (black lines) for a single stimulation case in Figure 23. While some differences were observed between levels, we did not identify any obvious trends. For both LFPs and DSRs, normalized activity due to DSS generally continued to increase with shorter IPIs, while activity in response to SSS typically decreased at shorter IPIs for all valid levels and stimulation cases across animals. Because the IPI-a curve accurately captured the typical cortical response for each stimulation case, we used the IPI-a curves to compare activity across A1 locations and layers in the following sections.

RESPONSES IN DIFFERENT A1 AND ICC LOCATIONS

We investigated whether the DSS curves varied between different cortical columns with similar BFs by comparing simultaneously recorded responses within a designated layer. Figure 24 shows three examples of LFP and DSR responses, such that each example (row) corresponds to layer I/II A1 activity simultaneously recorded in response to stimulation at one ICC location.

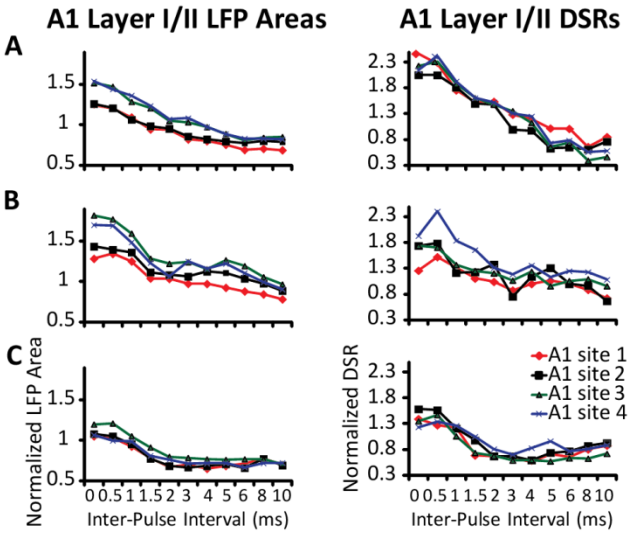

Figure 24: Typical examples of LFP (left column) and DSR (right column) normalized responses to DSS stimulation within three different ICC lamina locations (**A, B, C**). Each plot shows four IPI-a curves corresponding to sites simultaneously recorded in layer I/II across an isofrequency band of A1. The A1 sites in each plot are 400 µm apart and have similar BFs (1.2 kHz for **A** and **B**, 11.8 kHz for **C**). (**A**) and (**B**) responses were recorded in the same A1 location and animal but for different ICC stimulation locations, while (**C**) was recorded from a different animal. The shape and magnitude of IPI-a curves vary more between rather than within each plot (i.e., between **A, B**, and **C**), suggesting that differences in cortical location may not greatly vary the response patterns. Instead, there were greater differences in curve shapes between ICC locations (e.g., **A** and **B** correspond to the same A1 location but different ICC locations).

Layer I/II was presented since we observed the largest enhancement effects compared to those in deeper layers and therefore expect more pronounced differences. Similar trends were observed for the other layers and are not shown. Within each example, the general shape of the IPI-a curves was quite similar across A1 locations though the magnitude of cortical activity could vary. The shape of the IPI-a curves appeared to exhibit greater differences between ICC locations, though this observation needs to be validated in

further experiments (see Chapter 2B).

SUMMARY ACROSS LOCATIONS AND ANIMALS

Because of the similarity in patterns of IPI-a curves, we averaged IPI-a curves across all stimulation cases and animals to create **mean IPI-a curves** for a given layer, stimulation protocol, and data type (i.e., LFP or DSR) in Figure 25.

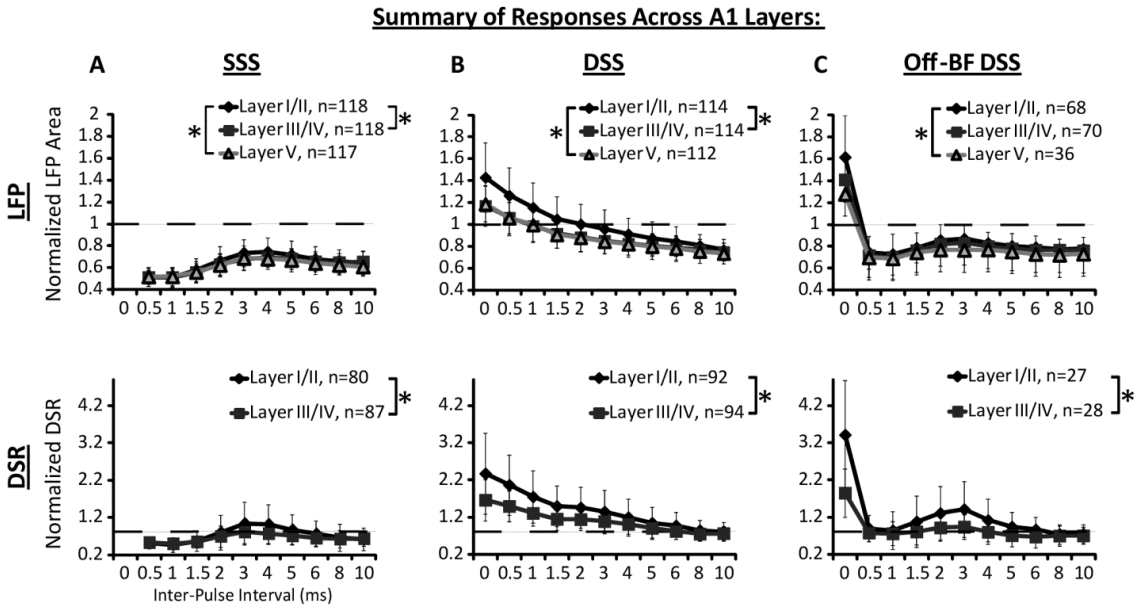

Figure 25: Summary of responses across A1 layers. LFP (top) and DSR (bottom) IPI-a curves were averaged across all stimulation cases and animals. These mean IPI-a curves were obtained for layers I/II, III/IV, and V of A1 in response to SSS (**A**), DSS (**B**) and Off-BF DSS (**C**) protocols. Significantly increased activity was found for layer I/II compared to the deeper layers for specific IPIs longer than 0 ms (marked by asterisks; see text for IPIs and p-values). n refers to the number IPI-a curves, each corresponding to a different stimulation case. Error bars are standard deviations across stimulation cases.

The LFP and DSR responses to DSS and SSS stimulation are shown in Figure 25A and Figure 25B for different cortical layers, confirming the results from the individual cases presented above. As shown in Figure 25B, similar trends were observed for both the LFP

and DSR results, though the DSR data showed larger values of normalized cortical activity. Within each mean IPI-a curve, normalized responses at each IPI were statistically compared to those at the 10 ms IPI, which was the longest IPI that consistently elicited a single continuous LFP or spiking response in the cortex. As IPIs decreased from 10 ms, SSS caused the LFP areas and DSRs to first increase and then decrease towards that of a single pulse for all cortical layers (Figure 25A). Responses to SSS were significantly below that of the 10 ms normalized response at IPIs of $\leq$ 1.5 ms for LFPs and $\leq$ 1 ms for DSRs ($P < 0.05$), with responses at 0.5 ms at or near the normalized value of 0.5. In addition, responses at 4-5 ms IPI were significantly above that of 10 ms IPI for LFPs and responses between 3-5 ms IPI were significantly above that of 10 ms IPI for DSRs ($P < 0.05$). These results suggest SSS may achieve some increased activity for shorter IPIs but is limited by the refractory-like properties of the same neurons being activated to the second pulse. In contrast, DSS caused responses to increase for decreasing IPIs with the short IPI responses exceeding 1 (dashed line) for all layers. Responses to DSS were significantly larger than that at 10 ms IPI for IPIs $\leq$ 6 ms for LFPs and DSRs ($P < 0.05$). These average results were consistent with almost all stimulation cases (99%), in which only 4 IPI-a curves out of 526 were approximately flat.

Consistent with the individual DSS examples shown in the previous sections, DSR and LFP responses in layer I/II were significantly larger than those in deeper layers for IPIs $\leq$ 8 ms ($P < 0.05$). Responses for SSS were also significantly larger for layer I/II compared to the deeper layers for IPIs between 2-6 ms for LFPs and 3-5 ms for DSRs ($P < 0.05$). These results suggest that co-activation of neurons within an ICC lamina elicits

greater enhanced activity along the thalamocortical or corticocortical pathway within supragranular layers of A1 compared to the deeper layers.

One relevant question is if this enhancement effect can also be achieved by co-activating neurons across different frequency laminae. Figure 25C shows the mean IPI-a curves when stimulating two sites located 100 μm apart in different frequency regions of the ICC with the Off-BF DSS protocol. Overall, the Off-BF DSS curves looked similar to those for SSS in which there was a slight rise in activity as the IPIs decreased from 10 ms that then started to decrease at about 2-3 ms. However, the curves did not approach a normalized value of 0.5 for short IPIs as occurred for SSS possibly because stimulation may not induce complete refraction to the first pulse. The two stimulated sites for Off-BF DSS are far enough apart that non-overlapping and non-activated neurons can still be activated by the second pulse (i.e., second site). At an IPI of 0 ms, there is a sudden increase in activity, which is likely caused by current summation that simultaneously activates a larger volume of neurons. An important observation from Figure 25C is that current summation seems to predominantly occur for IPIs less than 0.5 ms. Especially since the sites are spaced much farther apart for DSS than for Off-BF DSS, this further supports that the increase in activity for shorter IPIs for DSS, at least down to 0.5 ms, is caused by a functional interaction between neurons within an ICC lamina rather than an artificial effect of current summation.

It is evident that the Off-BF DSS responses are unlike the DSS in that the curves do not continue to increase with shorter IPIs. This indicates that the same integration mechanism achieved by stimulating different neural populations within an ICC lamina

cannot be effectively accessed by stimulating different neural populations across ICC laminae.

For both LFPs and DSRs ($P < 0.05$), the cortical activity at 0 ms IPI was significantly greater than that at the 10 ms IPI in layers I/II and III/IV in response to the Off-BF DSS protocol. Similar to the SSS data, the cortical activity for IPIs at 2-4ms for LFPs and DSRs ($P < 0.05$) in layers I/II and III/IV was significantly greater than that at the 10 ms IPI. Consistent with SSS and DSS, the activity was also significantly larger in layer I/II than deeper layers for IPIs between 2-6 ms for LFPs and DSRs ($P < 0.05$).

LATENCY

The previous results showed that, in response to DSS at short IPIs, normalized cortical activity was greater in supragranular than granular layers of A1. In order to better understand the mechanism involved in this increased supragranular enhancement, we calculated the mean FSL of each stimulation case for both A1 layers. The mean FSL was determined by averaging FSL across the same stimulation levels as the normalized LFP areas and DSRs above. We found the mean FSL was ~8 ms across all layer III/IV sites and ~ 11 ms for across all layer I/II sites, as shown by histograms in Figure 26A and B, respectively.

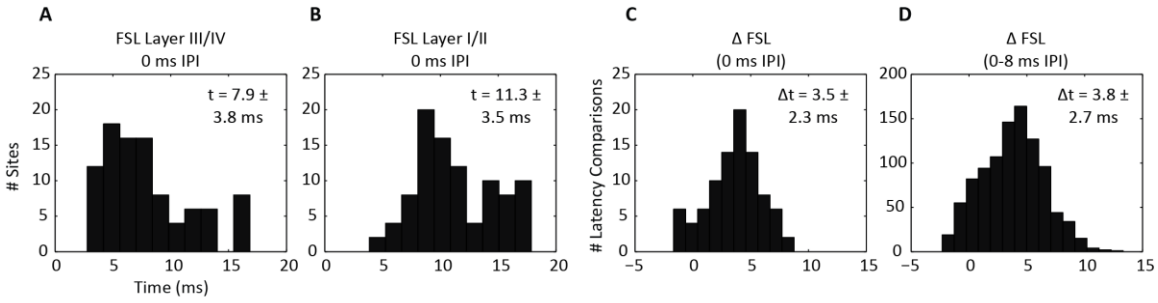

Figure 26: Histograms of FSLs for all stimulation cases recorded in layer III/IV (**A**) and layer I/II (**B**) at the 0 ms IPI. When comparing sites recorded from the same A1 location, FSLs recorded in layer I/II were on average ~ 4 ms longer than those in layer III/IV at the 0 ms IPI (**C**) as well as all IPIs from 0-8 ms (**D**).

For A1 placements from which both layer I/II and layer III/IV sites were simultaneously recorded, we calculated the difference between the FSL at layer I/II and layer III/IV and found this ΔFSL to be 3.5 ± 3.2 ms for the 0 ms IPI, as shown Figure 26C. This ΔFSL value was consistent for all IPIs, with no trends between ΔFSL and IPIs. Thus, the distribution of latencies for the 0 ms IPI (Figure 26C) was similar to the distribution of latencies for all IPIs (Figure 26D).

DISCUSSION

Repeated stimulation of a single ICC neural population induces strong refractory effects in A1 for IPIs shorter than 2-3 ms. In contrast, activation of two different ICC populations within the same lamina elicits increased A1 activity with shorter IPIs from 6 ms down to 0 ms. Increased A1 activity with shorter IPIs did not occur for stimulation of two sites in different ICC laminae, except at the 0 ms IPI associated with current summation. These results suggest that an enhancement mechanism exists within the ICC-to-A1 pathway that can functionally integrate activation on a fast temporal scale (<6 ms

window) from different neural populations mainly originating from the same ICC lamina. Enhanced activity was observed across layers I-V of A1, with the greatest increase in activity within layer I/II.

Functional Role of the Enhancement Mechanism

The differences observed between SSS and DSS activation for short IPIs are consistent with previous results presented by Calixto et al. (2012) in which the ICC was stimulated with an AMI array that consisted of much larger sites (126,000 μm^2 versus 413 μm^2) and only LFPs recorded in layer III/IV of A1 were used for analysis. In general, IPIs below 2-3 ms for SSS exhibit strong refractory effects, perhaps because ICC neurons are unable to be reactivated in such a short period of time (Sivaramakrishnan and Oliver 2006). However, as also reported by Calixto et al. (2012), we did not observe any obvious differences in this refractory-like effect across stimulation levels (e.g., SSS curves in Figure 23). It would be expected that increasing the current level would activate a larger population of neurons within the ICC. Considering that the ICC consists of an inhomogeneous network of different types of neurons (Oliver 1984; 2005), different levels should activate neurons with varying activation and refractory effects. Because of this inhomogeneity, we expected much greater differences in IPI curves across levels than observed in our study. At IPIs above 2-3 ms, the responses to SSS follow the same general pattern as observed for DSS. This suggests that both SSS and DSS may have access to the same enhancement mechanism, but SSS is limited by refractory effects.

We also showed that co-activation of neurons across different frequency regions was not able to access this enhancement mechanism, which is consistent with studies

showing that specific ICC regions project to and activate specific MGV and A1 regions in a tonotopic pattern (Lim and Anderson 2006; Malmierca et al. 1997; McMullen et al. 2005). The enhancement mechanism across frequency regions may have been masked by lateral inhibition, for bandwidths in the MGV and A1 have shown to be less than 0.2 octaves for sharply tuned units (Bartlett et al. 2011). However, excitatory bandwidths have shown to vary from 0.1 octaves to over an octave along an isofrequency band of A1 (Schreiner and Mendelson 1990; Schreiner et al. 2000; Schreiner and Sutter 1992), and we would expect this variation to cause large differences in the IPI-a curves across cortical locations. In contrast, we found similar profiles across medial-to-lateral locations along the isofrequency dimension of A1 that were recorded simultaneously in response to stimulation of the same ICC sites (data not shown). Moreover, the similarity in the shape of the IPI-a curves between the Off-BF DSS and SSS further suggests that the integration mechanism requires activation of neurons within multiple locations along an ICC lamina, which was not possible with both of these protocols. Regardless of the role of lateral inhibition, the integration mechanism could not be achieved by stimulating neurons in different ICC laminae.

We propose that the enhancement mechanism identified in this study is designed to integrate activation of different neurons within a given ICC isofrequency lamina and could contribute to the coding of various acoustic features that rely on a population code with short inter-spike intervals. One possible role of this enhancement mechanism relevant for the AMI is in coding for fast temporal information. Individual ICC neurons cannot follow fast temporal patterns beyond hundreds of hertz (within ~5-10 ms range)

(Joris et al. 2004; Krishna and Semple 2000). Instead, it seems plausible that populations of neurons along an ICC lamina are designed to code for fast features through a synchrony or spike-interval code that then results in converging activity onto different A1 neurons via the MGV to elicit varying firing rates. Consistent with this explanation, a previous study showed that individual ICC neurons fire in a sparse and precisely timed pattern to stimuli, rarely fire more than once within a 10 ms window, and are temporally correlated with other neurons mainly within the same lamina and with inter-spike delays of less than roughly 5 ms (Chen et al. 2012). In other words, coding for sound features within the ICC on a time scale of less than 10 ms should involve neurons within a similar lamina that fire in a correlated pattern. We have identified an integration mechanism from ICC to A1 that can actually process this type of co-activity across of multiple ICC neurons with spike-intervals less than 6 ms (Figure 25B) to elicit enhanced activity across A1, especially in supragranular layers.

Psychophysical results in humans further suggest that this enhancement mechanism may be involved with transmitting fast temporal features to higher cortical centers. Both acoustic and CI stimulation studies have identified short-term temporal integration in which presentation of repeated clicks or electrical pulses with shorter inter-stimulus intervals (within ~5 ms) elicits a louder sensation or lower detection threshold (Flanagan 1961; McKay and McDermott 1998; Viemeister and Wakefield 1991). Generally, short-term temporal integration can be viewed as a sliding neural window that integrates and tracks the rapid changes in the sound waveform (Forrest and Green 1987; Oxenham and Moore 1994; Viemeister 1979). The shape and time scale of this perceptual

short-term integrator as a function of IPI for acoustic clicks or CI pulses is quite similar to the IPI-a curves presented in Figure 25B. Therefore, short-term temporal integration may be coded from ICC to A1 by integrating inputs from different neurons along an ICC lamina.

It is important to note that our results are based on electrical stimulation of the ICC, which can induce greater synchronized activation across neurons surrounding the stimulated sites than typically occurs to acoustic stimulation. The neural integration and enhancement effect observed from ICC to A1 in our study needs to be further investigated in acoustic stimulation experiments, especially in identifying its functional role in processing different sound features. Nevertheless, our results demonstrate the existence of a neural mechanism for different neurons along an ICC lamina to interact with each other on a fast time scale and alter activity in A1, which is absent or at least differs from what exists across different ICC laminae.

Potential Neural Mechanisms Underlying Cortical Enhancement

The DSS enhancement effects were unlikely to have been caused by current summation or antidromic activation. Current summation can occur for short IPIs for overlapping current fields, but any charge accumulation on the membranes of overlapping stimulated neurons should dissipate faster than 1 ms based on chronaxie values (Grill et al. 2005; Miocinovic and Grill 2004; Ranck 1975). Moreover, increased activity was not present at the 0.5 ms IPI for the SSS or Off-BF DSS protocols, and thus any increased activity at or above 0.5 ms IPI for the DSS protocol cannot be simply due to current summation. In terms of antidromic activation effects, we observed antidromic

spikes in A1 layer V in response to stimulation of 62% of the ICC sites. It is possible that antidromically stimulating the corticofugal axons in ICC could activate axon collaterals projecting from layer V up to more superficial layers (Winer and Prieto 2001) that would then prime A1 neurons to enhance the activity to a second pulse. However, stimulating 38% of ICC sites did not elicit any noticeable antidromic activity across A1 at levels which orthodromic activity was prevalent, yet we still observed large increased or enhanced responses with almost every DSS case. Moreover, the cortical activity recorded across layers I-V in response to DSS was significantly larger when antidromic activity was not detected as compared to when it was detected for IPIs between 0.5-1.5 ms for LFP ($P < 0.03$) and 0.5-1 ms for DSR ($P < 0.02$), with other IPIs not showing statistical differences. If antidromic activity was the primary cause of the increased cortical activity, we would expect that the activity would have been greater rather than smaller when antidromic activity was detected. Therefore, it is unlikely that antidromic activation is the primary cause of the enhancement effect.

The enhanced activity in A1 can be observed in layer III/IV LFPs, which reflect the synaptic input from MGV, and layer III/IV DSRs, giving evidence that the tectothalamic, thalamocortical, or corticocortical pathways may be involved individually or in concert to integrate responses from an ICC lamina. In the tectothalamic pathway, ICC neurons diverge and synapse onto a larger span of isofrequency thalamic neurons and a large span of ICC neurons converge onto the same thalamic neurons with excitatory synapses (Bartlett and Smith 1999; Cetas et al. 2003; Lee and Sherman 2010b; McMullen et al. 2005). Therefore, stimulation of two different ICC populations with shorter

intervals could sufficiently activate overlapping MGV populations and transmit increased excitation to A1 (Broicher et al. 2010; Cruikshank et al. 2002). This increased excitation could be caused by several mechanisms within the thalamocortical pathway. A greater number of MGV neurons could be activated that then converge onto and elicit enhanced activity in the same A1 neurons. It is also possible that the same MGV neurons are repeatedly activated due to converging inputs from different ICC neurons, causing the thalamic neurons to fire in a burst mode (Sherman 2001; Swadlow and Gusev 2001). This high-frequency firing could elicit enhanced activity in the same A1 neurons. At least in the visual system, it has been shown that two thalamocortical neurons activated within ~7 ms window can more robustly elicit a cortical response (i.e., a supralinear effect that is stronger for shorter inter-spike intervals) compared to that of a single thalamocortical neuron (Usrey et al. 2000). Repeated activation of the same thalamocortical neuron can also elicit enhanced cortical activity but with a slower inter-spike interval scale (a window of ~15 ms). If similar synaptic effects exist between the visual and auditory systems and considering the similarity in the window time scale of ~7 ms with our results of 6 ms, the enhanced activity in layers III/IV of A1 could be largely attributed to activation of different MGV neurons caused by DSS, which is not possible with SSS. Moreover, in the auditory system of ketamine-anesthetized guinea pigs, most MGV neurons respond with single or double spikes while nonlemniscal thalamic neurons typically respond with bursting patterns (He and Hu 2002; Hu 1995). Further evidence that the enhancement effect may be associated with the thalamocortical pathway is provided by studies that have performed intracellular recordings in A1 neurons and

revealed a strong inhibitory component that quenches preceding excitatory inputs within about 4 ms (Tan and Wehr 2009; Wehr and Zador 2003), which is consistent with the time scale of our 6 ms enhancement window. Perhaps the same temporal sequence for thalamocortical transmission in which cortical neurons receive excitatory inputs, followed by inhibitory inputs, is also active in narrowing the window for the integration in our study.

We observed the greatest enhancement in supragranular layers of A1, which may be due to lemniscal or non-lemniscal thalamocortical projections as well as corticocortical projections as proposed in Figure 27.

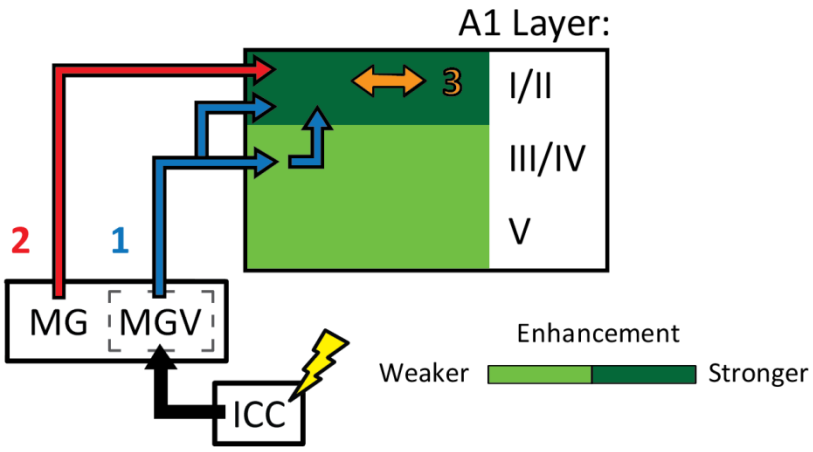

Figure 27: Pathways that may contribute to the enhanced activity within supragranular layers in response to co-activation of ICC neurons. Initial enhancement may occur via the lemniscal pathway (Pathway 1). The MGV could integrate responses from different neurons along an ICC lamina and then project to layer I/II in AI through layer III/IV and/or through direct feedforward mechanisms (Cetas et al. 1999; Huang and Winer 2000; Mitani et al. 1985). The feedforward axon collaterals originating from layer III/IV may prime responses in layer I/II. The supragranular layers could also be integrating converging responses from layer III/IV. In addition, layer I/II could be primed by giant axons from the MG (Pathway 2) (Huang and Winer

2000; Lee 2012; Winer et al. 2005) or via horizontal connections across supragranular layers (Pathway 3) (Lee 2012; Winer 2010; Winer 1985).

Within lemniscal projections, supragranular layers could integrate responses across granular layers or be primed by tonotopic thalamocortical projections, which primarily target layer III/IV but also have collaterals that extend to layer I (branching arrow in Pathway 1, Figure 27) (Cetas et al. 1999; Huang and Winer 2000; Mitani et al. 1985). These collaterals are thought to synchronize temporal feedback and feedforward processes between corticocortical and corticofugal circuits (Huang and Winer 2000; Lee 2012; Winer et al. 2005). Non-lemniscal projections could also prime supragranular layers (Pathway 2, Figure 27), in which the earliest thalamic signals may arrive at the cortex in layer I via giant axons that predominantly originate in the MGM (Huang and Winer 2000; Lee 2012). However, the longer latencies (of approximately 3 ms) in supragranular layers as compared to granular layers suggest that these pathways are unlikely to directly result in increased spiking. Moreover, this latency difference does not decrease with shorter IPIs despite the fact that shorter IPIS typically result in greater spiking rates. The consistency of ΔFSLs across IPIs suggests that this is not a result of any mechanism unique to DSS co-activation. Instead, it seems likely that the transmission time between layer III/IV and layer I/II is on average ~3 ms, and that the increased enhancement in supragranular layers is due to mechanisms with longer latencies than the enhancement seen in granular layers through either lemniscal thalamocortical or corticocortical projections. With the corticocortical projections, the horizontal projections in supragranular layers (Winer 2010) may contribute to lateral inhibition even at long

ranges (Moeller et al. 2010) that could alter spike timing and integration of the neurons (Pathway 3, Figure 27). In addition, supragranular layers may utilize several pathways, for layer II is thought to act as a hub which integrates responses from layer I and layer III cells before sending information to layer V and VI cells (Mitani et al. 1985). In other words, supragranular layers may be responsible for integrating thalamocortical and corticocortical information before sending it to corticofugal projections.

CHAPTER 3B: CORTICAL ENHANCEMENT FROM DSS VARIES WITH ICC BUT NOT A1 LOCATIONS

Repeated electrical stimulation of a single site in the ICC has been shown to cause strong suppressive and refractory effects in elicited responses within A1. These effects can be circumvented by stimulation of at least two sites within an isofrequency lamina, which at short inter-site delays (<5 ms) can elicit cortical activity which is enhanced beyond the summation of activity induced by the individual sites. This enhancement, prevalent throughout cortical layers, is largest in supragranular layers. In this study, we investigated whether cortical enhancement varies with the stimulation location of co-activated ICC neurons or recording location across A1. We electrically stimulated two locations within the 10 kHz ICC lamina with varying short delays and recorded activity in different locations of A1 of ketamine-anesthetized guinea pigs. Although the enhancement was not correlated with the A1 recording location, we found that rostral-lateral regions of the ICC resulted in greater normalized cortical activity at very short delays than caudal-medial regions. These ICC regions also differentially responded to both acoustic and electric stimulation. In response to pure tones, the rostral-lateral regions responded with greater spatial and temporal synchrony than caudal-medial regions. In response to electrical stimulation of A1, excitatory activity could be elicited from functional descending projections to caudal-medial and not rostral-lateral regions. These

results suggest that the two ICC regions are distinct, and that auditory neuroprostheses implanted in the midbrain may need to target rostral-lateral regions for better performance.

INTRODUCTION

Hearing loss has been treated with auditory prostheses such as the CI or ABI for decades. By stimulating along the tonotopic gradient of the auditory nerve within the cochlea, the CI is able to provide sufficient temporal and spectral cues required for speech understanding (Kral and O'Donoghue 2010; Shannon et al. 1995; Zeng 2004). For people without an implantable cochlea or functioning auditory nerve, ABIs have been used as an alternative to the CI. The primary patient group targeted for ABIs are those with NF2, a genetic disorder in which bilateral tumors develop along the auditory nerves. Unfortunately, ABIs typically results in poorer performance than CIs, particularly for NF2 patients (Colletti et al. 2009; Lim et al. 2009; Schwartz et al. 2008), though some recent ABI patients have shown performance levels approaching that of CI patients (Colletti et al. 2012; Sennaroglu et al. 2011). As an alternative approach to the ABI, a new AMI was developed for stimulation along the tonotopic gradient of the ICC (Lim et al. 2009; Lim et al. 2007). Consisting of a single-shank array (20 sites), the AMI was recently implanted in five NF2 patients. While AMI stimulation can activate frequency-specific neurons and transmit spectral cues to higher auditory centers, it appears to exhibit limited temporal coding abilities (Lenarz et al. 2006a; Lim and Anderson 2006; Lim et al. 2013; Lim et al. 2008b; McKay et al. 2013).

Calixto et al. (2012) investigated this limitation of the AMI by activating the ICC of guinea pigs with the AMI array and recording the evoked LFPs in the A1. They found that repeated stimulation of a population of neurons with the AMI causes refractory and suppressive neural effects of LFPs in layer III/IV of A1. These negative effects, which may have caused the limited temporal coding of the AMI, could be overcome by stimulating at multiple sites (and subsequently multiple neuronal populations) within an isofrequency lamina. Similar results were also seen for LFPs and spiking in supragranular, granular, and infragranular layers across A1 in response to ICC stimulation with much smaller sites (413 μm^2 versus 126,000 μm^2) (Straka et al. 2013). In addition, the co-activation of sites with short delays (<6 ms) resulted in cortical activity which was enhanced beyond a linear sum of activation elicited by the individual sites, with the strongest enhancement in supragranular layers. Although cortical enhancement did not appear to be affected by the recording location across A1, preliminary data suggested that it was influenced by the stimulation location across the ICC isofrequency lamina.

The location of stimulation across an ICC isofrequency lamina is expected to impact cortical responses because specific ICC regions differ in physiological responses as well as anatomical inputs and outputs. Maps for response properties have been found across the isofrequency lamina, including periodicity coding properties such as best modulation frequency and spike latencies (Schreiner and Langner 1988) (Langner et al. 2002), binaural properties (Brückner and Rübsamen 1995; Roth et al. 1978; Semple and Aitkin 1979; Wenstrup et al. 1985), and threshold and tuning properties (Hage and Ehret 2003;

Stiebler 1986; Stiebler and Ehret 1985). We had previously shown that first spike latency, first spike jitter, duration of the PSTH response, LFP peak magnitude, and LFP peak time vary caudal-medially to rostral-laterally in anesthetized guinea pig (see Chapter 2). These different response properties across the ICC isofrequency laminae may arise from differences in input and output projection patterns. Anatomical studies have found spatially distinct functional zones within the ICC as a result of different projections from the brainstem (Brunso-Bechtold et al. 1981; Cant and Benson 2006; Loftus et al. 2004; Oliver et al. 1997; Shneiderman and Henkel 1987). In the gerbil, the two zones are located in the rostral-lateral and caudal-medial regions of the ICC and differentially project to rostral and caudal regions of the MGV, respectively (Cant and Benson 2007).

Differences across the ICC isofrequency lamina are further supported by electrophysiological studies which found that stimulation of the rostral-lateral and caudal-medial regions of the ICC elicits different responses in A1. In contrast to rostral-lateral regions, stimulation of the caudal-medial regions of the ICC requires higher activation thresholds, and evoked potentials in A1 are smaller in magnitude, have longer latencies, and have larger discriminable level steps (Lim and Anderson 2007b; Neuheiser et al. 2010). Since these cortical activation properties are evident when stimulating with individual pulses across the ICC lamina, cortical activity is expected to also vary based on ICC location when co-activating multiple neuronal populations.

In this study, we investigated the relationship between cortical responses and the location of co-activating ICC neurons with short IPIs. By using fewer delays than in our previous study (Straka et al. 2013), we stimulated from more locations across the ICC

lamina per animal to create a more complete location map than possible in Chapter 3A. We also re-examined whether locations across A1 also contributed to varying degrees of enhancement. As with our previous study, we did not find differences in enhancement across cortical locations. However, we found that stimulating rostral-lateral regions of the ICC led to stronger cortical activity and even greater enhancement in supragranular layers in contrast to caudal-medial regions. When comparing with other studies from our lab, these caudal-medial regions exhibit different responses to acoustic tones (see Chapter 2) and can be driven by electrical stimulation of A1 (Markovitz et al. 2013), in contrast to rostral-lateral regions.

METHODS

OVERVIEW

Basic surgical procedures and methods for neural recording and stimulation were similar to those presented in previous work (Lim and Anderson 2007a; 2006; Straka et al. 2013). Ketamine-anesthetized guinea pigs were used in accordance with policies of the University of Minnesota's Institutional Animal Care and Use Committee. Silicon-substrate, 32-site Michigan electrode arrays (NeuroNexus Technologies, Ann Arbor, MI) were used to electrically stimulate the ICC and record the corresponding neural responses within A1. Appropriate placement of the array sites within the ICC and A1 was guided by acoustic-driven responses (Lim and Anderson 2007b; Snyder et al. 2004; Wallace et al. 2000). Multi-unit spiking activity and LFPs were recorded in response to application of a single pulse at each of two sites within the same isofrequency lamina with varying delays

between the two pulses. These experiments investigated how cortical activation throughout A1 varied when stimulating different neurons across an isofrequency lamina.

Surgery

Experiments were performed on thirteen male and female Hartley guinea pigs (387 ± 57 g, Elm Hill Breeding Labs, Chelmsford, MA). Animals were initially anesthetized with an intramuscular injection of ketamine (40 mg/kg) and xylazine (10 mg/kg), and were given periodic supplements to maintain an areflexive state. After fixing the animal into a stereotaxic frame (David Kopf Instruments, Tujunga, CA), the right side of the cortex was exposed from the caudal end of the occipital lobe to the middle cerebral artery of the temporal lobe. The dura was removed, micromanipulators were used to insert the arrays into the ICC and A1, and the exposed brain was covered with agarose gel.

Stimulation and Recording Setup

All experiments were performed in an acoustically- and electrically-shielded chamber and controlled by a computer interfaced with TDT System 3 hardware (Tucker-Davis Technology, Alachua, FL) using custom software written in MATLAB (MathWorks, Natick, MA). For acoustic stimulation, sound was presented via a speaker coupled to the left ear through a hollow ear bar. The speaker-ear bar system was calibrated using a 0.25-in. condenser microphone (ACO Pacific, Belmont, CA) connected to the ear bar via a short plastic tube representing the ear canal.

All neural signals were passed through analog DC-blocking and anti-aliasing filters from 1.6 Hz to 7.5 kHz. The sampling frequency used for acoustic stimulation was 195 kHz and for neural recording was 24 kHz. Electrical stimulation up to 100 μA was

presented on different sites on the ICC array in a monopolar configuration with a ground return in the neck muscles. The pulses were biphasic, charge-balanced, cathodic-leading, and 205 μs/phase. The recording ground needle was positioned either under the skin approximately 2 cm rostral to bregma or directly in the brain in the parietal lobe. No obvious differences in results were observed when using the different recording grounds.

PLACEMENT OF ARRAYS

PSTHs and FRMs of spiking activity were plotted online to confirm the array's position within the ICC or A1. Details on these analysis methods and example plots for similar types of arrays are presented in previous publications (Lenarz et al. 2006a; Lim and Anderson 2006; Neuheiser et al. 2010). The BF was taken as the centroid of frequencies which elicited spiking responses at 10 dB above the visually-determined threshold.

The A1 array consisted of four 5-mm-long shanks separated by 400 μm. Sites were linearly spaced at 200 μm along the shank and each had an area of 177 μm^2. The array was inserted approximately perpendicular to the cortical surface in an attempt to align each shank along a column in A1 (Abeles and Goldstein 1970; Redies et al. 1989b; Wallace et al. 2000). For each shank, the average **ΔBF** between sites in layers I/II, III/IV, and V was 0.08 ± 0.08 octaves (mean ± SD), which is less than the local critical frequency scatter of up to 0.4 octaves which can be seen in isofrequency bands of A1 (Schreiner et al. 2000; Schreiner and Sutter 1992). The similarity in BF suggests placements may have been in one BF column, though this was not confirmed with histology. Placement into A1 was confirmed when tonotopic shifts from low to high BFs

were observed for ventral-rostral to dorsal-caudal locations (Wallace et al. 2000). Only A1 sites with similar BFs to the stimulated ICC sites were analyzed (ICC-to-A1 ΔBF: 0.2 ± 0.1 octaves). To investigate differences across A1 locations, we reconstructed the site locations on the A1 surface based on microscope images (OPMI 1 FR pro, Zeiss, Dublin, CA) taken of our array placements and normalized based on various landmarks (e.g., middle cerebral artery, bregma and lateral suture lines, major blood vessels) as successfully used in previous studies (Eggermont and Roberts 2004; Schreiner et al. 2000; Wallace et al. 2000). These normalized locations and their respective BFs can be seen overlaid on the auditory cortex in Figure 28.

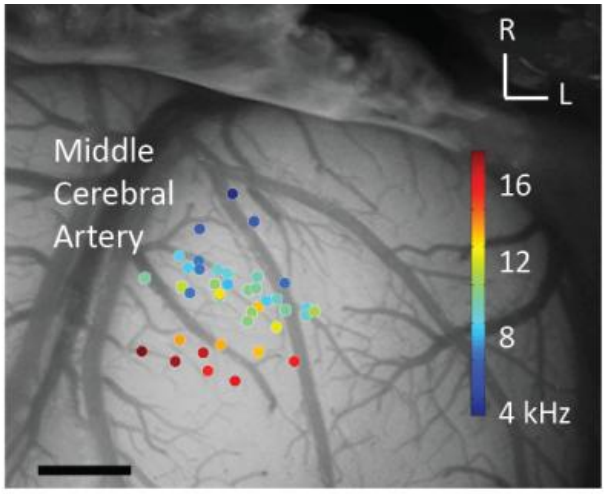

Figure 28: All recorded A1 locations which were BF-matched to ICC site pairs are overlaid on a typical guinea pig cortex. Colors represent the average BF recorded in that location from layers I-V. Scale bar is 1 mm.

The identification of A1 layers was accomplished by performing CSD analysis (Kral et al. 2000; Mitzdorf 1985; Muller-Preuss and Mitzdorf 1984) in response to 70 dB SPL broadband noise (100 trials) using the finite difference formula:

$$CSD(z) = \sigma_z \frac{\phi(z+\Delta z) - 2\phi(z) + \phi(z-\Delta z)}{(\Delta z)^2}$$

where ϕ is the averaged LFP across trials, z is the depth location of each site along an A1 array shank, Δz is the differentiation step size, and σ_z is the component of conductivity in the z-direction. Δz was equal to the A1 site spacing of 200 μm and σ_z was set to one since absolute CSD values were not required for analysis. The one-dimensional CSD approximation provides a consistent representation for the current sinks and sources associated with columnar synaptic activity in the guinea pig auditory cortex (Lim and Anderson 2007a; Middlebrooks 2008). The main input layer of A1, which is layer III/IV in guinea pig (Huang and Winer 2000; Smith and Populin 2001), corresponded to the site with the shortest latency current sink (i.e., positive CSD peak). Layer V was identified as the site with a current source (i.e., negative CSD peak), typically being two electrode sites (or 400 μm) deeper than layer III/IV. Supragranular layers, here combined as layer I/II, corresponded to two electrode sites (or 400 μm) shallower than layer III/IV.

The ICC array consisted either of four 8-mm-long shanks or of two 10-mm-long shanks. For both arrays, each shank was separated by 500 μm and sites were linearly spaced at 100 μm along the shank. Each site had an area of approximately 700 μm^2. Prior to the experiment, the sites on the ICC array were activated using cyclic voltammetry to enable both recording and stimulation up to 100 μA (Anderson et al. 1989; Lim and Anderson 2006). The ICC array was placed at a 45° angle to the sagittal plane through the visual cortex in order to be aligned along the tonotopic axis of the ICC (Malmierca et al. 1995; Snyder et al. 2004), with the shanks aligned in the caudal to rostral direction.

Proper array placement in the ICC was confirmed by observing FRMs that exhibited an orderly shift from low to high BFs from superficial to deeper locations along a shank (Lim and Anderson 2006; Snyder et al. 2004).

ELECTRICAL STIMULATION PARAMETERS

We electrically stimulated two sites within the ICC with similar BFs and characterized the corresponding LFP and spiking activity within A1 supragranular layers I/II, main input layers III/IV, and output layer V. For each ICC pair, the average ΔBF between the ICC sites was 0.08 ± 0.06 octaves. Across all animals, the ICC sites had an average BF of 10.3 kHz ± 0.3 octaves. Both the ΔBF between ICC pairs and the BF scatter across the lamina were within the bandwidth of ~0.3 octaves seen in an isofrequency lamina of cat (Schreiner and Langner 1997) and rat (Malmierca et al. 2008). Therefore, we analyzed how stimulation across the 10 kHz isofrequency lamina affected cortical activity, and the ICC locations were determined by histology (see Histological Reconstructions section). A total of 28 ICC site pairs were stimulated and responses were recorded in 117 A1 locations from 13 animals, for a total of 248 stimulation cases (i.e., ICC-A1 stimulation-recording site pairs).

Electrical stimulation was presented with different levels and varying IPIs, with each stimulus being randomly presented for a total of 20 trials. The IPIs included 0 (simultaneous stimulation), 0.5, 1, 2, 4, and 8 ms. The stimulation levels varied between the two pulses on different sites because stimulation of different ICC locations elicits A1 activity with different thresholds (Lim and Anderson 2007b; Neuheiser et al. 2010). Due to restrictions in time, we identified only two or three suprathreshold levels for one of the

sites while stimulating the other site with up to ten levels above its threshold across a 12 dB range. Only levels eliciting A1 activity above threshold but below saturation levels were analyzed. An average of 10 levels was used for each stimulation case. For each level, we plotted IPI curves in which the A1 response was shown as a function of IPI. Note that for a given pair of ICC sites for the DSS protocol, we could obtain two different IPI curves by reversing the order of which ICC site was stimulated first. Due to inherent differences in neural activation patterns, we considered each of these two scenarios as different stimulation cases when later presenting the summary data and statistical analyses. Moreover, when fitting neural responses to a linear mixed model, stimulation order proved to be a significant predictor (see Results for more details). Linear mixed models were performed using the nlme library in R (Team 2013).

HISTOLOGICAL RECONSTRUCTIONS

Prior to placement, the ICC array was dipped in a red stain (Di-I: 1, 1-dioctadecyl-3,3,3',3'-tetramethylindocarbocyanine perchlorate, Sigma-Aldrich, St. Louis, MO) to later identify array position within the ICC during histological analysis. Detailed description of the histological procedure, midbrain reconstruction, normalization, and approximation of frequency lamina is provided in a previous publication (Markovitz et al. 2012). Briefly, the midbrain was fixed with 3.7% paraformaldehyde and cryosectioned into sagittal sections at 60 μm using a sliding microtome (Leica, Buffalo Grove, IL). Images of each slice were taken using a Leica MZ FLIII fluorescence stereomicroscope (Leica, Buffalo Grove, IL), Leica DFC412 C peltier cooled CCD camera, and Image-Pro software (MediaCybernetics, Bethesda, MD). A single reflection white light image using a

variable intensity fiber optic light source (Fiber-Lit-PL800, Dolan-Jenner Industries, Boxborough, MA) was taken to determine the outline of each slice. Fluorescence images were later superimposed on the white light images for visualization of the reference and array shank points. The brain was then reconstructed in three dimensions using Rhinoceros (Seattle, WA), and the positions of the arrays were estimated by creating best fit lines through the points on individual slices.

The reconstructions for each brain were normalized to one standard brain using the reference needle point at the intersection of the superior colliculus, thalamus, and lateral extension from the IC, as well as using the curvature of the IC. The 10 kHz lamina was approximated by creating a plane orthogonal to the average insertion angle of all best fit lines of each array placement. The depth of the lamina was determined by calculating the distance from the surface of the IC, where neurons do not respond to broadband noise, to locations where neurons respond with specific BFs from previously published data (Markovitz et al. 2012). This distance was multiplied by a scaling factor to account for tissue changes due to histological process.

The reconstructions of each array placement stimulated, as well as the 10 kHz lamina, can be seen in Figure 29A within the normalized brain. Figure 29B shows the DSS locations across the 10 kHz lamina. In order to provide cues about the shape of the ICC, these DSS locations are shown along with locations found to be on the border or outside the ICC from previously published data (see Chapter 2). Locations were determined to be outside the ICC if the FRMs did not exhibit an orderly shift from low to high BFs for superficial to deeper sites along a shank. Locations were labeled ‘border’ if

the FRMs showed broad tuning with orderly shifts, if tonotopic shifts were not observed across the whole shank, or if a neighboring shank (which was simultaneously recorded) was outside the ICC. From the border information shown here, we believe we have sufficiently stimulated throughout the ICC lamina while avoiding other subnuclei of the inferior colliculus. In order to analyze how cortical activity varied due to stimulation across the isofrequency lamina, the average location between the two stimulated sites was used and are shown with the border points in Figure 29C.

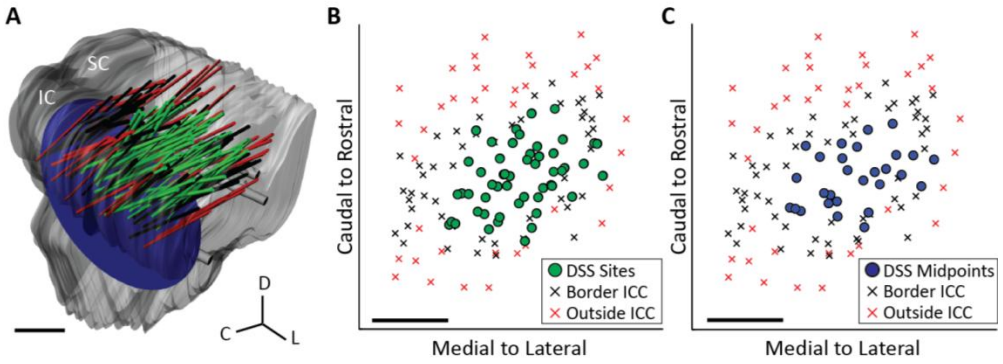

Figure 29: A, The midbrains and array placements were reconstructed in three dimensions and normalized onto a single brain. Green shanks correspond to ICC placements which were electrically stimulated (in pairs). Black and red shanks were placements which were on the border of or outside of the ICC, as determined by FRMs along the shank (see Results). The 10 kHz isofrequency lamina was approximated by a plane at a depth which corresponds to neurons with 10 kHz BF, the average BF of the stimulated ICC sites. **B**, The locations of the stimulated sites in the ICC were plotted along with the border and outside ICC sites across the 10 kHz lamina. **C**, Analysis for the location effects across the ICC lamina was performed by determining the midpoint between each stimulated pair of ICC neurons. Scale bars are 1 mm.

Data Analysis

Evoked Potential Activity

Analysis on evoked potentials and spiking activity was similar to previous studies (Straka et al. 2013). Briefly, for the IPIs used (up to 8 ms), only one response was present. The area of the negative LFP was calculated after removing the electrical artifact from each trace and averaging LFP traces across trials. To calculate the area, a horizontal line was created from the baseline just before the peak to the rising portion of the LFP, and the LFP response was quantified by calculating the area underneath this line with a trapezoidal function. To reduce variability in the LFP area calculation, we removed trials that exhibited large sporadic activity preceding our stimulus-driven activity (see Straka et al. 2013 for details). A trial was removed if the difference between its slope and that of the average slope for a given 25 ms sliding window was greater than three standard deviations. An average of about 17 trials, with a minimum of 14 trials, was included in the calculation of the LFP area for each stimulation case and level.

Spiking Activity

Spikes were detected offline using the same online method described above. The electrical artifact was already removed from the signal for each trial during LFP analysis and prior to filtering the signals from 300-3000 Hz for spike detection. Spikes were summed across a 45 ms window following the onset of the electrical stimulus for all of the same trials included for the LFP analysis. This window was sufficiently long to fully capture the A1 activity elicited by ICC stimulation. The DSR per trial was calculated by subtracting the spike rate obtained for this 45 ms window by the spontaneous rate obtained for the 20 ms window preceding the electrical stimulus.

Spiking activity in layer V often had putative antidromic activity, which was evident

because the spikes exhibited short latencies, low temporal jitter, a sudden increase from no activity to robust spiking per trial with a slight increase in current level above threshold, and isolated activity predominantly in layer V as characterized in a previous publication (Lim and Anderson 2007a). Due to the difficulty of accurately isolating antidromic spikes from the multiunit orthodromic activity, LFP analysis for layer V is included in this paper while DSR or FSL analysis for layer V is not.

Normalization

LFP and DSR responses at each IPI were normalized by summing the responses to stimulus pulses applied separately at each of two sites in the ICC. Normalized values greater than 1 were classified as enhanced.

Statistical Tests

Normalized, level-averaged cortical responses were fit to a mixed model, where the factors included the IPI, ICC location, A1 location, A1 layer, and stimulation order (whether the rostral ICC site or the caudal ICC site was stimulated first). The random variable for the model was the animal from which data was collected. Significance was determined when $P < 0.05$ after a Holm-Bonferroni correction. Comparisons within significant factors, such as between A1 layers or comparing specific IPIs to the 8 ms IPI, were made using Wilcoxon Signed-Rank tests after applying a Holm-Bonferroni correction, unless otherwise specified.

Two significant factors in the mixed model included the caudal-rostral and medial-lateral directions across the ICC. In order to quantify the directionality of this location effect, response properties were fit to the midpoint of the locations of ICC stimulation

pairs using two-dimensional, linear multiple regression analysis. The model determined the slope parameter here called the steepest gradient axis (i.e., the vector of greatest increase) for each response parameter.

RESULTS

TYPICAL CORTICAL RESPONSES TO DSS

Cortical responses to ICC stimulation varied depending on the delay between pulses delivered to two neural populations within the same ICC isofrequency lamina. Both LFPs and spiking across cortical layers increase as the IPI decreases in response to DSS at one stimulation level, as was shown in Figure 21 and Figure 22 in Chapter 3A and in a previous publication (Straka et al. 2013). The extent of the increase in activity was greater for layer I/II compared to the other layers for LFPs and spiking. Responses were quantified as LFP areas or DSR and then normalized to the sum of individual responses to show IPI curves. IPI curves indicate how normalized responses vary with IPI when stimulating at one level for a single stimulation case (i.e., one A1-ICC location pair from one animal). These IPI curves reveal that at short IPIs, DSS stimulation elicits enhanced cortical activity above a linear sum of the individual responses, or a normalized value of 1. In addition, the normalized values in the IPI curves highlight the difference between layers, showing stronger activity at shorter delays for the more superficial layers compared to the deeper layers. Cortical activity was recorded across many stimulation levels, and these levels were averaged to calculate the **IPI-a curves** for each single stimulation case, as shown in Figure 23 in Chapter 2A. While some differences were observed between levels, we did not identify any obvious trends. Because the IPI-a

curves accurately captured the typical cortical response for each stimulation case, they were used to compare activity across A1 and ICC locations and layers in the following sections.

To determine which factors played a significant role in cortical enhancement, we fit all of the IPI-a responses to a mixed model. In this model, the factors were IPI, ICC location, A1 location, A1 layer, stimulation order (whether the rostral or the caudal ICC site from the stimulation pair was stimulated first), and the random variable was the animal used in the data. Significant factors in this model included the medial to lateral direction ($P < 0.004$) and the rostral to caudal direction ($P < 0.002$) across the ICC lamina, the IPI ($P < 3x10^{-16}$), and the cortical layer ($P < 3x10^{-16}$). In addition, the stimulation order was significant ($P < 0.003$), and therefore we treated each order as independent stimulation pairs. Across A1, neither the medial to lateral nor the rostral to caudal direction was significant ($P > 0.05$). In the following sections we further investigate these location effects across the ICC and A1 in order to better understand potential mechanisms influencing the enhancement effect.

Responses Vary Between Different Cortical Layers

Normalized cortical responses varied significantly depending on the layer location of the recording site. Figure 30 shows the IPI-a curves for DSR and LFP activity across each cortical layer averaged across A1 and ICC locations.

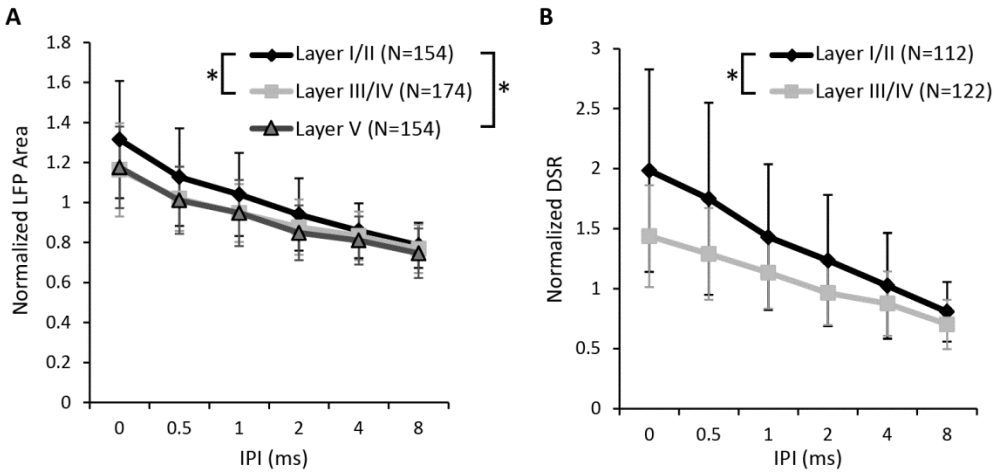

Figure 30: Summary of responses across A1 layers. LFP (**A**) and DSR (**B**) IPI-a curves were averaged across all stimulation cases and animals for layers I/II, III/IV, and V of A1. Significantly increased activity was found for layer I/II compared to the deeper layers for IPIs between 0-4 ms for LFP areas and 0-8 ms for DSRs (marked by asterisks; see text for p-values). N refers to the number IPI-a curves, each corresponding to a different stimulation case. Error bars are standard deviations across stimulation cases.

For all curves, it is evident that activity increases as delays decrease. For LFPs and DSRs recorded at each layer, we found that normalized cortical activity at the 0-4 ms IPIs were significantly larger than the cortical activity recorded at the 8 ms IPI ($P < 5x10^{-8}$). Therefore, the cortical activity is enhanced at shorter IPIs for all layers. When comparing between layers, normalized IPI-a curves for both LFP areas and DSRs appear larger in supragranular layers than deeper layers at shorter IPIs in Figure 30A and B, respectively. LFP activity in layer I/II was significantly larger than that recorded in layer III/IV or layer V for 0-4 ms IPIs ($P < 0.005$). No significant differences were detected between LFPs recorded in layer III/IV and layer V. In addition, DSR activity recorded in layer I/II was significantly larger than that recorded in layer III/IV for 0-8 ms IPIs ($P < 0.01$).

Therefore, enhancement was found at all layers, with a greater increase in cortical activity at short IPIs in the supragranular layer, consistent with Chapter 3A.

Responses Vary across the ICC Lamina

Next, we investigated how cortical responses vary depending on the stimulation location across the ICC lamina. Figure 31 highlights a case example of DSS stimulation of pairs of sites across the ICC eliciting different cortical responses when recording from one layer III/IV location in A1 in one animal.

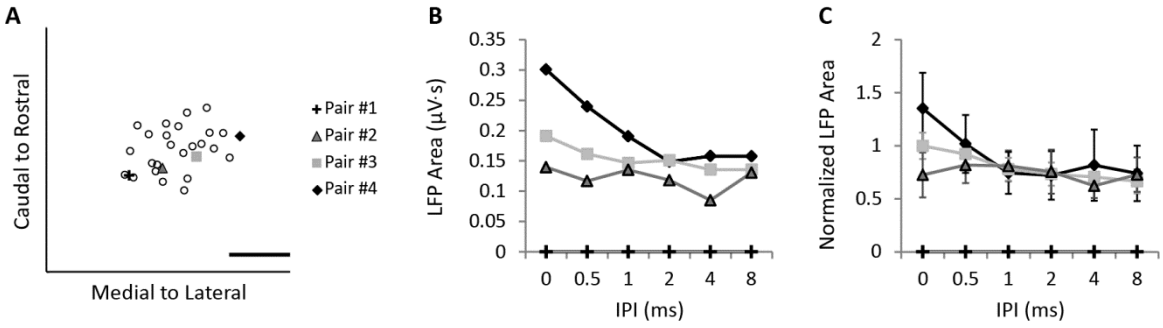

Figure 31: A case example of how stimulating different locations across the ICC isofrequency lamina alter IPI and IPI-a curves recorded in one cortical location from a single animal. **A**, The locations of four pairs of ICC sites stimulated across the ICC lamina, shown with other ICC sites for reference. Elicited activity was recorded in one cortical location in layer III/IV. **B**, For Pair #2-4, we found stimulation levels that elicited similar cortical activity at the 8 ms IPI, which allowed for direct comparison in terms of evoked activity. At those specific stimulation levels, we found that LFP areas increased to a greater extent for shorter IPIs with more rostral-lateral stimulation locations relative to the activity at the 8 ms IPI. Stimulating Pair #1 did not result in sufficient LFP activation for this cortical location within the current injection limits of our electrode arrays. **C**, When averaged across stimulation levels, the IPI-a curves confirm that more rostral-lateral locations reveal higher levels of cortical enhancement. Error bars are standard deviations across levels.

Figure 31A shows the location of four pairs of sites that were stimulated (symbols) along with the rest of the DSS stimulated sites (empty circles) for reference. Stimulation of the most caudal-medial pair of sites (Pair #1) did not elicit activity at this cortical location within the current injection limits for safety and stability of our electrode arrays. The most caudal-medial region has previously been shown to require much higher thresholds to activate A1 (Lim and Anderson 2007b), and therefore our inability to activate A1 was not unexpected. For the other stimulation pairs, we found electrical stimulation levels that elicited similar cortical activity at the 8 ms IPI and then plotted the IPI curves for those stimulation levels (Figure 31). Figure 31B shows that the cortical activity at shorter IPIs remains constant for Pair #2, while it increases for the site pairs that are located in more rostral-lateral locations. The fact that the difference in cortical activity at short IPIs varies with ICC locations, despite the similarity in activity at longer IPIs, suggests that this is not a result of a threshold effect limiting cortical activity. Instead, this difference in activity at short IPIs is indicative of a property specific to the ICC stimulation location. The IPI-a curves in Figure 31C further confirm that greater enhancement occurs due to stimulation of more rostral-lateral sites across all valid stimulation levels. This example shows that, when recording in a single cortical location, the ICC site pairs that were located in more rostral-lateral locations across the lamina elicited larger cortical activity at short IPIs.

To investigate this location effect across all animals, we plotted how the cortical response at specific IPIs varied depending on the locations of the stimulated ICC site pairs (i.e., the midpoint location of the site pairs). Figure 32A shows that the normalized

LFP responses to the 0 ms IPI are weakest in the caudal-medial region and strongest in the rostral-lateral region for all cortical layers.

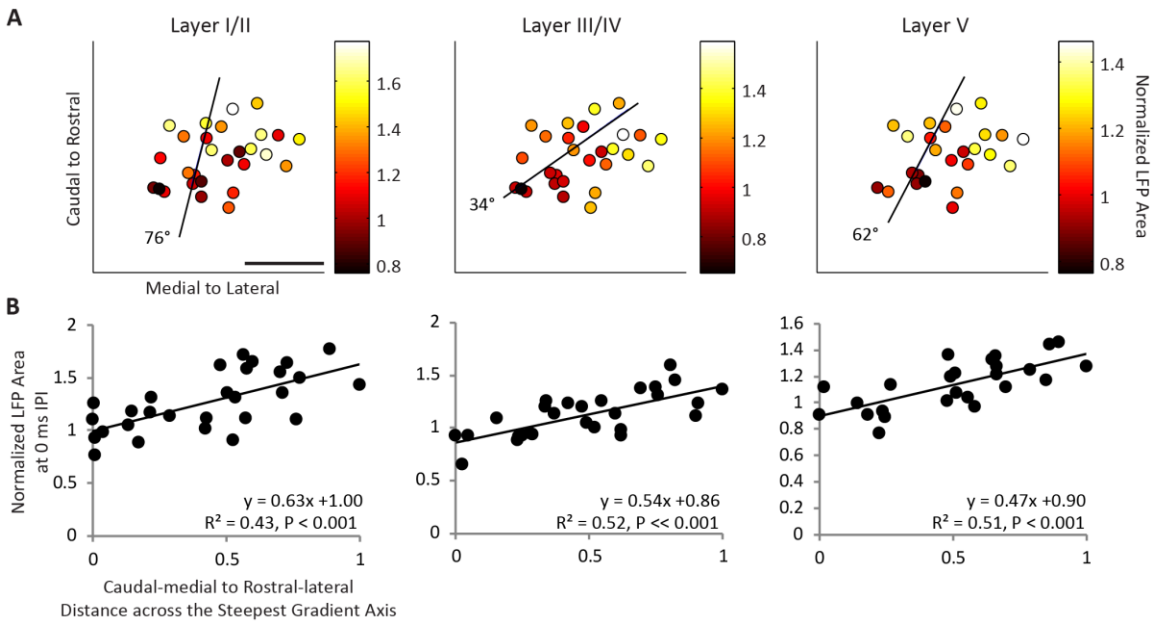

Figure 32: DSS in rostral-lateral ICC regions elicits greater normalized LFP areas across cortical layers than caudal-medial regions. **A**, The amount of elicited normalized LFP area (color) is shown for the midpoint between each pair of stimulated ICC sites (dots) at the 0 ms IPI. Cortical activity was averaged across A1 locations within a specific layer if multiple locations were recorded in response to stimulation of a given pair of sites. Using multiple linear regression to fit the cortical activity as a function of the ICC midpoint location, the steepest gradient axis was found (line). The angle of the steepest gradient is shown, where 0 would indicate alignment with the medial to lateral axis and 90 would indicate alignment with the caudal to rostral axis. The scale bar is 1 mm. **B**, Normalized LFP area is shown as a function of the ICC pair midpoint location along the steepest gradient axis, where 0 is the most caudal-medial location and 1 is the most rostral-lateral location.

In order to quantify this directionality, we fit responses to ICC locations using two-dimensional, linear multiple regression analysis and found the steepest gradient axis (black lines in Figure 32A), or the vector at which the responses increase the most. Next

we plotted how the normalized LFP area varies across the steepest gradient axis (Figure 32B). We collapsed the data along the caudal-medial to rostral-lateral axis, with 0 corresponding to the most caudal-medial point. Since several cortical locations could be recording activity from a single stimulation site, cortical activity was averaged across all relevant recording locations. We found that the normalized cortical activity was smallest in the caudal-medial region of the ICC and increased towards the rostral-lateral regions. As shown in Figure 33, similar trends were observed for normalized DSR across the ICC at the 0 ms IPI. In this paper, we show the 0 ms IPI map because the greatest amount of enhancement and thus the clearest trends were observed. Similar trends were observed for the 0.5 ms IPI and more diverse maps were observed for longer IPIs (data not shown, see summary in Table 2). The angle of the steepest gradient axis for LFPs and DSRs at each layer and IPI as well as descriptive statistics can be found in Table 2.

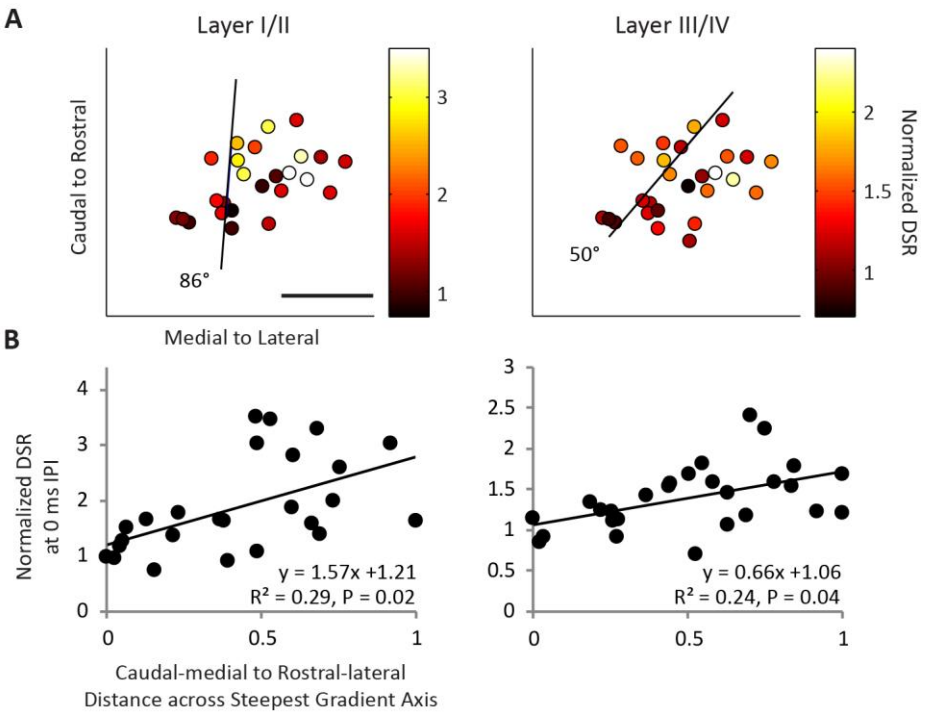

Figure 33: A, Normalized DSRs (color) recorded in supragranular and granular layers of the cortex are shown for the midpoint location for each stimulated ICC site pair. **B**, Normalized DSR is plotted as a function of the midpoint location across the steepest gradient axis (A, black line). Similar to **FIGURE 32**, DSS of rostral-lateral regions results in greater normalized DSR activity than caudal-medial regions. The scale bar is 1 mm.

Table 2: A summary of the results from the multiple regression performed on how cortical responses varied with ICC stimulation location. LFP area and DSR recorded within layers I-V of A1 in response to co-activation across the ICC isofrequency lamina (see Figure 32 and Figure 33 for ICC locations). For each ICC stimulation location, cortical activity was averaged across recording locations. The angle θ across the isofrequency lamina is the inverse tangent of the slope of the regression, where 90° would be aligned to the caudal to rostral axis and 0° would be aligned to the medial to lateral axis. Each regression was performed on the number of ICC site pairs, N, with the descriptive statistics of a coefficient of determination R^2 and probability P.

		0 ms IPI	0.5 ms IPI	1 ms IPI	2 ms IPI	4 ms IPI	8 ms IPI
LFP Layer I/II (N=28)	R^2	0.43	0.30	0.34	0.17	0.05	0.03
	P	0.001	0.025	0.005	0.096	0.515	0.704
	θ (^{0})	75.5	90.9	102.8	112.4	99.9	147.4
LFP Layer III/IV (N=28)	R^2	0.57	0.39	0.16	0.01	0.03	0.01
	P	0.000	0.007	0.129	0.940	0.688	0.843
	θ (^{0})	34.3	54.6	86.4	169.3	31.0	166.3
LFP Layer V (N=25)	R^2	0.51	0.41	0.35	0.10	0.07	0.09
	P	0.000	0.01	0.01	0.32	0.43	0.37
	θ (^{0})	62.3	79.6	96.0	98.1	58.9	55.4
DSR Layer I/II (N=25)	R^2	0.29	0.31	0.18	0.12	0.10	0.08
	P	0.023	0.035	0.106	0.232	0.306	0.401
	θ (^{0})	85.5	96.1	95.9	101.4	82.0	105.4
DSR Layer III/IV (N=27)	R^2	0.24	0.22	0.08	0.02	0.10	0.19
	P	0.035	0.078	0.354	0.757	0.296	0.078
	θ (^{0})	49.5	79.0	103.6	152.5	146.1	14.2

In summary, we found significant fits at the 0 and 0.5 ms IPI for LFP at all cortical layers and DSR for layer I/II ($P < 0.05$). For DSR at layer III/IV, significant fits were found for the 0 ms IPI ($P < 0.05$). The average angle of the steepest gradient axis, or **average steepest gradient angle**, was 71 ± 20^0 across both IPIs (where 90^0 would be

aligned with the caudal to rostral axis and 0^0 would be aligned with medial to lateral axis). Therefore, we conclude that DSS stimulation of rostral-lateral regions of the ICC lamina results in greater cortical activity in comparison to caudal-medial regions.

RESPONSES IN DIFFERENT A1 LOCATIONS

Although the mixed model did not find significant trends that responses to DSS varied across A1 locations, we wanted to further investigate whether cortical locations played a subtle role. First, we determined whether responses to caudal-medial verses rostral-lateral ICC locations were evenly sampled throughout A1. With this aim, we found the line perpendicular to the average steepest gradient angle (i.e., perpendicular to the 71^0 line defined above). This line separated the ICC into rostral-lateral and caudal-medial regions, each with an equal number of stimulation locations (Figure 34A). A1 locations for each stimulated ICC location appeared to be evenly spread across A1 (Figure 34B).

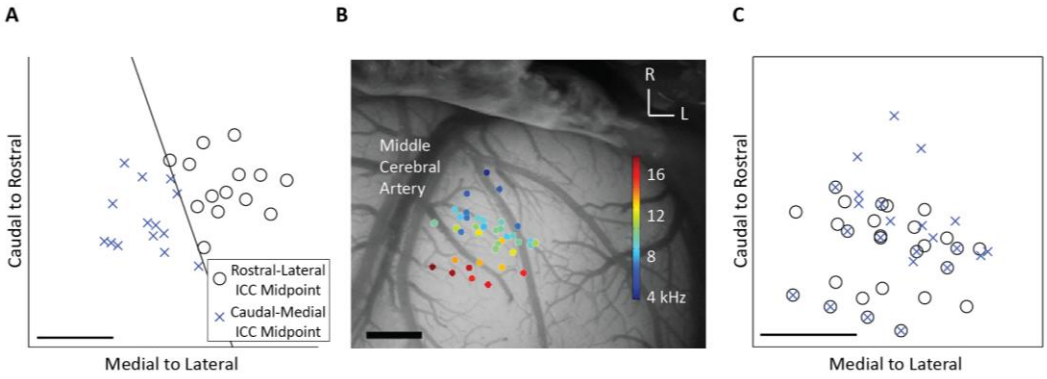

Figure 34: The ICC lamina was split into caudal-medial verses rostral lateral regions (**A**) by the line perpendicular to the average steepest gradient axis, which is the average direction where cortical activity varies the most for the 0 and 0.5 ms IPI. The midpoint between each stimulation pair was determined to originate from one of those two regions. Overlaid on the cortex with BF values (**B**), the A1 locations corresponding to cortical activity elicited from the stimulated caudal-medial ICC region spanned across

similar cortical locations as those for the rostral-lateral ICC region (**C**). The scale bars are 1 mm. Note that panels within (**A**) correspond to ICC locations while the panels within (**B**) and (**C**) correspond to A1 locations.

This was further confirmed when comparison tests did not find a significant difference between the cortical locations recording activity elicited from caudal-medial vs. rostral lateral ICC regions (using a two-sided Wilcoxon rank sum test, $P > 0.05$). Because these locations were similarly distributed across A1, we could further investigate trends across the cortex. Since several ICC stimulation locations were recorded per A1 site, we found the mean cortical activity for each delay at each A1 site by averaging across all relevant ICC stimulation locations. Figure 35 shows the mean LFP or DSR activity recorded in layer I/II, III/IV, or V for each cortical location at the 0 ms IPI.

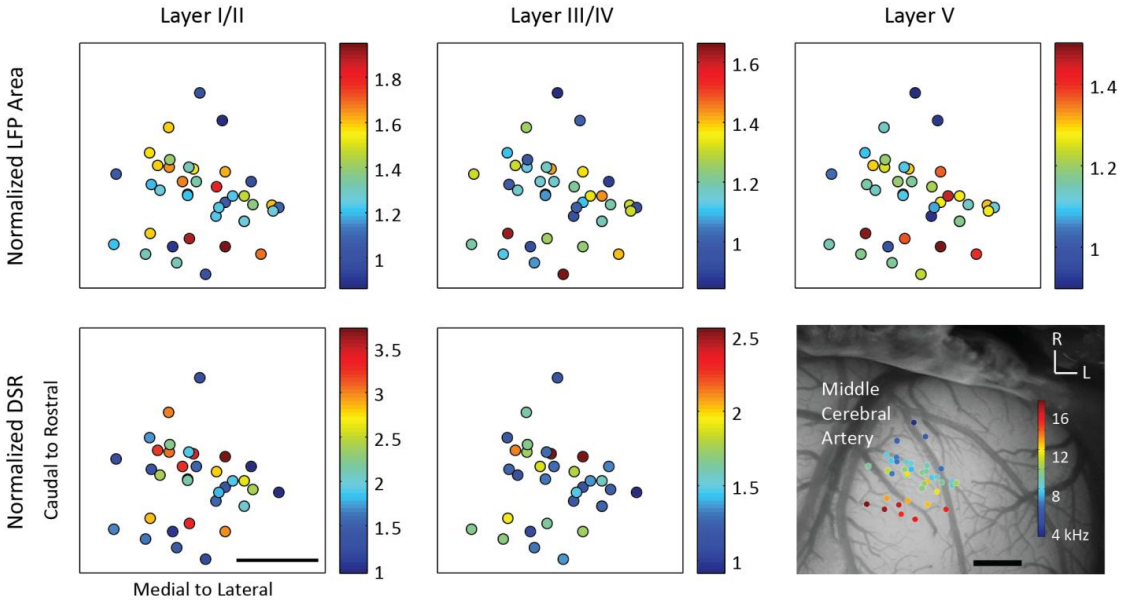

Figure 35: The location of sites across A1 does not have a clear impact in the amount of normalized LFP Area (top) or DSRs (bottom) recorded across different layers (columns). Indicated by color (no units), the

normalized cortical activity for each A1 location was averaged across stimulated locations in the ICC. The scale bars are 1 mm.

Confirming the results from the statistical model, we did not find trends of enhanced activity across the cortex for the 0 ms or other IPIs (data not shown).

DISCUSSION

Stimulation of two different ICC populations within the same lamina elicits increased A1 activity across layers I-V at IPIs shorter than 4 ms. This time window agrees with previous studies where a ~6 ms window was determined using more IPIs (Calixto et al. 2012; Straka et al. 2013). Here we also found that the increased A1 activity greatly depends on the stimulation location across the ICC lamina, as caudal-medial regions increases in activity while rostral-lateral regions resulted in large enhancement. Finally, we found that greater enhancement was found in supragranular layers, though recording location across each cortical layer was not significant. These results suggest that an enhancement mechanism exists within the ICC-to-A1 pathway that can functionally integrate activation on a fast temporal scale (<6 ms window) and depends on the stimulation location of neurons across the ICC lamina.

ANESTHESIA EFFECTS

In our study, we used an anesthetized preparation in order to position the electrode array into multiple ICC locations for an animal. We chose ketamine as the anesthetic because it is thought to suppress the auditory cortex less than other anesthetics, particularly pentobarbital (Astl et al. 1996; Wehr and Zador 2005). Ketamine has been shown to affect cortical activity by reducing spontaneous activity (Syka et al. 2005;

Zurita et al. 1994), typically inhibiting sound-evoked responses (Syka et al. 2005; Wang et al. 2005; Zurita et al. 1994), and altering temporal processing in response to electrical stimulation of the cochlea (Kirby and Middlebrooks 2012). Particularly at medium anesthesia depths, ketamine induces strong oscillatory responses in the auditory cortex (Eggermont 1992; Kisley and Gerstein 1999; Rennaker et al. 2007), which results in greater variability to sound-evoked responses (Kisley and Gerstein 1999). To minimize the impact of these bursts, we removed sweeps with aberrant activity, though the increased variability in cortical responses may have confounded some of our location results, especially at longer IPIs. Despite these cortical effects, it is unlikely that ketamine caused the DSS enhancement since it was not present when repeatedly stimulating an individual site or when stimulating two sites in different isofrequency laminae at similar IPIs with the same experimental methods as this DSS study (Straka et al. 2013). Moreover, the primary finding of this study is not the exact values of enhancement but rather the relative changes based on location across the ICC, where ketamine has been shown to have minimal or no effects on sound-evoked or spontaneous activity (Astl et al. 1996; Suta et al. 2003; Ter-Mikaelian et al. 2007; Torterolo et al. 2002).

Differences in Caudal-medial verses Rostral-lateral Regions in the ICC

We found little if any enhancement when co-activating sites in the caudal-medial region and very strong enhancement in the rostral-lateral region, which may reflect differing activation properties between the regions. When electrically stimulating single ICC sites and recording evoked responses in A1, the caudal-dorsal (which is equivalent to caudal-medial along the tilted ICC lamina) ICC region achieved higher thresholds, larger

discriminable levels steps, and smaller evoked potentials than stimulating in the rostral-ventral region (Lim and Anderson 2007b). However, it is unlikely that activation properties alone cause the difference in cortical activation because rostral-lateral regions had much larger amounts of cortical enhancement than caudal-medial regions at short IPIs even when both produced similar amounts of activity within A1 at the 8 ms IPI (Figure 31). Instead, it appears that the enhancement mechanism, whether on the tectothalamic, thalamocortical, or corticocortical level, integrates activity variably depending on the location of electrical stimulation across the ICC lamina.

Several recent studies within our lab have shown systematic differences in responses between the caudal-medial and rostral-lateral regions across the ICC laminae. In response to pure tones, neurons in the rostral-lateral as compared to the caudal-medial region of the ICC respond with shorter first spike latencies, less spiking jitter, larger LFPs that occur earlier, and PSTHs that are shorter in duration and have more predominant onsets (see Chapter 2). In addition, electrical stimulation of A1 elicits descending excitatory activation in the caudal-medial ICC but with little or no activation within the rostral-lateral ICC (Markovitz et al. 2013). Since both of these studies were performed with similar histological reconstruction techniques to this DSS study, we normalized all midbrains and array placements onto a common standard brain (Figure 36) to determine if these regions were consistent across studies.

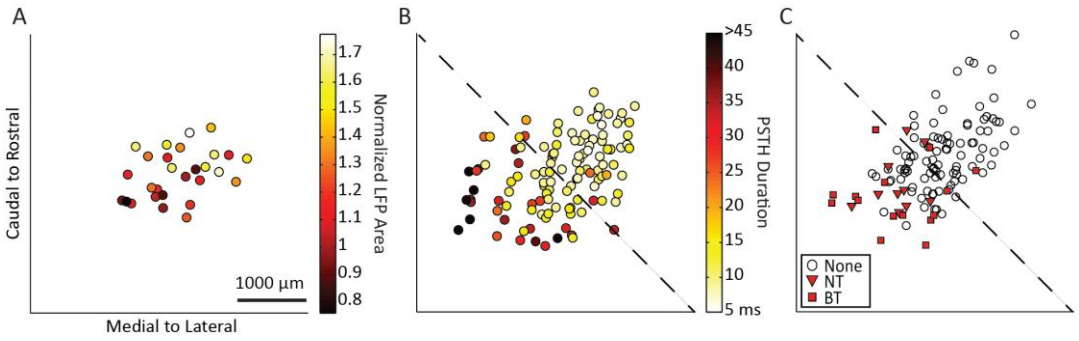

Figure 36: Comparisons across different studies showing that caudal-medial ICC regions exhibit different response properties than rostral-lateral regions in locations which, when electrically stimulated, elicit different cortical responses. **A**, Normalized LFPs recorded in layer I/II of A1 (color) were typically smaller when stimulating in the caudal-medial region and enhanced in the rostral-lateral region for the 10 kHz isofrequency lamina of the ICC. **B**, In response to 10 kHz pure tones (0.5 ms), the duration of PSTHs were longer in the caudal-medial region and shorter in the rostral-lateral region across the 10 kHz isofrequency lamina of the ICC (Data originally presented in Chapter 2). **C**, A1 stimulation caused excitatory responses in the caudal-medial but not the rostral-lateral region of the ICC for A1 sites with BFs of 10- 16 kHz (data originally presented in Markovitz et al. (2013)). These excitatory responses could be present across few or many ICC frequency laminae (i.e., narrowly tuned, NT, or broadly tuned, BT respectively). Locations from A, B, and C were normalized to the same standard brain and locations were taken across the 10 kHz ICC lamina.

We found that the rostral-lateral ICC region, which elicited stronger enhanced cortical activity (Figure 36A), responded with shorter PSTH durations to pure tones (Figure 36B) as well as differences in other response features listed in Chapter 2 corresponding to greater spatial and temporal synchrony. In addition, little to no activity was present in these rostral-lateral regions in response to electrical stimulation of A1 (Figure 36C). In contrast, caudal-medial regions, which elicited little or weak cortical enhancement in this study, typically responded to acoustic stimuli with weaker temporal and spatial

synchrony, and often responded to electric stimulation of A1 with activity that was either narrowly localized or broadly spread across frequency laminae.

In order to map locations across a given ICC lamina, we targeted only the 10 kHz lamina and therefore cannot claim that these trends occur throughout all ICC laminae, which roughly span 50 Hz to 50 kHz in guinea pig (Prosen et al. 1978). However, a previous study in guinea pig has shown a similar spatial segregation of activation properties from the ICC up to the granular layer in A1 for different frequency laminae spanning 9-23 kHz (Lim and Anderson 2007b). In addition, segregated caudal-medial versus rostral-lateral ICC regions were anatomically demonstrated throughout low, middle and high frequency regions in gerbil (Cant and Benson 2007; 2006). In response to electrical stimulation of A1, descending projections elicited activity in caudal-medial but not rostral-lateral regions for low, middle, and high frequency lamina spanning from 2- 16 kHz (Markovitz et al. 2013). Finally, caudal-medial versus rostral-lateral regions have been shown to exhibit differential properties in response to pure tones at the 10 kHz and 20 kHz laminae (Straka et al. 2013). Considering the consistency in ICC location trends across frequency regions for these different studies, we expect that the distinct activation properties between the caudal-medial and rostral-lateral regions would also occur in the other isofrequency laminae throughout the ICC.

Subprojection Pathway Hypothesis

We have found that DSS of the rostral-lateral and caudal-medial regions across the ICC lamina result in different degrees of normalized cortical activity, and that these regions show different responses to acoustic and electric stimulation. These differences

across the ICC lamina are likely due to differences in input and output projection patterns that are maintained through the ascending lemniscal system. Anatomical studies in gerbil have shown that the caudal-medial and rostral-lateral regions of the ICC receive different inputs from the brainstem and project differentially to the caudal and rostral regions of the MGV, respectively (Cant and Benson 2007; 2006). The anatomical segregation of the MGV is also continued in thalamocortical outputs, as demonstrated by studies in the cat and rat, which found that the rostral MGV projects throughout the auditory cortex, including A1, whereas the caudal MGV projects to core cortical regions predominantly outside of A1 (Morel and Imig 1987; Polley et al. 2007; Rodrigues-Dagaeff et al. 1989; Storace et al. 2012; Storace et al. 2010). These segregated thalamic and cortical regions reveal differences in acoustic response properties similar to those seen in the ICC. In comparison to caudal regions, the neurons in rostral MGV respond to acoustic stimuli with stronger excitatory activation, shorter latencies with less jitter, more precise time-locking to click trains, and stricter tonotopic organization with narrower tuning curves (Rodrigues-Dagaeff et al. 1989). The cortical regions that receive inputs from caudal MGV neurons typically exhibit responses with longer latencies, greater spiking jitter, less excitatory activity, and less precise tonotopic organization compared to A1 regions, which receive inputs from rostral MGV neurons. (Morel and Imig 1987; Polley et al. 2007; Rodrigues-Dagaeff et al. 1989; Schreiner et al. 2011; Storace et al. 2012; Storace et al. 2010).

The differences in projection patterns from the brainstem and up to the cortex have led to the hypothesis that at least two subprojection pathways exist in the lemniscal

system. Across lemniscal nuclei, these response properties of the "rostral" pathway suggests it may be designed for stronger activation and more precise transmission of sound information to higher centers compared to the caudal pathway. At least in the ICC, electrical stimulation of the A1 results in excitatory activation only in the caudal-medial region (Markovitz et al. 2013). Combined with the more robust and precise activation properties identified for the rostral pathway, these findings suggest that the rostral pathway may serve as the main ascending pathway for transmitting sound cues to higher perceptual centers while the caudal pathway, at least within the midbrain, may serve a more modulatory and integrative role with the rostral neurons.

Clinical Relevance

Co-activating neural populations across an ICC isofrequency lamina has been shown to overcome suppressive neural effects observed when repeatedly stimulating an individual site. To utilize this strategy in patients for the goal of improving speech perception, the second generation of the AMI will consist of two parallel linear arrays in order to stimulate along as well as within the isofrequency axis. As shown by this study, stimulating the more rostral-lateral region will likely lead to better cortical activation at short IPIs than caudal-medial regions, and therefore the rostral-lateral region should be targeted for implantation. However, though greater normalized cortical activity was elicited when stimulating the rostral-lateral region of the ICC, clinical trials will need to be performed to determine whether this stimulation strategy and implantation location will lead to improved speech understanding.

CHAPTER 4: CONCLUSION

SUMMARY OF RESULTS

The lack of thorough understanding of the lemniscal system has been a limiting factor in developing and improving auditory neuroprostheses, particularly in the midbrain. Traditionally, the lemniscal system has been considered as one pathway, but recent evidence has found differences in anatomical projection patterns from the brainstem to the cortex. Moreover, physiological differences in MGV and A1 responses have been consistent with these anatomical projection patterns. Together, this suggests that there may be sub-projection pathways through the lemniscal system. However, maps of physiological response properties across the ICC have previously not matched the anatomical projection patterns. This inconsistency has called into question the presence of sub-projection pathways through the midbrain. The existence of these dual lemniscal pathways would fundamentally change how auditory researchers investigate the lemniscal system because studies would need to determine how results differ between sub-projection pathways rather than grouping results into one lemniscal system. Moreover, property differences between sub-projection pathways would alter the approach for implantation location and stimulation of the AMI.

In Chapter 2, we investigated the functional organization of responses across the ICC in order to better understand the lemniscal system. Specifically, we analyzed how neurons across the ICC isofrequency lamina vary in response to pure tones by

investigating parameters including first spike latency, latency jitter, PSTH duration and shape, peak magnitude of the LFP, and time at which the LFP peak occurs. With these parameters, we were able to investigate synaptic inputs (through LFPs) as well as the timing properties of outputs (through spiking activity). We found differences between the rostral-lateral and caudal-medial regions of the ICC, which were consistent with anatomical projection patterns observed in previous studies. In addition to confirming that dual lemniscal projections exist at the level of the midbrain, these results will guide identification of optimal target locations for neuroprostheses within the lemniscal system.

The next goal of this thesis in Chapter 3 was to identify better stimulation strategies and implantation locations in order to improve the implementation of the AMI. In the first clinical trial, the AMI array was chosen to be a single-shank penetrating array rather than a three-dimensional array because of a lack of evidence showing that the benefits would overcome the implantation safety risks, including a higher likelihood of hemorrhage and edema (Liu et al. 1997). Moreover, good results were expected from the AMI single shank because it would be able to present a dynamic temporal pattern via ICC neuron synchronization to the sound envelope for different frequency channels (Lim et al. 2007; Rode et al. 2013) in which even crude temporal patterns have shown to be sufficient for speech recognition (Shannon et al. 1995). However, the initial clinical trials showed poor speech perception, which was most likely due to implantation in sub-optimal locations and limited temporal coding abilities (Calixto et al. 2012; Lim et al. 2008a; McKay et al. 2013). While Calixto et al. (2012) demonstrated that three-dimensional stimulation may be required to sufficiently code for temporal information

through DSS to improve hearing performance, this study was limited by large stimulation sites of the AMI. The results in Chapter 3A extended this study by using smaller electrode sites, thus minimizing the current spread and antidromic activity, allowing us to record LFPs as well as spiking activity at several cortical layers. We found enhanced cortical activity for both LFPs and spiking, which was strongest in supragranular layers. In addition, we determined that this enhancement only occurred when co-activating neurons along an isofrequency ICC lamina, and not across different laminae.

From previous studies, including the response characterizations in Chapter 2, it was known that locations along the ICC isofrequency lamina have different neural properties. Therefore, we investigated location trends of DSS, both in the ICC and in A1. In Chapter 3 we show that the greatest enhancement, which could occur across A1, was a result of stimulating rostral-lateral rather than caudal-medial ICC regions. The results in Chapter 3B found that an optimal implantation location for the DSS may be the rostral-lateral region of the ICC.

Comparing results across studies, this rostral-lateral ICC region identified in Chapter 3 is consistent with the rostral-lateral region identified from Chapter 2, which responds to pure tones with shorter PSTH durations, shorter first spike latencies with less jitter, more onset responses, and larger LFPs that occur earlier than responses in the caudal-medial region. In addition, this rostral-lateral region is consistent with studies that have shown none or minimal excitatory responses to electrical stimulation of A1, while the caudal-medial region exhibits significant excitatory responses. The difference in excitation patterns suggests that the caudal-medial region may receive different

corticofugal projections than the rostral-lateral region of ICC (further investigated in a study presented in Appendix A).

FUTURE WORK

In Chapter 2, we found that physiological responses vary between different subregions of the ICC, and that the locations of these subregions are consistent with the dual lemniscal pathway hypothesis derived from studies across species. However, to truly confirm this dual lemniscal pathway hypothesis, both anatomical and physiological studies from the ICC, MGV, and ACC should be performed within the same species. This is important in order to confirm that the same locations for the differential anatomical projection patterns correspond to the different response properties. In addition, more complex and natural response properties (e.g., speech-like features) should be investigated more fully across different laminae. As more realistic models of the lemniscal pathway are being developed (Dugue et al. 2010; Guerin et al. 2006; Hewitt and Meddis 1994; Jepsen et al. 2008; Meddis et al. 2001; Nelson and Carney 2004; Rode et al. 2013; Sumner et al. 2003), they will need to begin incorporating these differences in coding properties between sub-projection ascending pathways.

In Chapter 3, we found that DSS of rostral-lateral regions results in greater cortical enhancement, particularly in supragranular cortical layers. Future studies should record responses in MGV to determine whether it is the source of the integration of neural responses across the ICC. In addition, the mechanism for increased enhancement in the supragranular layers should also be probed to determine whether it is due to thalamocortical or corticocortical projections. Previous studies have investigated how

these two projections alter responses to a pure tone for single cells in A1 by comparing typical responses to responses due to thalamocortical excitation alone, which was achieved by silencing the cortex by applying muscimol, a $GABA_A$ agonist (Happel et al. 2010). Neighboring cortical regions could also be silenced or altered with other pharmacological agents, such as $GABA_B$ agonists (Happel et al. 2010; Yamauchi et al. 2000) or the $GABA_A$ antagonist gabazine (Moeller et al. 2010), or with cryogenic cooling of the cortex (Coomber et al. 2011). With these techniques, any resulting differences in the degree of enhancement could be attributed to differences in corticocortical projections. Conversely, constant enhancement throughout these manipulations would indicate that the thalamus is the source of the enhancement.

Clinical Application

Since the initial AMI clinical trial resulted in limited speech perception, evidence of real and substantive improvements in the stimulation and implantation strategies had to be shown in order to gain funding and approval for future clinical trials. Moreover, while it was expected than multiple penetrating electrodes through the ICC could improve performance, sufficient data had to determine that the expected benefit would outweigh the increased surgical risk (Liu et al. 1997). Through the work presented in this thesis, we found that the optimal stimulation strategy may need to co-activate neurons along the ICC isofrequency laminae, particularly within the rostral-lateral region of the ICC. To implement this, the next clinical trial will need to implant at least two AMI shanks into the ICC to be able to co-activate neurons along a lamina as well as across laminae. The

next clinical trial with a two-shank AMI array that will utilize these strategies is awaiting approval, and is expected to begin in the summer of 2014.

The results from the clinical trial will reveal whether the increased cortical enhancement seen when using DSS to stimulate the rostral-lateral region of the ICC in animal studies will translate to increased speech understanding with the AMI in patients. Other benefits of DSS may include a wider dynamic stimulation range and a decrease in the amount of current necessary per site. This lower current level should also reduce tissue damage and power consumption. Moreover, current steering can be used with a three dimensional array, which may enable activation of more specific ICC regions (Butson and McIntyre 2008). From this upcoming clinical trial, we will not only be able to correlate the neural activity results found in this thesis to potential improvements in perception, but we will also be able to compare how these technological improvements will affect speech understanding, which is the ultimate goal of this research.

BIBLIOGRAPHY

Abeles M, and Goldstein MH, Jr. Functional architecture in cat primary auditory cortex: columnar organization and organization according to depth. *J Neurophysiol* 33: 172-187, 1970.

Adams JS, Hasenstab MS, Pippin GW, and Sismanis A. Telephone use and understanding in patients with cochlear implants. *Ear Nose Throat J* 83: 96, 99-100, 102-103, 2004.

Aitkin L, Tran L, and Syka J. The responses of neurons in subdivisions of the inferior colliculus of cats to tonal, noise and vocal stimuli. *Exp Brain Res* 98: 53-64, 1994.

Aitkin LM, Dickhaus H, Schult W, and Zimmermann M. External nucleus of inferior colliculus: auditory and spinal somatosensory afferents and their interactions. *J Neurophysiol* 41: 837-847, 1978.

Aitkin LM, Kenyon CE, and Philpott P. The representation of the auditory and somatosensory systems in the external nucleus of the cat inferior colliculus. *J Comp Neurol* 196: 25-40, 1981.

Aitkin LM, Webster WR, Veale JL, and Crosby DC. Inferior colliculus. I. Comparison of response properties of neurons in central, pericentral, and external nuclei of adult cat. *J Neurophysiol* 38: 1196-1207, 1975.

Andersen RA, Snyder RL, and Merzenich MM. The topographic organization of corticocollicular projections from physiologically identified loci in the AI, AII, and anterior auditory cortical fields of the cat. *J Comp Neurol* 191: 479-494, 1980.

Anderson DJ, Najafi K, Tanghe SJ, Evans DA, Levy KL, Hetke JF, Xue XL, Zappia JJ, and Wise KD. Batch-fabricated thin-film electrodes for stimulation of the central auditory system. *IEEE Trans Biomed Eng* 36: 693-704, 1989.

Astl J, Popelar J, Kvasnak E, and Syka J. Comparison of response properties of neurons in the inferior colliculus of guinea pigs under different anesthetics. *Audiology* 35: 335-345, 1996.

Bajo VM, and Moore DR. Descending projections from the auditory cortex to the inferior colliculus in the gerbil, Meriones unguiculatus. *J Comp Neurol* 486: 101-116, 2005.

Bajo VM, Nodal FR, Bizley JK, Moore DR, and King AJ. The ferret auditory cortex: descending projections to the inferior colliculus. *Cereb Cortex* 17: 475-491, 2007.

Bajo VM, Nodal FR, Moore DR, and King AJ. The descending corticocollicular pathway mediates learning-induced auditory plasticity. *Nat Neurosci* 13: 253-260, 2010.

Banks M, and Smith P. Thalamocortical Relations. In: *The Auditory Cortex*, edited by Winer JA, and Schreiner CESpringer US, 2011, p. 75-97.

Bartlett EL, Sadagopan S, and Wang X. Fine frequency tuning in monkey auditory cortex and thalamus. *J Neurophysiol* 106: 849-859, 2011.

Bartlett EL, and Smith PH. Anatomic, intrinsic, and synaptic properties of dorsal and ventral division neurons in rat medial geniculate body. *J Neurophysiol* 81: 1999-2016, 1999.

Bartlett EL, and Smith PH. Effects of paired-pulse and repetitive stimulation on neurons in the rat medial geniculate body. *Neuroscience* 113: 957-974, 2002.

Britten KH, Shadlen MN, Newsome WT, and Movshon JA. The analysis of visual motion: a comparison of neuronal and psychophysical performance. *J Neurosci* 12: 4745-4765, 1992.
Broicher T, Bidmon HJ, Kamuf B, Coulon P, Gorji A, Pape HC, Speckmann EJ, and Budde T. Thalamic afferent activation of supragranular layers in auditory cortex in vitro: a voltage sensitive dye study. *Neuroscience* 165: 371-385, 2010.
Brunso-Bechtold JK, Thompson GC, and Masterton RB. HRP study of the organization of auditory afferents ascending to central nucleus of inferior colliculus in cat. *J Comp Neurol* 197: 705-722, 1981.
Brückner S, and Rübsamen R. Binaural response characteristics in isofrequency sheets of the gerbil inferior colliculus. *Hear Res* 86: 1-14, 1995.
Butler AB, and Hodos W. Auditory and Vocal Forebrain in Amniotes. In: *Comparative Vertebrate Neuroanatomy*John Wiley & Sons, Inc., 2005, p. 571-591.
Butson CR, and McIntyre CC. Current Steering to Control the Volume of Tissue Activated During Deep Brain Stimulation. *Brain Stimulat* 1: 7-15, 2008.
Calford MB, and Aitkin LM. Ascending projections to the medial geniculate body of the cat: evidence for multiple, parallel auditory pathways through thalamus. *J Neurosci* 3: 2365-2380, 1983.
Calixto R, Lenarz M, Neuheiser A, Lenarz T, and Lim HH. Cortical Responses to a new Double-Shank Auditory Midbrain Implant (AMI) in the Guinea Pig. *Assoc Res Otolaryng Abstr* 33: 95, 2010.
Calixto R, Lenarz M, Neuheiser A, Scheper V, Lenarz T, and Lim HH. Co-activation of different neurons within an isofrequency lamina of the inferior colliculus elicits enhanced auditory cortical activation. *J Neurophysiol* 2012.
Cant NB, and Benson CG. Multiple topographically organized projections connect the central nucleus of the inferior colliculus to the ventral division of the medial geniculate nucleus in the gerbil, Meriones unguiculatus. *J Comp Neurol* 503: 432-453, 2007.
Cant NB, and Benson CG. Organization of the inferior colliculus of the gerbil (Meriones unguiculatus): differences in distribution of projections from the cochlear nuclei and the superior olivary complex. *J Comp Neurol* 495: 511-528, 2006.
Cetas JS, de Venecia RK, and McMullen NT. Thalamocortical afferents of Lorente de No: medial geniculate axons that project to primary auditory cortex have collateral branches to layer I. *Brain Res* 830: 203-208, 1999.
Cetas JS, Price RO, Crowe J, Velenovsky DS, and McMullen NT. Dendritic orientation and laminar architecture in the rabbit auditory thalamus. *J Comp Neurol* 458: 307-317, 2003.
Cetas JS, Price RO, Velenovsky DS, Sinex DG, and McMullen NT. Frequency organization and cellular lamination in the medial geniculate body of the rabbit. *Hear Res* 155: 113-123, 2001.
Chen C, Read HL, and Escabi MA. Precise feature based time scales and frequency decorrelation lead to a sparse auditory code. *J Neurosci* 32: 8454-8468, 2012.
Cohen YE, and Knudsen EI. Maps versus clusters: different representations of auditory space in the midbrain and forebrain. *Trends Neurosci* 22: 128-135, 1999.

Colletti L, Shannon R, and Colletti V. Auditory brainstem implants for neurofibromatosis type 2. *Curr Opin Otolaryngol Head Neck Surg* 20: 353-357, 2012.
Colletti V, and Shannon RV. Open set speech perception with auditory brainstem implant? *Laryngoscope* 115: 1974-1978, 2005.
Colletti V, Shannon RV, Carner M, Veronese S, and Colletti L. Progress in restoration of hearing with the auditory brainstem implant. *Progress in brain research* 175: 333-345, 2009.
Coomber B, Edwards D, Jones SJ, Shackleton TM, Goldschmidt J, Wallace MN, and Palmer AR. Cortical inactivation by cooling in small animals. *Front Syst Neurosci* 5: 53, 2011.
Coomes DL, Schofield RM, and Schofield BR. Unilateral and bilateral projections from cortical cells to the inferior colliculus in guinea pigs. *Brain Res* 1042: 62-72, 2005.
Cruikshank SJ, Rose HJ, and Metherate R. Auditory thalamocortical synaptic transmission in vitro. *J Neurophysiol* 87: 361-384, 2002.
Doucet JR, Molavi DL, and Ryugo DK. The source of corticocollicular and corticobulbar projections in area Te1 of the rat. *Exp Brain Res* 153: 461-466, 2003.
Dugue P, Le Bouquin-Jeannes R, Edeline JM, and Faucon G. A physiologically based model for temporal envelope encoding in human primary auditory cortex. *Hear Res* 268: 133-144, 2010.
Edeline J-M. Physiological Properties of Neurons in the Medial Geniculate Body. In: *The Auditory Cortex*, edited by Winer JA, and Schreiner CESpringer US, 2011, p. 251-274.
Eggermont JJ. Stimulus induced and spontaneous rhythmic firing of single units in cat primary auditory cortex. *Hear Res* 61: 1-11, 1992.
Eggermont JJ, and Roberts LE. The neuroscience of tinnitus. *Trends Neurosci* 27: 676-682, 2004.
Eggermont JJ, and Smith GM. Synchrony between single-unit activity and local field potentials in relation to periodicity coding in primary auditory cortex. *J Neurophysiol* 73: 227-245, 1995.
Ehret G, and Romand R. *The Central Auditory System*. New York: Oxford University Press, Inc., 1997.
Faye-Lund H. The neocortical projection to the inferior colliculus in the albino rat. *Anat Embryol (Berl)* 173: 53-70, 1985.
Faye-Lund H, and Osen KK. Anatomy of the inferior colliculus in rat. *Anat Embryol (Berl)* 171: 1-20, 1985.
Feliciano M, and Potashner SJ. Evidence for a glutamatergic pathway from the guinea pig auditory cortex to the inferior colliculus. *J Neurochem* 65: 1348-1357, 1995.
Flanagan JL. Audibility of periodic pulses and a model for threshold. *J Acoust Soc Am* 33: 1540-1548, 1961.
Forrest TG, and Green DM. Detection of partially filled gaps in noise and the temporal modulation transfer function. *J Acoust Soc Am* 82: 1933-1943, 1987.
Gao E, and Suga N. Experience-dependent corticofugal adjustment of midbrain frequency map in bat auditory system. *Proc Natl Acad Sci U S A* 95: 12663-12670, 1998.

Gao E, and Suga N. Experience-dependent plasticity in the auditory cortex and the inferior colliculus of bats: role of the corticofugal system. *Proc Natl Acad Sci U S A* 97: 8081-8086, 2000.
Green D, and Swets J. *Signal Detection Theory and Psychophysics*. New York: Wiley, 1966.
Grill WM, Simmons AM, Cooper SE, Miocinovic S, Montgomery EB, Baker KB, and Rezai AR. Temporal excitation properties of paresthesias evoked by thalamic microstimulation. *Clin Neurophysiol* 116: 1227-1234, 2005.
Guerin A, Jeannes Rle B, Bes J, Faucon G, and Lorenzi C. Evaluation of two computational models of amplitude modulation coding in the inferior colliculus. *Hear Res* 211: 54-62, 2006.
Hage SR, and Ehret G. Mapping responses to frequency sweeps and tones in the inferior colliculus of house mice. *Eur J Neurosci* 18: 2301-2312, 2003.
Happel MF, Jeschke M, and Ohl FW. Spectral integration in primary auditory cortex attributable to temporally precise convergence of thalamocortical and intracortical input. *J Neurosci* 30: 11114-11127, 2010.
Harris KD, Bartho P, Chadderton P, Curto C, de la Rocha J, Hollender L, Itskov V, Luczak A, Marguet SL, Renart A, and Sakata S. How do neurons work together? Lessons from auditory cortex. *Hear Res* 271: 37-53, 2011.
Hattori T, and Suga N. The inferior colliculus of the mustached bat has the frequency-vs-latency coordinates. *J Comp Physiol A* 180: 271-284, 1997.
He J, and Hu B. Differential distribution of burst and single-spike responses in auditory thalamus. *J Neurophysiol* 88: 2152-2156, 2002.
Heil P, Rajan R, and Irvine DR. Sensitivity of neurons in cat primary auditory cortex to tones and frequency-modulated stimuli. II: Organization of response properties along the 'isofrequency' dimension. *Hear Res* 63: 135-156, 1992.
Herbert H, Aschoff A, and Ostwald J. Topography of projections from the auditory cortex to the inferior colliculus in the rat. *J Comp Neurol* 304: 103-122, 1991.
Hewitt MJ, and Meddis R. A computer model of amplitude-modulation sensitivity of single units in the inferior colliculus. *J Acoust Soc Am* 95: 2145-2159, 1994.
Hu B. Cellular basis of temporal synaptic signalling: an in vitro electrophysiological study in rat auditory thalamus. *J Physiol* 483 (Pt 1): 167-182, 1995.
Hu B. Functional organization of lemniscal and nonlemniscal auditory thalamus. *Exp Brain Res* 153: 543-549, 2003.
Huang CL, and Winer JA. Auditory thalamocortical projections in the cat: laminar and areal patterns of input. *J Comp Neurol* 427: 302-331, 2000.
Huffman RF, and Henson OW, Jr. The descending auditory pathway and acousticomotor systems: connections with the inferior colliculus. *Brain Res Brain Res Rev* 15: 295-323, 1990.
Hyde PS, and Knudsen EI. Topographic projection from the optic tectum to the auditory space map in the inferior colliculus of the barn owl. *J Comp Neurol* 421: 146-160, 2000.
Imig TJ, and Morel A. Tonotopic organization in ventral nucleus of medial geniculate body in the cat. *J Neurophysiol* 53: 309-340, 1985.

Jepsen ML, Ewert SD, and Dau T. A computational model of human auditory signal processing and perception. *J Acoust Soc Am* 124: 422-438, 2008.
Ji W, Gao E, and Suga N. Effects of acetylcholine and atropine on plasticity of central auditory neurons caused by conditioning in bats. *J Neurophysiol* 86: 211-225, 2001.
Jones EG, and Burton H. Areal differences in the laminar distribution of thalamic afferents in cortical fields of the insular, parietal and temporal regions of primates. *J Comp Neurol* 168: 197-247, 1976.
Joris PX, Schreiner CE, and Rees A. Neural processing of amplitude-modulated sounds. *Physiol Rev* 84: 541-577, 2004.
Kaas J. The Evolution of Auditory Cortex: The Core Areas. In: *The Auditory Cortex*, edited by Winer JA, and Schreiner CESpringer US, 2011, p. 407-427.
Kirby AE, and Middlebrooks JC. Unanesthetized auditory cortex exhibits multiple codes for gaps in cochlear implant pulse trains. *J Assoc Res Otolaryngol* 13: 67-80, 2012.
Kisley MA, and Gerstein GL. Trial-to-trial variability and state-dependent modulation of auditory-evoked responses in cortex. *J Neurosci* 19: 10451-10460, 1999.
Knudsen EI. Instructed learning in the auditory localization pathway of the barn owl. *Nature* 417: 322-328, 2002.
Kral A, Hartmann R, Tillein J, Heid S, and Klinke R. Congenital auditory deprivation reduces synaptic activity within the auditory cortex in a layer-specific manner. *Cereb Cortex* 10: 714-726, 2000.
Kral A, and O'Donoghue GM. Profound deafness in childhood. *N Engl J Med* 363: 1438-1450, 2010.
Kreft HA, Donaldson GS, and Nelson DA. Effects of pulse rate on threshold and dynamic range in Clarion cochlear-implant users. *J Acoust Soc Am* 115: 1885-1888, 2004.
Krishna BS, and Semple MN. Auditory temporal processing: responses to sinusoidally amplitude-modulated tones in the inferior colliculus. *J Neurophysiol* 84: 255-273, 2000.
Langner G. Periodicity coding in the auditory system. *Hear Res* 60: 115-142, 1992.
Langner G, Albert M, and Briede T. Temporal and spatial coding of periodicity information in the inferior colliculus of awake chinchilla (Chinchilla laniger). *Hear Res* 168: 110-130, 2002.
Lee CC. Thalamic and cortical pathways supporting auditory processing. *Brain and language* 2012.
Lee CC, and Sherman SM. Drivers and modulators in the central auditory pathways. *Front Neurosci* 4: 79, 2010a.
Lee CC, and Sherman SM. Modulator property of the intrinsic cortical projection from layer 6 to layer 4. *Frontiers in Systems Neuroscience* 3: 2009.
Lee CC, and Sherman SM. On the classification of pathways in the auditory midbrain, thalamus, and cortex. In: *Hear Res*. Netherlands: 2010 Elsevier B.V, 2011, p. 79-87.
Lee CC, and Sherman SM. Topography and physiology of ascending streams in the auditory tectothalamic pathway. *Proc Natl Acad Sci U S A* 107: 372-377, 2010b.
Lenarz M, Lim HH, Lenarz T, Reich U, Marquardt N, Klingberg MN, Paasche G, Reuter G, and Stan AC. Auditory midbrain implant: histomorphologic effects of long-

term implantation and electric stimulation of a new deep brain stimulation array. *Otol Neurotol* 28: 1045-1052, 2007.
Lenarz M, Lim HH, Patrick JF, Anderson DJ, and Lenarz T. Electrophysiological validation of a human prototype auditory midbrain implant in a guinea pig model. *J Assoc Res Otolaryngol* 7: 383-398, 2006a.
Lenarz T, Lim HH, Reuter G, Patrick JF, and Lenarz M. The auditory midbrain implant: a new auditory prosthesis for neural deafness-concept and device description. *Otol Neurotol* 27: 838-843, 2006b.
Lim HH, and Anderson DJ. Antidromic activation reveals tonotopically organized projections from primary auditory cortex to the central nucleus of the inferior colliculus in guinea pig. *J Neurophysiol* 97: 1413-1427, 2007a.
Lim HH, and Anderson DJ. Auditory cortical responses to electrical stimulation of the inferior colliculus: implications for an auditory midbrain implant. *J Neurophysiol* 96: 975-988, 2006.
Lim HH, and Anderson DJ. Spatially distinct functional output regions within the central nucleus of the inferior colliculus: Implications for an auditory midbrain implant. *J Neurosci* 27: 8733-8743, 2007b.
Lim HH, Lenarz M, Joseph G, and Lenarz T. Frequency representation within the human brain: Stability versus plasticity. *Sci Rep* 3: 1474, 2013.
Lim HH, Lenarz M, and Lenarz T. Auditory midbrain implant: a review. *Trends in amplification* 13: 149-180, 2009.
Lim HH, Lenarz T, Anderson DJ, and Lenarz M. The auditory midbrain implant: effects of electrode location. *Hear Res* 242: 74-85, 2008a.
Lim HH, Lenarz T, Joseph G, Battmer RD, Patrick JF, and Lenarz M. Effects of phase duration and pulse rate on loudness and pitch percepts in the first auditory midbrain implant patients: Comparison to cochlear implant and auditory brainstem implant results. *Neuroscience* 154: 370-380, 2008b.
Lim HH, Lenarz T, Joseph G, Battmer RD, Samii A, Samii M, Patrick JF, and Lenarz M. Electrical stimulation of the midbrain for hearing restoration: insight into the functional organization of the human central auditory system. *J Neurosci* 27: 13541-13551, 2007.
Lipski J. Antidromic activation of neurones as an analytic tool in the study of the central nervous system. *J Neurosci Methods* 4: 1-32, 1981.
Liu X, McPhee G, Seldon HL, and Clark GM. Histological and physiological effects of the central auditory prosthesis: surface versus penetrating electrodes. *Hear Res* 114: 264-274, 1997.
Loftus WC, Bishop DC, Saint Marie RL, and Oliver DL. Organization of binaural excitatory and inhibitory inputs to the inferior colliculus from the superior olive. *J Comp Neurol* 472: 330-344, 2004.
Ma X, and Suga N. Augmentation of plasticity of the central auditory system by the basal forebrain and/or somatosensory cortex. *J Neurophysiol* 89: 90-103, 2003.
Malmierca M, and Ryugo D. Descending Connections of Auditory Cortex to the Midbrain and Brain Stem. In: *The Auditory Cortex*, edited by Winer JA, and Schreiner CESpringer US, 2011, p. 189-208.

Malmierca MS. The structure and physiology of the rat auditory system: an overview. *Int Rev Neurobiol* 56: 147-211, 2003.
Malmierca MS, Blackstad TW, Osen KK, Karagulle T, and Molowny RL. The central nucleus of the inferior colliculus in rat: a Golgi and computer reconstruction study of neuronal and laminar structure. *J Comp Neurol* 333: 1-27, 1993.
Malmierca MS, and Hackett TA. Structural organization of the ascending auditory pathway. In: *The Oxford Handbook of Auditory Science: The Auditory Brain*, edited by Palmer AR, and Rees A. New York: Oxford University Press, 2010, p. 9-41.
Malmierca MS, Izquierdo MA, Cristaudo S, Hernandez O, Perez-Gonzalez D, Covey E, and Oliver DL. A discontinuous tonotopic organization in the inferior colliculus of the rat. *J Neurosci* 28: 4767-4776, 2008.
Malmierca MS, Rees A, Le Beau FE, and Bjaalie JG. Laminar organization of frequency-defined local axons within and between the inferior colliculi of the guinea pig. *J Comp Neurol* 357: 124-144, 1995.
Malmierca MS, Rees A, and Le Beau FEN. Ascending projections to the medial geniculate body from physiologically defined loci in the inferior colliculus. In: *Acoustical Signal Processing in the Central Auditory System*, edited by Syka J. New York: Plenum, 1997, p. 295-302.
Markovitz CD, Tang TT, Edge DP, and Lim HH. Three-dimensional brain reconstruction of in vivo electrode tracks for neuroscience and neural prosthetic applications. *Frontiers in Neural Circuits* 6: 2012.
Markovitz CD, Tang TT, and Lim HH. Tonotopic and localized pathways from primary auditory cortex to the central nucleus of the inferior colliculus. *Front Neural Circuits* 7: 77, 2013.
McKay CM, Lim HH, and Lenarz T. Temporal processing in the auditory system: insights from cochlear and auditory midbrain implantees. *J Assoc Res Otolaryngol* 14: 103-124, 2013.
McKay CM, and McDermott HJ. Loudness perception with pulsatile electrical stimulation: the effect of interpulse intervals. *J Acoust Soc Am* 104: 1061-1074, 1998.
McMullen NT, Velenovsky DS, and Holmes MG. Auditory thalamic organization: Cellular slabs, dendritic arbors and tectothalamic axons underlying the frequency map. *Neuroscience* 136: 927-943, 2005.
Meddis R, O'Mard LP, and Lopez-Poveda EA. A computational algorithm for computing nonlinear auditory frequency selectivity. *J Acoust Soc Am* 109: 2852-2861, 2001.
Middlebrooks JC. Auditory cortex phase locking to amplitude-modulated cochlear implant pulse trains. *J Neurophysiol* 100: 76-91, 2008.
Middlebrooks JC, and Zook JM. Intrinsic organization of the cat's medial geniculate body identified by projections to binaural response-specific bands in the primary auditory cortex. *J Neurosci* 3: 203-224, 1983.
Miocinovic S, and Grill WM. Sensitivity of temporal excitation properties to the neuronal element activated by extracellular stimulation. *J Neurosci Methods* 132: 91-99, 2004.

Mitani A, Shimokouchi M, Itoh K, Nomura S, Kudo M, and Mizuno N. Morphology and laminar organization of electrophysiologically identified neurons in the primary auditory cortex in the cat. *J Comp Neurol* 235: 430-447, 1985.
Mitzdorf U. Current source-density method and application in cat cerebral cortex: investigation of evoked potentials and EEG phenomena. *Physiol Rev* 65: 37-100, 1985.
Moeller CK, Kurt S, Happel MF, and Schulze H. Long-range effects of GABAergic inhibition in gerbil primary auditory cortex. *Eur J Neurosci* 31: 49-59, 2010.
Morel A, and Imig TJ. Thalamic projections to fields A, AI, P, and VP in the cat auditory cortex. *J Comp Neurol* 265: 119-144, 1987.
Morest DK, and Oliver DL. The neuronal architecture of the inferior colliculus in the cat: defining the functional anatomy of the auditory midbrain. *J Comp Neurol* 222: 209-236, 1984.
Muller-Preuss P, and Mitzdorf U. Functional anatomy of the inferior colliculus and the auditory cortex: current source density analyses of click-evoked potentials. *Hear Res* 16: 133-142, 1984.
Nakamoto KT, Jones SJ, and Palmer AR. Descending projections from auditory cortex modulate sensitivity in the midbrain to cues for spatial position. *J Neurophysiol* 99: 2347-2356, 2008.
Nelson PC, and Carney LH. A phenomenological model of peripheral and central neural responses to amplitude-modulated tones. *J Acoust Soc Am* 116: 2173-2186, 2004.
Neuheiser A, Lenarz M, Reuter G, Calixto R, Nolte I, Lenarz T, and Lim HH. Effects of pulse phase duration and location of stimulation within the inferior colliculus on auditory cortical evoked potentials in a guinea pig model. *J Assoc Res Otolaryngol* 11: 689-708, 2010.
Oliver DL. Neuron types in the central nucleus of the inferior colliculus that project to the medial geniculate body. *Neuroscience* 11: 409-424, 1984.
Oliver DL. Neuronal organization in the inferior colliculus. In: *The Inferior Colliculus*, edited by Winer JA, and Schreiner CE. New York: Springer Science+Business Media, Inc., 2005, p. 69-114.
Oliver DL, Beckius GE, Bishop DC, and Kuwada S. Simultaneous anterograde labeling of axonal layers from lateral superior olive and dorsal cochlear nucleus in the inferior colliculus of cat. *J Comp Neurol* 382: 215-229, 1997.
Oxenham AJ, and Moore BC. Modeling the additivity of nonsimultaneous masking. *Hear Res* 80: 105-118, 1994.
Pfingst BE, Zwolan TA, and Holloway LA. Effects of stimulus configuration on psychophysical operating levels and on speech recognition with cochlear implants. *Hear Res* 112: 247-260, 1997.
Phillips DP, and Orman SS. Responses of single neurons in posterior field of cat auditory cortex to tonal stimulation. *J Neurophysiol* 51: 147-163, 1984.
Phillips DP, Semple MN, and Kitzes LM. Factors shaping the tone level sensitivity of single neurons in posterior field of cat auditory cortex. *J Neurophysiol* 73: 674-686, 1995.
Polley DB, Read HL, Storace DA, and Merzenich MM. Multiparametric auditory receptive field organization across five cortical fields in the albino rat. *J Neurophysiol* 97: 3621-3638, 2007.

Popper AN, and Fay RR. *Hearing by bats*. Springer-Verlag, 1995.
Portfors CV, Mayko ZM, Jonson K, Cha GF, and Roberts PD. Spatial organization of receptive fields in the auditory midbrain of awake mouse. *Neuroscience* 193: 429-439, 2011.
Portfors CV, and Wenstrup JJ. Topographical distribution of delay-tuned responses in the mustached bat inferior colliculus. *Hear Res* 151: 95-105, 2001.
Prosen CA, Petersen MR, Moody DB, and Stebbins WC. Auditory thresholds and kanamycin-induced hearing loss in the guinea pig assessed by a positive reinforcement procedure. *The Journal of the Acoustical Society of America* 63: 559-566, 1978.
Ranck JB, Jr. Which elements are excited in electrical stimulation of mammalian central nervous system: a review. *Brain Res* 98: 417-440, 1975.
Rauschecker J, and Romanski L. Auditory Cortical Organization: Evidence for Functional Streams. In: *The Auditory Cortex*, edited by Winer JA, and Schreiner CESpringer US, 2011, p. 99-116.
Read HL, Winer JA, and Schreiner CE. Functional architecture of auditory cortex. *Current Opinion in Neurobiology* 12: 433-440, 2002.
Redies H, Brandner S, and Creutzfeldt OD. Anatomy of the auditory thalamocortical system of the guinea pig. *J Comp Neurol* 282: 489-511, 1989a.
Redies H, Sieben U, and Creutzfeldt OD. Functional subdivisions in the auditory cortex of the guinea pig. *J Comp Neurol* 282: 473-488, 1989b.
Rees A, and Palmer A. *The Auditory Brain*. Oxford ; New York: Oxford University Press, 2010, p. x, 450 p.
Rennaker RL, Carey HL, Anderson SE, Sloan AM, and Kilgard MP. Anesthesia suppresses nonsynchronous responses to repetitive broadband stimuli. *Neuroscience* 145: 357-369, 2007.
Rode T, Hartmann T, Hubka P, Scheper V, Lenarz M, Lenarz T, Kral A, and Lim HH. Neural representation in the auditory midbrain of the envelope of vocalizations based on a peripheral ear model. *Front Neural Circuits* 7: 166, 2013.
Rodrigues-Dagaeff C, Simm G, De Ribaupierre Y, Villa A, De Ribaupierre F, and Rouiller EM. Functional organization of the ventral division of the medial geniculate body of the cat: evidence for a rostro-caudal gradient of response properties and cortical projections. *Hear Res* 39: 103-125, 1989.
Roth GL, Aitkin LM, Andersen RA, and Merzenich MM. Some features of the spatial organization of the central nucleus of the inferior colliculus of the cat. *J Comp Neurol* 182: 661-680, 1978.
Rouiller EM. Functional Organization of the Auditory Pathways. In: *The Central Auditory System*, edited by Ehret G, and Romand R. New York: Oxford University Press, Inc., 1997.
Saldana E, Feliciano M, and Mugnaini E. Distribution of descending projections from primary auditory neocortex to inferior colliculus mimics the topography of intracollicular projections. *J Comp Neurol* 371: 15-40, 1996.
Schreiner C, Froemke R, and Atencio C. Spectral Processing in Auditory Cortex. In: *The Auditory Cortex*, edited by Winer JA, and Schreiner CESpringer US, 2011, p. 275-308.

Schreiner CE, and Langner G. Laminar fine structure of frequency organization in auditory midbrain. *Nature* 388: 383-386, 1997.
Schreiner CE, and Langner G. Periodicity coding in the inferior colliculus of the cat. II. Topographical organization. *J Neurophysiol* 60: 1823-1840, 1988.
Schreiner CE, and Mendelson JR. Functional topography of cat primary auditory cortex: distribution of integrated excitation. *J Neurophysiol* 64: 1442-1459, 1990.
Schreiner CE, Read HL, and Sutter ML. Modular organization of frequency integration in primary auditory cortex. *Annu Rev Neurosci* 23: 501-529, 2000.
Schreiner CE, and Sutter ML. Topography of excitatory bandwidth in cat primary auditory cortex: single-neuron versus multiple-neuron recordings. *J Neurophysiol* 68: 1487-1502, 1992.
Schwartz MS, Otto SR, Shannon RV, Hitselberger WE, and Brackmann DE. Auditory brainstem implants. *Neurotherapeutics* 5: 128-136, 2008.
Semple MN, and Aitkin LM. Representation of sound frequency and laterality by units in central nucleus of cat inferior colliculus. *J Neurophysiol* 42: 1626-1639, 1979.
Sennaroglu L, Colletti V, Manrique M, Laszig R, Offeciers E, Saeed S, Ramsden R, Sarac S, Freeman S, Andersen HR, Zarowski A, Ziyal I, Sollmann WP, Kaminsky J, Bejarano B, Atas A, Sennaroglu G, Yucel E, Sevinc S, Colletti L, Huarte A, Henderson L, Wesarg T, and Konradsson K. Auditory brainstem implantation in children and non-neurofibromatosis type 2 patients: a consensus statement. *Otol Neurotol* 32: 187-191, 2011.
Shannon RV. Threshold and loudness functions for pulsatile stimulation of cochlear implants. *Hear Res* 18: 135-143, 1985.
Shannon RV, Zeng FG, Kamath V, Wygonski J, and Ekelid M. Speech recognition with primarily temporal cues. *Science* 270: 303-304, 1995.
Sherman SM. Tonic and burst firing: dual modes of thalamocortical relay. *Trends Neurosci* 24: 122-126, 2001.
Sherman SM, and Guillery RW. *Exploring the Thalamus*. Elsevier Science, 2001.
Shneiderman A, and Henkel CK. Banding of lateral superior olivary nucleus afferents in the inferior colliculus: a possible substrate for sensory integration. *J Comp Neurol* 266: 519-534, 1987.
Sivaramakrishnan S, and Oliver DL. Neuronal responses to lemniscal stimulation in laminar brain slices of the inferior colliculus. *J Assoc Res Otolaryngol* 7: 1-14, 2006.
Smith PH, and Populin LC. Fundamental differences between the thalamocortical recipient layers of the cat auditory and visual cortices. *J Comp Neurol* 436: 508-519, 2001.
Snyder RL, Bierer JA, and Middlebrooks JC. Topographic spread of inferior colliculus activation in response to acoustic and intracochlear electric stimulation. *J Assoc Res Otolaryngol* 5: 305-322, 2004.
Stiebler I. Tone-threshold mapping in the inferior colliculus of the house mouse. *Neurosci Lett* 65: 336-340, 1986.
Stiebler I, and Ehret G. Inferior colliculus of the house mouse. I. A quantitative study of tonotopic organization, frequency representation, and tone-threshold distribution. *J Comp Neurol* 238: 65-76, 1985.

Storace DA, Higgins NC, Chikar JA, Oliver DL, and Read HL. Gene expression identifies distinct ascending glutamatergic pathways to frequency-organized auditory cortex in the rat brain. *J Neurosci* 32: 15759-15768, 2012.
Storace DA, Higgins NC, and Read HL. Thalamic label patterns suggest primary and ventral auditory fields are distinct core regions. *J Comp Neurol* 518: 1630-1646, 2010.
Storace DA, Higgins NC, and Read HL. Thalamocortical pathway specialization for sound frequency resolution. *J Comp Neurol* 519: 177-193, 2011.
Straka M, Schendel D, and Lim HH. Neural integration and enhancement from the inferior colliculus up to different layers of auditory cortex. *J Neurophysiol* 2013.
Sumner CJ, O'Mard LP, Lopez-Poveda EA, and Meddis R. A nonlinear filter-bank model of the guinea-pig cochlear nerve: rate responses. *J Acoust Soc Am* 113: 3264-3274, 2003.
Suta D, Kvasnak E, Popelar J, and Syka J. Representation of species-specific vocalizations in the inferior colliculus of the guinea pig. *J Neurophysiol* 90: 3794-3808, 2003.
Swadlow HA, and Gusev AG. The impact of 'bursting' thalamic impulses at a neocortical synapse. *Nat Neurosci* 4: 402-408, 2001.
Syka J, Popelar J, Kvasnak E, and Astl J. Response properties of neurons in the central nucleus and external and dorsal cortices of the inferior colliculus in guinea pig. *Exp Brain Res* 133: 254-266, 2000.
Syka J, Suta D, and Popelar J. Responses to species-specific vocalizations in the auditory cortex of awake and anesthetized guinea pigs. *Hear Res* 206: 177-184, 2005.
Tan AY, and Wehr M. Balanced tone-evoked synaptic excitation and inhibition in mouse auditory cortex. *Neuroscience* 163: 1302-1315, 2009.
Team RC. R: A language and environment for statistical computing. Vienna, Austria: R Foundation for Statistical Computing, 2013.
Ter-Mikaelian M, Sanes DH, and Semple MN. Transformation of temporal properties between auditory midbrain and cortex in the awake Mongolian gerbil. *J Neurosci* 27: 6091-6102, 2007.
Torterolo P, Falconi A, Morales-Cobas G, and Velluti RA. Inferior colliculus unitary activity in wakefulness, sleep and under barbiturates. *Brain Res* 935: 9-15, 2002.
Usrey WM, Alonso JM, and Reid RC. Synaptic interactions between thalamic inputs to simple cells in cat visual cortex. *J Neurosci* 20: 5461-5467, 2000.
Velenovsky DS, Cetas JS, Price RO, Sinex DG, and McMullen NT. Functional subregions in primary auditory cortex defined by thalamocortical terminal arbors: an electrophysiological and anterograde labeling study. *J Neurosci* 23: 308-316, 2003.
Viemeister NF. Temporal modulation transfer functions based upon modulation thresholds. *J Acoust Soc Am* 66: 1364-1380, 1979.
Viemeister NF, and Wakefield GH. Temporal integration and multiple looks. *J Acoust Soc Am* 90: 858-865, 1991.
Wallace MN, Rutkowski RG, and Palmer AR. Identification and localisation of auditory areas in guinea pig cortex. *Exp Brain Res* 132: 445-456, 2000.
Wang X, Lu T, Snider RK, and Liang L. Sustained firing in auditory cortex evoked by preferred stimuli. *Nature* 435: 341-346, 2005.

Webster DB, Popper AN, and Fay RR. *The Mammalian auditory pathway : neuroanatomy*. New York: Springer-Verlag, 1992, p. xi, 485 p.
Wehr M, and Zador AM. Balanced inhibition underlies tuning and sharpens spike timing in auditory cortex. *Nature* 426: 442-446, 2003.
Wehr M, and Zador AM. Synaptic mechanisms of forward suppression in rat auditory cortex. *Neuron* 47: 437-445, 2005.
Wenstrup JJ, Larue DT, and Winer JA. Projections of physiologically defined subdivisions of the inferior colliculus in the mustached bat: targets in the medial geniculate body and extrathalamic nuclei. *J Comp Neurol* 346: 207-236, 1994.
Wenstrup JJ, Ross LS, and Pollak GD. A functional organization of binaural responses in the inferior colliculus. *Hear Res* 17: 191-195, 1985.
Winer J, and Schreiner C. The Central Auditory System: A Functional Analysis. In: *The Inferior Colliculus*, edited by Winer J, and Schreiner CSpringer New York, 2005, p. 1-68.
Winer JA. A Profile of Auditory Forebrain Connections and Circuits. In: *The Auditory Cortex*, edited by Winer JA, and Schreiner CE. New York: Springer Science+Business Media, Inc., 2010.
Winer JA. Decoding the auditory corticofugal systems. *Hear Res* 212: 1-8, 2006.
Winer JA. Structure of layer II in cat primary auditory cortex (AI). *J Comp Neurol* 238: 10-37, 1985.
Winer JA. Three systems of descending projections to the inferior colliculus. In: *The Inferior Colliculus*, edited by Winer JA, and Schreiner CE. New York: Springer Science+Business Media, Inc., 2005, p. 231-247.
Winer JA, and Larue DT. Populations of GABAergic neurons and axons in layer I of rat auditory cortex. *Neuroscience* 33: 499-515, 1989.
Winer JA, Larue DT, Diehl JJ, and Hefti BJ. Auditory cortical projections to the cat inferior colliculus. *J Comp Neurol* 400: 147-174, 1998.
Winer JA, Miller LM, Lee CC, and Schreiner CE. Auditory thalamocortical transformation: structure and function. *Trends Neurosci* 28: 255-263, 2005.
Winer JA, and Prieto JJ. Layer V in cat primary auditory cortex (AI): cellular architecture and identification of projection neurons. *J Comp Neurol* 434: 379-412, 2001.
Winer JA, and Schreiner C. *The Auditory Cortex*. Springer, 2010.
Xiong Y, Zhang Y, and Yan J. The neurobiology of sound-specific auditory plasticity: a core neural circuit. *Neurosci Biobehav Rev* 33: 1178-1184, 2009.
Yamauchi T, Hori T, and Takahashi T. Presynaptic inhibition by muscimol through GABAB receptors. *Eur J Neurosci* 12: 3433-3436, 2000.
Yan J, Zhang Y, and Ehret G. Corticofugal shaping of frequency tuning curves in the central nucleus of the inferior colliculus of mice. *J Neurophysiol* 93: 71-83, 2005.
Yan W, and Suga N. Corticofugal modulation of the midbrain frequency map in the bat auditory system. *Nat Neurosci* 1: 54-58, 1998.
Yost WA. *Fundamentals of hearing : an introduction*. San Diego: Academic Press, 2007, p. xiii, 338 p.
Zeng FG. Trends in cochlear implants. *Trends in amplification* 8: 1-34, 2004.

Zhang Y, Hakes JJ, Bonfield SP, and Yan J. Corticofugal feedback for auditory midbrain plasticity elicited by tones and electrical stimulation of basal forebrain in mice. *Eur J Neurosci* 22: 871-879, 2005.
Zhou J, and Shore S. Convergence of spinal trigeminal and cochlear nucleus projections in the inferior colliculus of the guinea pig. *The Journal of comparative neurology* 495: 100-112, 2006.
Zurita P, Villa AE, de Ribaupierre Y, de Ribaupierre F, and Rouiller EM. Changes of single unit activity in the cat's auditory thalamus and cortex associated to different anesthetic conditions. *Neurosci Res* 19: 303-316, 1994.

APPENDIX A: CORTICOFUGAL PROJECTIONS

The IC receives massive corticofugal projections that mediate plastic changes, such as frequency tuning. Fibers originating from the A1 have been detected throughout the ICC and are tonotopic in organization. Secondary cortical areas have not necessarily been shown to have descending projections to the ICC, and no studies have investigated ICC corticofugal projections originating from the small, weakly tonotopic region in guinea pig called ventrorostral belt (**VRB**). Using antidromic stimulation to detect monosynaptic connections, we investigated the spatial organization and physiological properties of corticofugal fibers originating from A1 or VRB to the ICC of ketamine-anesthetized guinea pig. Using three dimensional histological techniques to reconstruct the ICC, we found that A1 has ample, tonotopically organized projections throughout the ICC isofrequency laminae. This study found that VRB also has monosynaptic projections to the ICC lamina, but, in contrast to A1 fibers, have a weaker tonotopic organization and primarily project to the caudal-medial and not rostral-lateral regions across the ICC laminae. In addition, no spatial organizations across isofrequency regions of A1 or VRB were detected.

INTRODUCTION

All areas of the auditory cortex have been shown to have descending corticofugal projections that target the inferior colliculus, the main auditory nucleus of the midbrain, in which projections originating from A1 have been the most accurately characterized. Traditionally, anatomical tracer studies have found that these A1 fibers primarily terminate in the nonlemniscal external cortices rather than the lemniscal ICC (Faye-Lund 1985; Herbert et al. 1991; Huffman and Henson 1990; Winer et al. 1998). However, recent anatomical evidence found projections from A1 to the ICC that are tonotopically organized (Andersen et al. 1980; Bajo and Moore 2005; Bajo et al. 2007; Coomes et al. 2005; Feliciano and Potashner 1995; Malmierca and Ryugo 2011; Saldana et al. 1996; Xiong et al. 2009). While these tracer studies could only analyze corticofugal projections from large neural populations, Lim et al. (2007a) investigated the spatial distribution and physiological properties of smaller populations of A1-ICC projections by electrically stimulating the ICC and recording antidromic spikes in the cortex. By using this antidromic stimulation method, monosynaptic projections could be identified and physiological properties of neurons from both areas could be characterized. Lim et al. (2007a) found that A1 corticofugal projections are amply distributed throughout the ICC and that they are tonotopically organized. However, the spatial resolution of the histological reconstructions limited the analysis of how these projections were organized across the ICC lamina, and the spatial organization across the cortex was not investigated.

These tonotopically organized, A1-ICC corticofugal projections have been shown to play a role in plastic changes within the auditory system. The frequency coding

properties of ICC neurons can be shifted towards those of the stimulated A1 neurons when paired with acoustic stimulation (Yan et al. 2005; Yan and Suga 1998), electrical stimulation of neuromodulatory pathways (Ma and Suga 2003; Zhang et al. 2005), or fear conditioning paradigms (Gao and Suga 1998; 2000; Ji et al. 2001). Lesions or suppression of activity within the auditory cortex limits this frequency shift in the ICC (Zhang et al. 2005) and can induce other effects in the IC such as altering responses for sound localization (Bajo et al. 2010; Nakamoto et al. 2008).Considering that these corticofugal projections are primarily glutamatergic (Feliciano and Potashner 1995), these plasticity studies suggest that A1 can alter the excitatory responses in ICC through this pathway. This was further confirmed by Markovitz et al. (2013), where focal electrical stimulation of A1 caused excitatory activity in the ICC with tonotopic patterns that either show strict or broad frequency alignment. Moreover, the excitatory activity was primarily observed in the caudal-medial and not rostral-lateral region along the ICC isofrequency laminae, which suggests that the corticofugal projections may exhibit differential patterns across the ICC laminae.

Together, these previous studies have found direct corticofugal projections from A1to ICC that are tonotopically arranged and can affect plastic changes in frequency-specific collicular responses. However, the spatial distribution across A1 and ICC of these projections have not been adequately investigated, even though there is evidence that A1 results in differential excitatory activity across the ICC laminae (Markovitz et al. 2013). Moreover, the majority of physiological studies have focused on corticofugal projections arising from A1. Considering that other cortical areas show differential

descending projection patterns, the contrast between the spatial distribution and physiological properties of various corticofugal patterns may provide insight into the function of the descending auditory system as a whole. For example, in the guinea pig the VRB is located laterally and ventrally to A1, has a weaker tonotopic arrangement that is aligned in the same direction as the tonotopic organization of A1 (Wallace et al. 2000). Due to VRB's location and similarity in tonotopic alignment as A1, VRB is often misidentified as A1. VRB's small area also makes its descending projections difficult to study with anatomical tracers. Though comparing cortical areas between species is often complicated, VRB likely corresponds to posterior auditory field (**PAF**) in cat since both fields are known for having the longest latencies in response to pure tones of the tonotopically arranged cortical fields (Kaas 2011; Phillips and Orman 1984; Wallace et al. 2000). Though the PAF has corticofugal projections to the inferior colliculus, the projection targets have not been shown to include the ICC, in contrast to the A1 corticofugal projections (Winer et al. 1998).

In this study, we investigated corticofugal projections originating in A1 and VRB by recording antidromic activity elicited by electrical stimulation of the ICC. We found that both A1 and VRB respond with antidromic spiking, thus giving evidence of monosynaptic projections from both areas are present in the ICC. We analyzed physiological responses to compare the tonotopic arrangement of corticofugal projections arising from each cortical area. In addition to assessing the spatial distribution of these connections across the cortex, we used detailed histological reconstructions of the

midbrain to analyze the spatial organization across the ICC isofrequency lamina, in which we discovered significant differences between the VRB and A1.

METHODS

OVERVIEW

Basic surgical procedures and methods for neural recording and stimulation were similar to those presented in previous work (Lim and Anderson 2007a; 2006; Straka et al. 2013). Ketamine-anesthetized guinea pigs were used in accordance with policies of the University of Minnesota's Institutional Animal Care and Use Committee. Silicon-substrate, 32-site Michigan electrode arrays (NeuroNexus Technologies, Ann Arbor, MI) were used to electrically stimulate the ICC and record the corresponding neural responses within AC. Appropriate placement of the array sites within the ICC and AC was guided by acoustic-driven responses (Lim and Anderson 2007b; Snyder et al. 2004; Wallace et al. 2000). Array sites in the ICC were individually stimulated and multi-unit spiking responses were recorded in A1 and VRB. When antidromic activity was detected in A1 or VRB, the minimal stimulation threshold and location across the ICC was found to determine if there is a spatial distribution across the ICC lamina for corticofugal projections.

SURGERY

Experiments were performed on 23 male and female Hartley guinea pigs (380 ± 53 g, Elm Hill Breeding Labs, Chelmsford, MA). Animals were initially anesthetized with an intramuscular injection of ketamine (40 mg/kg) and xylazine (10 mg/kg), and were given periodic supplements to maintain an areflexive state. After fixing the animal into a

stereotaxic frame (David Kopf Instruments, Tujunga, CA), the right side of the cortex was exposed from the caudal end of the occipital lobe to the middle cerebral artery of the temporal lobe. The dura was removed, micromanipulators were used to insert the arrays into the ICC and AC, and the exposed brain was covered with agarose gel.

Stimulation and Recording Setup

All experiments were performed in an acoustically- and electrically-shielded chamber and controlled by a computer interfaced with TDT System 3 hardware (Tucker-Davis Technology, Alachua, FL) using custom software written in MATLAB (MathWorks, Natick, MA). For acoustic stimulation, sound was presented via a speaker coupled to the left ear through a hollow ear bar. The speaker-ear bar system was calibrated using a 0.25-in. condenser microphone (ACO Pacific, Belmont, CA) connected to the ear bar via a short plastic tube representing the ear canal.

All neural signals were passed through analog DC-blocking and anti-aliasing filters from 1.6 Hz to 7.5 kHz. The sampling frequency used for acoustic stimulation was 195 kHz and for neural recording was 24 kHz. Electrical stimulation up to 100 μA was presented on different sites on the ICC array in a monopolar configuration with a ground return in the neck muscles. The pulses were biphasic, charge-balanced, cathodic-leading, and 205 μs/phase. The recording ground needle was positioned either under the skin approximately 2 cm rostral to bregma or directly in the brain in the parietal lobe. No obvious differences in results were observed when using the different recording grounds.

Placement of Arrays

PSTHs and FRMs of spiking activity were plotted online to confirm the array's

position within the ICC or AC. Details on these analysis methods and example plots for similar types of arrays are presented in previous publications (Lenarz et al. 2006a; Lim and Anderson 2006; Neuheiser et al. 2010). Briefly, we bandpass filtered the neural signals (300-3000 Hz) on each site and detected spikes that exceeded a threshold of three standard deviations above the background activity. For FRMs, four trials were presented for each pure tone (1-40 kHz, 8 steps/octave) and level (0-70 dB, 10 dB steps) stimulus. The BF was taken as the centroid of frequencies which elicited spiking responses at 10 dB above the visually-determined threshold.

The AC array consisted of four 5-mm-long shanks separated by 400 μm. Sites were linearly spaced at 200 μm along the shank and each had an area of 177 μm^2. The array was inserted approximately perpendicular to the cortical surface in an attempt to align each shank along a column in AC (Abeles and Goldstein 1970; Redies et al. 1989b; Wallace et al. 2000). Placement into A1 or VRB was confirmed when tonotopic shifts from low to high BFs were observed for ventral-rostral to dorsal-caudal locations (Wallace et al. 2000). To investigate differences across AC locations, we reconstructed the site locations on the cortical surface based on microscope images (OPMI 1 FR pro, Zeiss, Dublin, CA) taken of our array placements and normalized based on various landmarks (e.g., middle cerebral artery, bregma and lateral suture lines, major blood vessels) as successfully used in previous studies (Eggermont and Roberts 2004; Schreiner et al. 2000; Wallace et al. 2000). These normalized locations and their respective BFs can be seen overlaid on the auditory cortex in Figure 37.

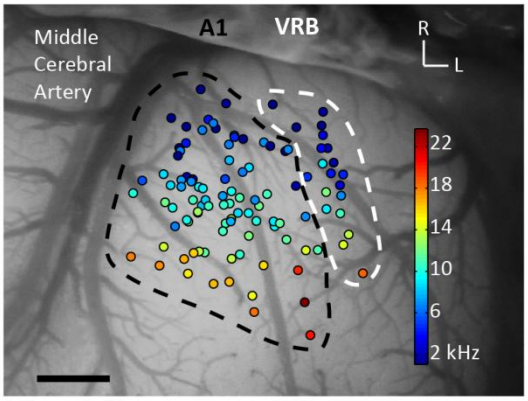

Figure 37: BF of each recording site in A1 and VRB, overlaid on a typical guinea pig cortex. Locations were determined to be in A1 or VRB based on cortical location as well as latency responses (see Methods). Scale bar is 1 mm. R, rostral; L, lateral.

Data was analyzed on a total of 88 A1 placements from 20 guinea pigs and 20 VRB placements from 4 guinea pigs, where multiple AC placements were made in two guinea pigs. AC placements were determined to be in A1 or VRB by the location on the cortex seen in Figure 37, where VRB placements were more lateral than A1 placements. These locations are similar to those previously determined by Wallace et al. in guinea pig (Wallace et al. 2000). The identification of analysis was confirmed by differences in the FSL responses, which are significantly longer in VRB (Wallace et al. 2000). The FSL was calculated by computing the mean latency of the first spike to noise stimuli at 70 dB SPL across 100 trials, and the FSL for a specific cortical shank was determined by averaging across all sites which responded to noise. Across all of the A1 and VRB locations, the mean FSL for A1 was 21 ± 5 ms (N=85 sites), which was significantly different from the 33 ± 5 ms FSL for VRB (N=18 sites), ($P < 3 \times 10^{-10}$ using two-tailed, unequal variance t-tests, some sites responded weakly to noise and were not included). Thus, we were confident that VRB and A1 were appropriately differentiated.

The identification of AC layers was accomplished by performing CSD analysis (Kral et al. 2000; Mitzdorf 1985; Muller-Preuss and Mitzdorf 1984) in response to 70 dB SPL broadband noise (100 trials) using the finite difference formula:

$$CSD(z) = \sigma_z \frac{\phi(z+\Delta z) - 2\phi(z) + \phi(z-\Delta z)}{(\Delta z)^2}$$

where ϕ is the averaged LFP across trials, z is the depth location of each site along an AC array shank, Δz is the differentiation step size, and σ_z is the component of conductivity in the z-direction. Δz was equal to the AC site spacing of 200 μm and σ_z was set to one since absolute CSD values were not required for analysis. The one-dimensional CSD approximation provides a consistent representation for the current sinks and sources associated with columnar synaptic activity in the guinea pig auditory cortex (Lim and Anderson 2007a; Middlebrooks 2008). The main input layer of AC, which is layer III/IV in guinea pig (Huang and Winer 2000; Smith and Populin 2001), corresponded to the site with the shortest latency current sink (i.e., positive CSD peak). Layer V was identified as the site with a current source (i.e., negative CSD peak), typically being two electrode sites (or 400 μm) deeper than layer III/IV. Since CSD analysis has not been well described in VRB, we also determined the cortical depth of the site determined to be in layer V. This was accomplished by determining the shallowest site along each shank with spiking responses to 100 trials of broadband noise 70 dB SPL. Since layer I has few neurons which are primarily GABAergic (Winer and Larue 1989) and layer II has more pyramidal neurons (Winer 1985), this shallow site is referred to as the layer II site.

Averaged across placements, sites identified as layer V were 920 ± 160 μm and 860 ± 170 μm below layer II for A1 (N= 87 layer differences) and VRB (N=18), respectively (placements with bad sites or invalid data at shallow sites were not included). Anatomical analysis using Nissl staining preparations in cat found that layer V is typically ~800-1300 μm below layer II for A1 and ~700-1200 μm below layer II in the temporal cortex (Huang and Winer 2000). Though our depths were determined with physiological recordings with a resolution of 200 μm between sites, the similarity with expected anatomical depths suggests that the CSD analysis correctly identified sites in layer V.

The ICC array consisted either of four 8-mm-long shanks or of two 10-mm-long shanks. For both arrays, each shank was separated by 500 μm and sites were linearly spaced at 100 μm along the shank. Each site had an area of approximately 700 μm^2. Prior to the experiment, the sites on the ICC array were activated using cyclic voltammetry to enable both recording and stimulation up to 100 μA (Anderson et al. 1989; Lim and Anderson 2006). The ICC array was placed at a 45° angle to the sagittal plane through the visual cortex in order to be aligned along the tonotopic axis of the ICC (Malmierca et al. 1995; Snyder et al. 2004). Proper array placement in the ICC was confirmed by observing FRMs that exhibited an orderly shift from low to high BFs from superficial to deeper locations along a shank (Lim and Anderson 2006; Snyder et al. 2004).

ELECTRICAL STIMULATION AND DATA ANALYSIS

For each ICC array placement, electrical stimulation was presented individually on several sites at stimulation levels from 16 to 36 dB in 2 dB steps, while randomizing

level and stimulation site. We did not stimulate at higher levels in order to remain within the threshold limits for safety and stability of our electrode arrays. Stimulation evoked multi-unit spiking activity in the AC, and spiking activity in layer V often had antidromic activity. As characterized in a previous publication (Lim and Anderson 2007a), antidromic activity was determined when spikes exhibited short latencies with low temporal jitter, the activity was predominantly isolated in layer V, and a slight increase in current level above threshold resulted in a sudden increase from no activity to robust spiking per trial. Though more definitive tests for antidromicity include spike collisions and the ability to follow at high stimulation rates (Lipski 1981), Lim et al. showed that these characteristics were consistent with A1-to-ICC projections that could also follow at high frequencies (2007a). The minimal stimulation threshold which resulted in antidromic activity was noted for each stimulation-recording ICC-AC site pair.

HISTOLOGICAL RECONSTRUCTIONS

Prior to placement, the ICC array was dipped in a red stain (Di-I: 1, 1-dioctadecyl-3,3,3',3'-tetramethylindocarbocyanine perchlorate, Sigma-Aldrich, St. Louis, MO) to later identify array position within the ICC during histological analysis. Detailed description of the histological procedure, midbrain reconstruction, normalization, and approximation of frequency lamina is provided in a previous publication (Markovitz et al. 2012). Briefly, the midbrain was fixed with 3.7% paraformaldehyde and cryosectioned into sagittal sections at 60 μm using a sliding microtome (Leica, Buffalo Grove, IL). Images of each slice were taken using a Leica MZ FLIII fluorescence stereomicroscope (Leica, Buffalo Grove, IL), Leica DFC412 C peltier cooled CCD camera, and Image-Pro software

(MediaCybernetics, Bethesda, MD). A single reflection white light image using a variable intensity fiber optic light source (Fiber-Lit-PL800, Dolan-Jenner Industries, Boxborough, MA) was taken to determine the outline of each slice. Fluorescence images were later superimposed on the white light images for visualization of the reference and array shank points. The brain was then reconstructed in three dimensions using Rhinoceros (Seattle, WA), and the positions of the arrays were estimated by creating best fit lines through the points on individual slices.

The reconstructions for each brain were normalized to one standard brain using the reference needle point at the intersection of the superior colliculus, thalamus, and lateral extension from the IC, as well as using the curvature of the IC. Isofrequency laminae were approximated by creating a plane orthogonal to the average insertion angle of all best fit lines of each array placement. The depth of each lamina was determined by calculating the distance from the surface of the IC, where neurons do not respond to broadband noise, to locations where neurons respond with specific BFs. This distance was multiplied by a scaling factor to account for tissue changes due to histological process.

A total of 437 ICC sites were stimulated. To analyze location effects across the ICC lamina, we created four laminae at frequencies which would include the majority of sites. We chose each lamina to have a bandwidth of approximately 0.6 octaves, which corresponds to two critical bands (Malmierca et al. 2008; Schreiner and Langner 1997), in order to have sufficient points for analysis. If there was more than one ICC site for a placement within the frequency lamina, the site resulting in the lowest threshold

antidromic activity was chosen for data analysis. Thus, we identified locations for ICC sites across these four isofrequency laminae with the following frequencies: 1.1-1.7 kHz (N=51 ICC sites), 3.8-6.1 kHz (N=44), 6.2-10 kHz (N=107) and 11-17 kHz (N=72). The locations of all array positions on the normalized brain can be seen in Figure 38A along with the four isofrequency laminae. We determined ICC locations across these laminae and showed whether antidromic activity was recorded in A1 or VRB in Figure 38B.

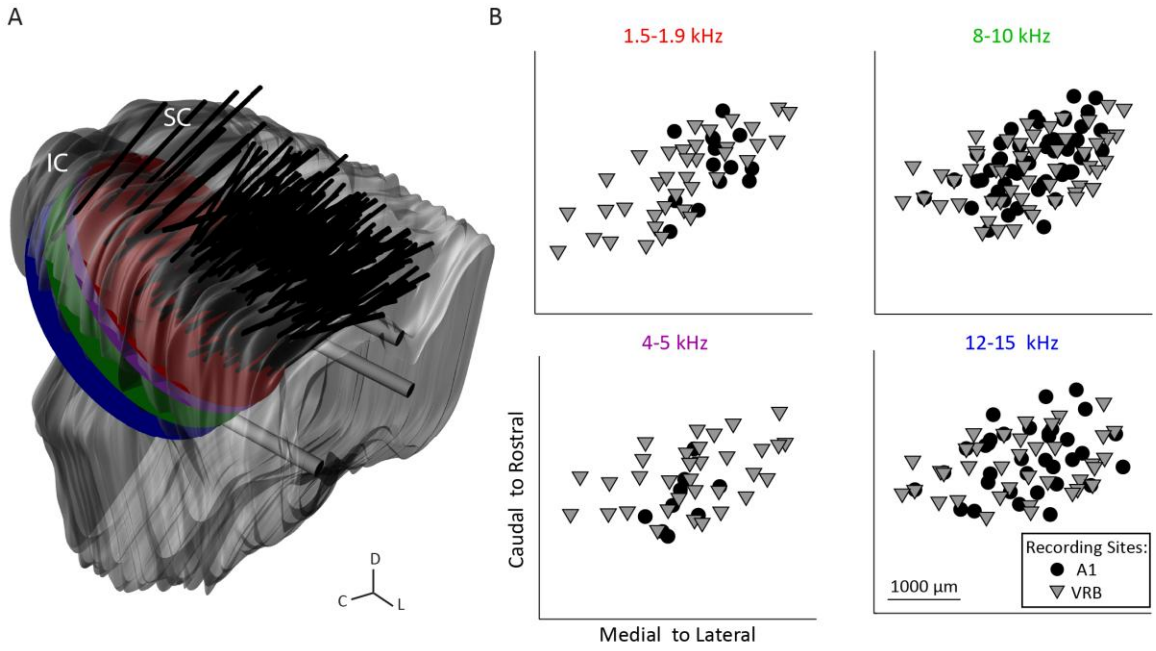

Figure 38: A, The midbrains and array placements were reconstructed in three dimensions and normalized onto a single brain. Each placement was determined to be in the ICC due to the presence of tonotopic shifts of increasing BFs with deeper sites for each shank (see Methods). The four isofrequency laminae were approximated by a plane at a depth in which neurons respond at those BFs. **B**, Each ICC site was electrically stimulated and elicited activity was recorded in VRB (triangles) or A1 (circles). The location of stimulated ICC sites was found across each lamina for sites with corresponding BFs (i.e., the locations were not determined for ICC sites with BFs beyond a lamina's bandwidth). Direct corticofugal projections were determined when antidromic activity was elicited in the cortex. D, dorsal; C, caudal.

RESULTS

OVERVIEW OF APPROACH

We compared corticofugal projections to the ICC arising from A1 and VRB (Figure 37) to determine whether tonotopically organized primary cortical areas have different projection patterns through the ICC. Corticofugal projections were identified when layer V sites in the AC had antidromic activity in response to electrical stimulation of the ICC. In the following sections, we characterize theses corticofugal projections by analyzing their tonotopic arrangement and spatial distribution across the AC as well as the isofrequency laminae of the ICC.

TONOTOPIC ARRANGEMENT OF DESCENDING PROJECTIONS

Since corticofugal projections from A1 to ICC have previously found to be tonotopically organized, the first goal of this project was to confirm this in A1 and assess this in VRB. Considering that high stimulation thresholds could be activating fibers from other laminae, we first determined how the frequency specificity of the fibers related to the current level used for stimulation. For each ICC-AC stimulation-recording site pair for which antidromic activity was detected, we found the threshold of stimulation that elicited antidromic activity and compared it to the ΔBF between the two sites. Figure 39A shows that as the stimulation threshold increased, so did the difference in BF's between A1 and ICC. A similar trend for VRB and ICC can be seen in Figure 39B, though the BF mismatch is much larger with the VRB sites than the A1 sites even at thresholds below 30 μA. Thus both A1 and VRB corticofugal fibers elicited by low stimulation thresholds

had a smaller ΔBF to the ICC sites than ones with higher stimulation thresholds (which resulted greater current spread).

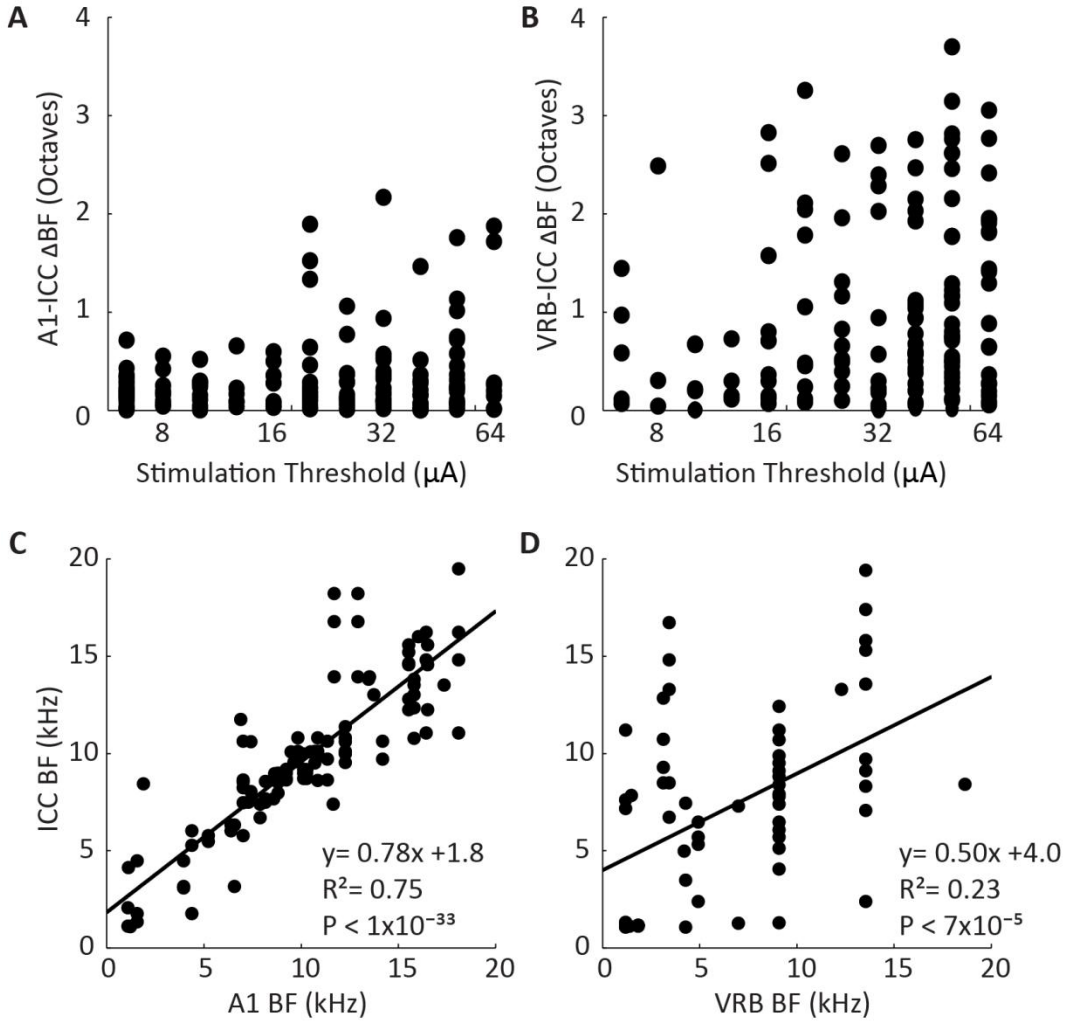

Figure 39: For each AC-ICC site pair with a monosynaptic projection, the ΔBF between each site pair was correlated to the minimum amount of current necessary to evoke antidromic activity. For both A1 (**A**) and VRB (**B**), the higher stimulation thresholds activate sites which have greater BF-mismatch, though neurons in A1 show more similar BFs to the ICC than do neurons in VRB. For corticofugal projections at which antidromic activity could observed in the AC at low stimulation levels (≤ 32μA), the BF of the stimulation site in ICC was correlated to the recording site in A1 (**C**) or VRB (**D**). While a strict tonotopy was found for corticogfugual projections from A1, weak tonotopy was observed for projections from VRB.

In order to characterize the tonotopic arrangement for stimulation cases at these low stimulation thresholds, we first needed to determine a criterion for the maximum current spread that would provide sufficient spatial discrimination. Lim et al. (2007a) previously showed that most A1-ICC antidromic thresholds occurred below 30 µA, which corresponds to a maximal spread of approximately 250 µm (Lim and Anderson 2007a; Ranck 1975). From ICC-A1 site pairs for which antidromic activity was present, we found that 73% (or 111 out of 153 sites) occurred at stimulation levels at or below 30 µA. Since each frequency lamina is approximately 175 µm in cat (Schreiner and Langner 1997) and 150 µm in rat (Malmierca et al. 2008), current applied to the center of a lamina would be unlikely to spread beyond its neighboring lamina. For cases where antidromic activity was elicited at thresholds at or below 30 µA, Figure 39C found that the BF of the A1 recording site was similar to the BF of the stimulating ICC site. Since linear regression found a significant correlation between the BFs ($P < 1x\ 10^{-30}$), we conclude that corticofugal projections from A1 are tonotopically organized. Figure 39D shows that the BF's of VRB and ICC sites were also significantly correlated ($P < 2x\ 10^{-5}$), though this relationship was much weaker and the mismatch between the two sites was still relatively high. For cases where stimulation threshold was at or below 30 µA, the average ΔBF was 0.3 ± 0.4 octaves for A1-ICC sites (N=111 pairs) and 0.8 ± 0.9 octaves for VRB-ICC sites (N=64 pairs).

LOCATION EFFECTS OF CORTICOFUGAL PROJECTIONS

Next, we wanted to determine the spatial distribution of the corticofugal projections across A1. Since each AC site was paired with at least two ICC sites, for each

recording location we found the minimum stimulation threshold elicited across all stimulated ICC sites. Antidromic activity was evident throughout the dorsal-medial to ventral-lateral AC, and no correlation could be determined between the recording location across this tonotopic axis and stimulation threshold for either A1 or VRB (data not shown).

Though a spatial distribution could not be determined across tonotopic areas of the cortical surface, we examined location trends across the isofrequency laminae of the ICC. ICC stimulation sites were separated into one of four isofrequency laminae based on their BF, and the minimal stimulation threshold from all AC sites was deteremined. The location of each stimulation site was determined within the respective lamina using histological reconstructions of each array placement and midbrain (see *Histological Reconstructions*). Thus, in the following analyses, only sites with BF's within the frequency band were analyzed. If a placement had more than one ICC site within an isofrequency lamina, the site that resulted in the lowest stimulation threshold was analyzed. Since we established that these descending projections were primarily tonotopically organized, we compared A1 sites which were BF-matched to the ICC site. Sites were determined to be BF-matched when ΔBF's were less than 0.4 octaves (the standard deviation of the A1-ICC ΔBFs at thresholds below 30 μA).

As shown in Figure 40A, there was no trend for minimal A1 stimulation threshold across any of the four isofrequency laminae. Although the lower frequency laminae had fewer points which did not fully span the lamina, these results sufficiently demonstrate that stimulation of all regions in the ICC could result in cortical antidromic activation.

Low thresholds (<12 µA, which has a current spread of <150 µm) were observed even within central regions of the ICC lamina, and therefore corticofugal fibers are present throughout the ICC lamina (Lim and Anderson 2007a; Ranck 1975).

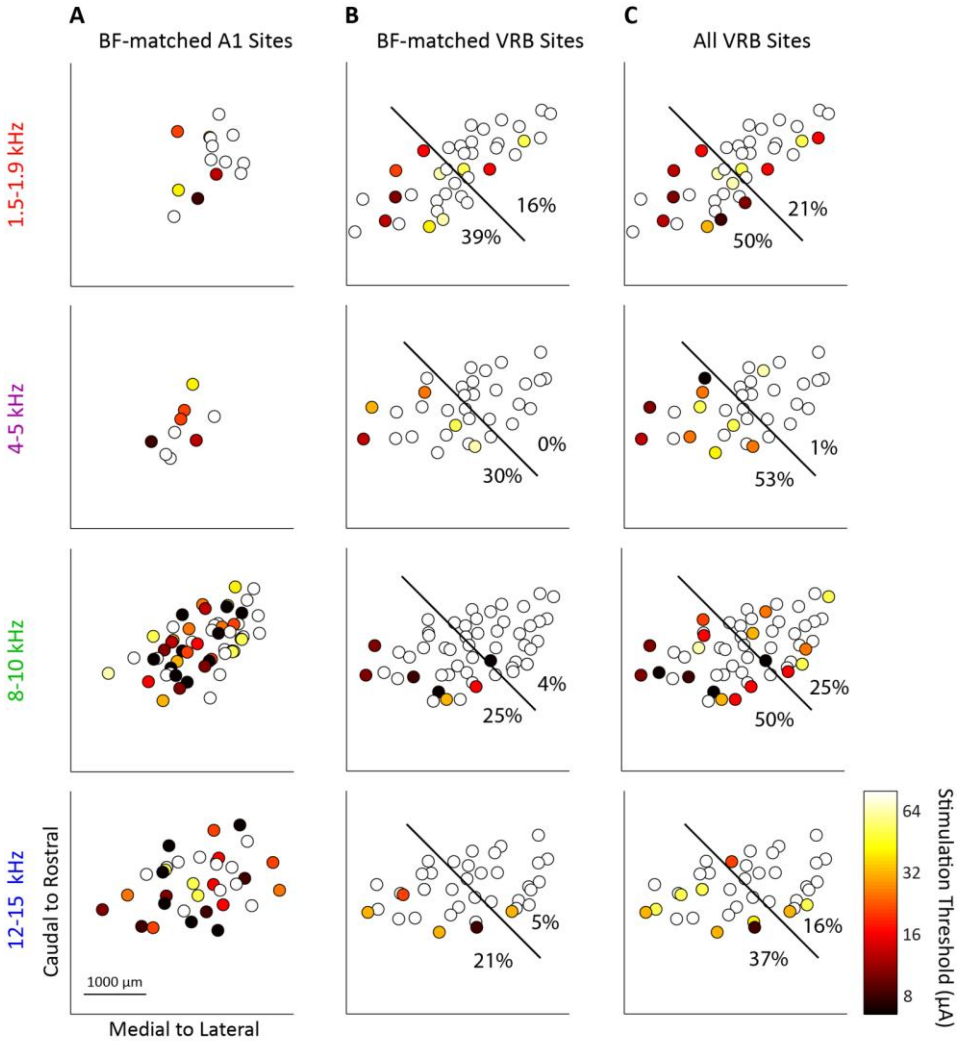

Figure 40: At each location across the four ICC isofrequency laminae, the minimum stimulation threshold evoked from BF-matched A1 sites (A), BF-matched VRB sites (B), or all VRB sites (C) was found. ICC sites which could not elicit antidromic activity in any cortical site even at the highest stimulation threshold (64 µA) are marked as white. While no spatial trend was observed across the ICC lamina for A1 corticofugal projections, VRB fibers were typically found in the caudal-medial regions of the ICC. Each lamina was split into a caudal-medial and rostral-lateral half (based on the average location of all measured

sites, marked by a diagonal line), and the percentage of sites which evoked antidromic activity was found for each half.

While A1 tonotopic corticofugal fibers were present throughout the ICC lamina, VRB corticofugal fibers, which are weakly tonotopic, could be stimulated primarily in the caudal-medial region for all four laminae, as shown in Figure 40B. To quantify this, each lamina was separated into a caudal-medial and a rostral-lateral half as indicated by the line in each pane, using the average location of points as the criterion. The percentage of sites within each half which elicited antidromic activation in VRB, indicated in each pane, was greater in the caudal-medial half for each lamina. Across all laminae, corticofugal projections were evident when stimulating 6% of the sites in rostral-lateral regions as compared to 28% of the sites in the caudal-medial regions.

Since VRB sites had greater mismatch in BF with ICC sites, we also plotted the location of ICC sites and found the minimum stimulation threshold across all VRB sites, regardless of BF, in Figure 40C. In comparison to the BF-matched only connections in Figure 40B, a greater percentage of sites throughout each laminae had corticofugal projections to at least one VRB site. However, the rostral-lateral regions still had a smaller percentage of sites with corticofugal projections, with a total of 18 % versus 47% of sites responding in the rostral-lateral and caudal-medial regions, respectively. Moreover, the thresholds in the rostral-lateral regions were also significantly higher ($P < 4 \times 10^{-5}$ using the Mann-U Whitney test, combining all laminae together and using 38 dB as the threshold for sites where antidromic activity could not be detected). Therefore,

stimulation of caudal-medial locations in the ICC could elicit antidromic activity in VRB even at low thresholds.

DISCUSSION

Our results demonstrate that corticofugal fibers from A1 are distributed throughout ICC isofrequency laminae and have a strict tonotopic organization, confirming a previous study (Lim and Anderson 2007a). In contrast to A1, fibers from VRB to ICC exhibit greater mismatch in tonotopic organization and are primarily localized in the caudal-medial region of the ICC. The differences in corticofugal projections from A1 and VRB in relation to spatial distribution and frequency organization suggest these two cortical areas may have different roles within the descending auditory system.

TONOTOPIC ORGANIZATION

These results confirm that most A1 corticofugal projections are arranged tonotopically. Of the projections which could be activated with relatively low current levels ($\leq$30μA), the average ΔBF was 0.3 ± 0.4 octaves, similar to the bandwidth of an ICC isofrequency lamina (Malmierca et al. 2008; Schreiner and Langner 1997). This suggests that frequency-specific A1 corticofugal fibers generally remain within an isofrequency lamina of the ICC. Projections originating in VRB are loosely tonotopically organized, with an average ΔBF of 0.8 ± 0.9 octaves for fibers with thresholds equal to or below 30μA . The weaker tonotopic organization of the VRB projections in comparison to A1 could be associated with a more diffuse and diverging projection pattern to the ICC

than those from A1, though it is also possible that it reflects the weaker tonotopic organization directly within VRB compared to A1 (Wallace et al. 2000).

Methodological Considerations of Antidromic Stimulation

Using antidromic stimulation as a method to study the spatial distribution of monosynaptic corticofugal projections allowed us to characterize the anatomical and physiological properties of small neural populations in both the cortex and ICC. Moreover, the analysis of the spatial distribution allowed us to determine the spatial organization of projections with greater resolution than possible with traditional histological tracers. Specifically, injections into the small region of VRB would likely diffuse into the lateral area of A1, and thus differentiation between the two regions would prove difficult.

Though the antidromic stimulation method has many benefits, caution must be used in the interpretation of the results because of some important limitations. Due to the design of our arrays, we could not ensure that that single units were recorded within A1. In addition, stimulation of ICC regions may cause antidromic activity in cortical regions which were not recorded, though the design of our array allowed us to record from four A1 locations at a time. We did not find spatial patterns across isofrequency regions of A1 or VRB, though perhaps more complex topographic patterns of the corticofugal projections exist. The second drawback limiting the analysis of these results is that antidromic stimulation can activate both axon terminals as well as passing fibers. Therefore, ICC locations may cause antidromic activity in the cortex from corticofugal fibers either directly innervating those regions or passing through those locations en route

to synapses with more distant neurons. Therefore, we can conclude that A1 corticofugal fibers pass through the entire ICC lamina in a strictly tonotopic organization, while VRB corticofugal fibers only pass through the most caudal-medial locations in VRB.

Descending Corticofugal Projections

Our results provide clear evidence that corticofugal projections from A1 and VRB are present in the ICC. For corticofugal fibers originating from both A1 and VRB, antidromic activation could be elicited even with very low stimulation thresholds of <12 µA, which corresponds to a maximal current spread distance of ~150 µm (i.e., smaller than the diameter of the circles in Figure 40) (Lim and Anderson 2007a; Ranck 1975). While we found that fibers originating from VRB primarily target the caudal-medial regions of the ICC laminae, fibers originating from A1 are ample throughout the ICC lamina.

The lack of spatial organization of A1 corticofugal projections was unexpected considering that Markovitz et al. (2013) found that activation of A1 resulted in excitatory responses in caudal-medial and not rostral-lateral regions along the ICC lamina. These seemingly contradictory results could be due to several issues. First of all, activating A1 neurons could have resulted in excitation of neurons either in secondary areas of the cortex such as VRB or in the cortices of the IC before these regions would excite the ICC. However, it is unlikely that A1 first projected to other cortical areas since the lowest current threshold which elicited activity in ICC was found when stimulating layer V neurons, which primarily send descending projections, rather than to layer I or II, where horizontal connections to other cortical areas primarily reside (unpublished findings in

lab). In addition, it is unlikely that cortices of the IC, which have little or no tonotopy (Aitkin et al. 1975), would act as a relay for the ICC in those cases due to the tonotopic nature of the activity. It is more likely that in this study, corticofugal projections could be passing through rostral-lateral regions en route to their target of the caudal-medial regions, but electrical stimulation of the ICC with our antidromic approach activates these passing fibers. Another possible scenario could be that the fibers terminate throughout the ICC but that inhibition in the rostral-lateral region restricts excitatory responses.

In this study, we discovered that VRB has monosynaptic corticofugal projections to the ICC, which, to the best of our knowledge, has not previously been investigated. Due to similarities in long responses latencies and weak tonotopy in comparison to A1, VRB is likely related to the PAF in cat (Kaas 2011; Phillips and Orman 1984; Wallace et al. 2000). Previous tracer studies found that PAF corticofugal projections exclusively target the outer cortices of the IC and not the ICC (Winer et al. 1998). The contrasting conclusions from our results and this previous tracer study may be due to differences in species or the methodology. The latter seems likely given that many previous tracer studies had shown no or minimal projections from A1 to ICC though more recent studies with detailed tracer and histology methods have been able to identify a greater number of projections to ICC across species (Bajo and Moore 2005; Bajo et al. 2007; Coomes et al. 2005; Feliciano and Potashner 1995; Malmierca and Ryugo 2011; Saldana et al. 1996).

The differential VRB projection patterns to the caudal-medial verses rostral-lateral regions along the ICC isofrequency laminae is one of many studies which have

found anatomical and physiological differences between these two regions. Moreover, studies across various species have found that these regional differences are maintained throughout the ascending lemniscal system. In the gerbil, the caudal-medial and rostral-lateral ICC regions receive differential projections from the brainstem and projection to rostral and caudal regions, respectively, of the MGV along its isofrequency dimension (Cant and Benson 2007; 2006). In addition, studies in the cat and rat have demonstrated that the rostral MGV projects throughout the auditory cortex, including A1, whereas the caudal MGV projects to regions predominantly outside of A1 (Morel and Imig 1987; Polley et al. 2007; Rodrigues-Dagaeff et al. 1989; Storace et al. 2012; Storace et al. 2010). Comparing responses to acoustic stimuli between these two regions within the ICC, MGV, and A1, neurons in the 'rostral' pathway typically respond with shorter latencies, less spiking jitter, shorter duration responses, and stronger excitatory activity than neurons in the 'caudal' pathway (Phillips et al. 1995; Polley et al. 2007; Rodrigues-Dagaeff et al. 1989; Schreiner et al. 2011; Storace et al. 2012; Wallace et al. 2000) (for ICC responses, see Chapter 2).

The differences in response properties and projection patterns between the two regions have led to an emerging hypothesis that dual sub-projection pathways are present through the lemniscal system. While most of the work supporting this hypothesis has primarily considered the ascending lemniscal system, it appears that the descending system may be a part of the sub-projection pathways, at least with corticotectal projections. This evident in the ICC, where primarily the caudal-medial and not rostral-lateral regions along the ICC isofrequency laminae have excitatory responses to

electrical stimulation of A1 (Markovitz et al. 2013) and have VRB corticofugal projections (as shown in this study). Future studies should investigate whether other corticofugal projections, including corticothalamic ones, also differentially project to the caudal regions within the sub-projection pathways. In addition to contributing to the understanding of the structure of the descending system, these studies could also illuminate the role of the subprojection pathways. With the current studies from the ascending and descending systems, it appears that the rostral pathway, with more robust and precise activation properties, may serve as the main ascending auditory pathway while the caudal pathway, with more diffuse activation properties and greater corticotectal projections, may serve a more modulatory role for sound processing.